

The HARPS search for southern extra-solar planets [★]

XLI. A dozen planets around the M dwarfs GJ 3138, GJ 3323, GJ 273, GJ 628, and GJ 3293

N. Astudillo-Defru^{1,2}, T. Forveille², X. Bonfils², D. Ségransan¹, F. Bouchy¹, X. Delfosse², C. Lovis¹, M. Mayor¹, F. Murgas², F. Pepe¹, N. C. Santos^{3,4}, S. Udry¹, A. Wünsche²

¹ Observatoire de Genève, Université de Genève, 51 ch. des Maillettes, 1290 Sauverny, Switzerland

² Univ. Grenoble Alpes, CNRS, IPAG, F-38000 Grenoble, France

³ Instituto de Astrofísica e Ciências do Espaço, Universidade do Porto, CAUP, Rua das Estrelas, PT4150-762 Porto, Portugal

⁴ Departamento de Física e Astronomia, Faculdade de Ciências, Universidade do Porto, Portugal

ABSTRACT

Context. Low mass stars are currently the best targets for searches for rocky planets in the habitable zone of their host star. Over the last 13 years, precise radial velocities measured with the HARPS spectrograph have identified over a dozen super-Earths and Earth-mass planets ($m \sin i \leq 10 M_{\oplus}$) around M dwarfs, with a well understood selection function. This well defined sample informs on their frequency of occurrence and on the distribution of their orbital parameters, and therefore already constrains our understanding of planetary formation. The subset of these low-mass planets that were found within the habitable zone of their host star also provide prized targets for future atmospheric biomarkers searches.

Aims. We are working to extend this planetary sample to lower masses and longer periods through dense and long-term monitoring of the radial velocity of a small M dwarf sample.

Methods. We obtained large numbers of HARPS spectra for the M dwarfs GJ 3138, GJ 3323, GJ 273, GJ 628 and GJ 3293, from which we derived radial velocities (RVs) and spectroscopic activity indicators. We searched them for variabilities, periodicities, Keplerian modulations and correlations, and attribute the radial-velocity variations to combinations of planetary companions and stellar activity.

Results. We detect 12 planets, of which 9 are new with masses ranging from 1.17 to 10.5 M_{\oplus} . Those planets have relatively short orbital periods ($P < 40$ d), except two of them with periods of 217.6 and 257.8 days. Among these systems, GJ 273 harbor two planets with masses close to the one of the Earth. With a distance of 3.8 parsec only, GJ 273 is the second nearest known planetary system – after Proxima Centauri – with a planet orbiting the circumstellar habitable zone.

Key words. stars: individual: GJ 3138, GJ 3323, GJ 273, GJ 628, GJ 3293 – stars: planetary systems – stars: late-type – planets and satellites: detection – technique: radial velocities

1. Introduction

M dwarfs lie at the bottom of the main sequence, and consequently are small, cool and intrinsically faint. These physical characteristics are as many advantages when looking for smaller, cooler and fainter planets. For orientation, an Earth-mass planet in the habitable zone of a 0.2- M_{\odot} M dwarf, produces a radial-velocity (RV) wobble that is over an order of magnitude larger than that of the Earth on our Sun. When caught in transit, this Earth-size planet decreases the flux of the M dwarf (with a 0.2 R_{\odot} radius) by 25 times as much as the Earth does when it crosses the Sun. This makes planets around M dwarfs easier to *detect*, and even more importantly easier to *characterize*. M dwarfs with transiting planets, like GJ436 (Butler et al. 2004; Gillon et al. 2007), GJ1214 (Charbonneau et al. 2009), GJ3470 (Bonfils et al. 2012), GJ1132 (Berta-Thompson et al. 2015) and K2-3 (Crossfield et al. 2015; Almenara et al. 2015) are therefore

very popular targets in the exoplanet characterization community. Our HARPS program has made significant contributions to the detection, confirmation and/or characterization of all of those. Some of the more numerous HARPS detections that do not transit may become amenable to characterization once future instruments (e.g. METIS@E-ELT – Snellen et al. 2015) will be able to resolve them angularly

In this paper, we report a total of twelve planet detections in five planetary systems. The five stars, GJ 3138, GJ 3323, GJ 273, GJ 628, and GJ 3293, were observed with the HARPS spectrograph as part of our long-term effort to search for planets around bright, nearby M dwarfs. Section 2 summarizes the stellar properties of each host star, while Section 3 shortly describes our dataset and how both radial velocities and spectroscopic indices are measured from the HARPS spectra. In Section 4 we identify periodic signals and ascribe them to either planets or activity-induced variations. Finally, Sect 5 presents our conclusions.

2. Stellar properties

GJ 3138, GJ 3323, GJ 273, GJ 628 and GJ 3293 are part of our HARPS sample of M dwarfs because their distance is $d < 11$ pc, their V band magnitude $V < 14$ mag, and their rotational velocity $v \sin i < 6.5$ km/s (Bonfils et al. 2013). We retrieved their

[★] Based on observations made with the HARPS instrument on the ESO 3.6 m telescope under the program IDs 180.C-0886(A), 183.C-0437(A), and 191.C-0873(A) at Cerro La Silla (Chile). Tables X are available in electronic form at <http://www.aanda.org>. Radial velocity data (X) are only available in electronic form at the CDS via anonymous ftp to cdsarc.u-strasbg.fr (130.79.128.5) or via <http://cdsweb.u-strasbg.fr/cgi-bin/qcat?J/A+A/>

	GJ 3138	GJ 3323	GJ 273	GJ 628	GJ 3293
Spectral Type ⁽¹⁾	M0	M4	M3.5	M3.5	M2.5
α (J2000)	02 ^h 09 ^m 10.9 ^s	05 ^h 01 ^m 57.5 ^s	07 ^h 27 ^m 24.49 ^s	16 ^h 30 ^m 18.1 ^s	04 ^h 28 ^m 35.6 ^s
δ (J2000)	-16°20'22.5''	-06°56'45.9''	+05°13'32.8''	-12°39'45.3''	-25°10'16''
V ⁽²⁾	10.98	12.22	9.872	10.03	11.962
J ⁽³⁾	8.076 ± 0.019	7.617 ± 0.032	5.714 ± 0.032	5.950 ± 0.024	8.362 ± 0.024
H ⁽³⁾	7.412 ± 0.031	7.065 ± 0.046	5.219 ± 0.063	5.373 ± 0.040	7.749 ± 0.038
K _S ⁽³⁾	7.246 ± 0.016	6.736 ± 0.024	4.857 ± 0.023	5.075 ± 0.024	7.486 ± 0.033
μ [mas] ^(4,5,5)	33.44 ± 2.17	187.92 ± 1.26	262.98 ± 1.39	232.98 ± 1.60	55 ± 9
M_V	8.6 ± 0.13	13.59 ± 0.01	12.26 ± 0.01	11.87 ± 0.01	10.66 ± 0.31
M_K	4.87 ± 0.13	8.11 ± 0.03	6.96 ± 0.03	6.91 ± 0.03	6.19 ± 0.31
BC_K	2.62 ± 0.05	2.72 ± 0.07	2.68 ± 0.08	2.71 ± 0.06	2.71 ± 0.08
L [L _{sun}] ⁽⁶⁾	0.045 ±0.007	0.0027 ±0.0066	0.0088 ±0.0066	0.0102 ±0.0066	0.022 ±0.0066
M [M _⊙] ⁽⁷⁾	0.681	0.164	0.29	0.294	0.42
R [R _⊙] ⁽⁶⁾	0.50 ± 0.03	0.119 ± 0.027	0.293 ± 0.027	0.307 ± 0.027	0.404 ± 0.027
T _{eff} [K] ⁽⁶⁾	3717 ± 49	3159 ± 49	3382 ± 49	3342 ± 49	3466 ± 49
[Fe/H] ⁽⁸⁾	-0.30 ± 0.12	-0.27 ± 0.09	0.09 ± 0.17	-0.09 ± 0.09	0.02 ± 0.09
μ_α [mas/yr] ^(4,9,2)	517.58 ± 1.98	-550.2 ± 8	572.51 ± 1.50	-94.81 ± 2.30	-87 ± 5
μ_δ [mas/yr] ^(4,9,2)	78.39 ± 1.63	-533.3 ± 8	-3693.51 ± 0.96	-1183.43 ± 1.74	-475 ± 5
dv_r/dt [m/s/yr]	0.188 ± 0.014	0.073 ± 0.001	1.221 ± 0.007	0.139 ± 0.001	0.097 ± 0.018
Rad. Vel [km/s] ^(1,10,11,11,10)	2.90 ± 10	39.42 ± 2.55	18.22 ± 0.10	-21.22 ± 0.10	826 ± 112
U [km/s]	59.7 ± 51.7	21.2 ± 2.3	-15.9 ± 0.1	12.91 ± 0.02	-27.3 ± 17.1
V [km/s]	-38.7 ± 64.6	-16.8 ± 3.2	-65.7 ± 0.1	-21.01 ± 0.01	-25.9 ± 6.6
W [km/s]	21.2 ± 7.0	-34.6 ± 1.1	-17.3 ± 0.1	-20.63 ± 0.01	-22.2 ± 23.1
Dyn. Pop.	-	YD/OD	YD/OD	YD	YD or YD/OD
Multiplicity ^(12,13)	-	No	No	No	-
HZ _{In} S/S _⊕ ^(14, conservative, 1M_⊕)	0.937	0.925	0.929	0.928	0.931
HZ _{In} S/S _⊕ ^(14, conservative, 5M_⊕)	1.006	0.993	0.997	0.996	0.999
HZ _{In} S/S _⊕ ^(15, [Fe/H]=-0.5,-0.3,0.3,0.3)	1.69	-	1.64	1.63	1.68
HZ _{Out} S/S _⊕ ^(14, conservative, 1M_⊕)	0.254	0.237	0.243	0.242	0.246
log(R' _{HK}) ⁽¹⁶⁾	-4.855	-4.839	-5.560	-5.523	-5.114
P _{Rot.} [days] ⁽¹⁶⁾	34	33	99	93	50
P _{Rot.} [days] ⁽¹⁷⁾	42.5	-	-	95	41

Table 1. Stellar properties and parameters. (1) Hawley et al. (1996); (2) Gaidos et al. (2014); (3) Cutri et al. (2003); (4) van Leeuwen (2007); (5) Henry et al. (2006); (6) Boyajian et al. (2012); (7) Delfosse et al. (2000); (8) Neves et al. (2013); (9) Zacharias et al. (2012); (10) Kordopatis et al. (2013); (11) Nidever et al. (2002); (12) Rodriguez et al. (2015); (13) Ward-Duong et al. (2015); (14) Kopparapu et al. (2013, 2014); (15) Kopparapu et al. (2016) (16) From Astudillo-Defru et al. (2016), where the typical error is 8.7%; (17) This work. From the periodogram of activity indices. On the dynamical population we use the abbreviation YD: young disk; OD: old disk.

spectral types, photometry, coordinates, proper motions, parallaxes, and multiplicity from the literature, with full references in Table 1. The secular acceleration (dv/dr) is calculated following Eq. 2 from Zechmeister et al. (2009). We computed their luminosities using Leggett et al. (2001) bolometric corrections. We estimated their physical parameters using calibrations by Delfosse et al. (2000) for stellar mass, Boyajian et al. (2012) for stellar radius and effective temperature, and Neves et al. (2013) for metallicity. We computed their UVW galactic velocities using the Johnson & Soderblom (1987) conventions and assigned them to dynamical population following the Leggett (1992) prescription, except for GJ 3138 where the uncertainty in the absolute radial velocity is too high. We computed the limit of the habitable zone of each star with the Kopparapu et al. (2013, 2014) online calculator¹, in addition to adopt the new inner limit of the HZ from Kopparapu et al. (2016). This new inner limit incorporates 3D global climate models (GCM) in tidally locked exoplanets around cool stars. We quantified their magnetic activity by measuring their Mount Wilson S index (Wilson 1968;

Vaughan et al. 1978) on their average HARPS spectra. We converted the S index into R'_{HK} values following the procedure described in Astudillo-Defru et al. (2016). With $\log(R'_{HK})$ between -4.78 and -5.60, all five stars are magnetically quiet, or at most very moderately active. While GJ 628 has been catalogued as a BY-Dra variable (Nakajima & Morino 2012), its photometric variability is only moderate since the dispersion of its V band flux is just 16 ± 7 mmag (Hosey et al. 2015). As discussed below, we find its variations consistent with a magnetic cycle. Table 1 summarizes these stellar properties.

3. Data

We obtained spectra of the five targets with HARPS (Mayor et al. 2003), a cross-dispersed echelle spectrograph fibre-fed by the 3.6m telescope at ESO/La Silla Observatory (Chile). The instrument has a resolving power of $R \sim 115,000$ and almost full wavelength coverage between 380 nm and 690 nm. It is enclosed in a vacuum vessel and temperature-stabilised so as to reach a long-term radial-velocity precision < 1 m/s. Calibrations are performed daily with a ThAr lamp (Lovis & Pepe 2007) and, since 2010, additionally with a white-light-illuminated Fabry-

¹ <http://depts.washington.edu/naivpl/sites/default/files/hz.shtml>

Pérot étalon (Wildi et al. 2010). Between those calibrations, the sub-m/s drift of the instrument can be measured by illuminating a second fiber with a calibration lamp while the first fiber collects the light of the star. The offset between the simultaneous and daily calibrations can be subtracted from the radial velocity measurement of the star to improve its precision to a few tens of cm/s (see Sect. 2.6 in Fischer et al. 2016). We did not initially rely on this simultaneous calibration for our program, because some very strong ThAr lines spill from the calibration fiber into the stellar spectra to degrade our measurements of some important spectroscopic diagnostics in the blue-part of M dwarf spectra. The Fabry-Pérot calibration source has much more uniform line intensities, and therefore does not significantly contaminate the stellar spectrum. From 2012 on, we thus changed our observing strategy and use simultaneous calibration with the Fabry-Pérot source for stars brighter than $V=11$ mag. For fainter targets, we use the second fiber to monitor the sky background.

The use of octagonal cross-section fibers in the entrance of the spectrograph demonstrate the ability to stabilize the illumination of the spectrograph, decreasing the effect of imperfect guiding or seeing variations (Perruchot et al. 2011). The HARPS fiber link was upgraded with such fiber on May 28th 2015 (Lo Curto et al. 2015), stabilizing its line-spread function but introducing a zero point in our measurement series.

3.1. Radial velocities

The HARPS Data Reduction Software (DRS) provides a quasi-real-time estimate of the radial velocity through cross correlation (CCF) of the stellar spectrum with a software mask (Baranne et al. 1979; Pepe et al. 2002). This measurement, although a very good first estimate, uses a fixed template across M sub-types and discards the information contained in the many blended and weak lines were rejected at its construction. It therefore has a sub-optimal signal to noise ratio, and we recompute improved velocities off-line through a few steps (Astudillo-Defru et al. 2015). We first align all spectra of a given star to a common frame using RV_{CCF} as a first guess, and co-add them into a high signal-to-noise stellar template. We then produce a high signal-to-noise template of the telluric absorption, subtracting the average stellar template contribution from each observed spectrum and co-adding the residuals in the laboratory frame. Whereas the stellar spectrum moves on the CCD according to the projection of the radial velocity of the Earth toward the star, the telluric lines are fixed on the detector. The stellar and telluric spectra can thus be disentangled. Armed with these two templates, we measure a radial velocity from each observed spectrum as the Doppler shift that maximizes the likelihood between this spectrum and the high signal-to-noise template, using the telluric template to mask out the pixels most affected by telluric lines. Extracting the RV through maximum-likelihood optimization against a high signal-to-noise template was already proposed long ago (e.g. Howarth et al. 1997; Zucker & Mazeh 2006), and independent implementations were applied to HARPS data by Chelli (2000); Galland et al. (2005, in Fourier space) and by Anglada-Escudé & Butler (2012).

Compared to the online pipeline, this reprocessing reduces the error bars by typically 20 to 30%. Since the HARPS upgrade with an introduction of a section of octagonal fiber altered the line spread function, we opted to process the *pre*- and *post*-upgrade epochs independently. For each star we thus produce *pre*- and *post*-upgrade templates, and we adjust a zero point offset when analyzing the time series.

3.2. Activity proxies

Because stellar activity can confuse planet searches, we need to monitor its strength and its variation on time-scales that range from the stellar rotation period (a few to 100 days) to the length of a magnetic cycle (a few hundred days to a dozen years). We therefore monitor the shape of the spectral lines and measure spectroscopic indices in our HARPS spectra, and we also use publicly available photometry.

3.2.1. Spectroscopic indices

Table 2. Wavelengths for the pass-bands defining $H\beta$, $H\gamma$ and Na D spectroscopic activity proxies.

Index	C	V	R
	$[\lambda_i, \lambda_f]$ [Å]	$[\lambda_i, \lambda_f]$ [Å]	$[\lambda_i, \lambda_f]$ [Å]
$H\beta$	[4861.04, 4861.60]	[4855.04, 4860.04]	[4862.6, 4867.2]
$H\gamma$	[4340.16, 4340.76]	[4333.60, 4336.80]	[4342.00, 4344.00]
Na D	[5889.70, 5890.20] [5895.67, 5896.17]	[5860.00, 5870.00]	[5904.00, 5908.00]

The HARPS DRS provides the Full-Width-at-Half-Maximum (FWHM) and the bisector span of the cross-correlation function (Queloz et al. 2001), which both are useful probes of stellar activity. We also measure from the spectra the chromospheric emission in the Ca II H&K lines, as well as in the $H\alpha$, $H\beta$, and $H\gamma$ and Na D lines (Wilson 1968; Giampapa et al. 1978; Linsky et al. 1982). Our measurements of the Ca II H&K follow Vaughan et al. (1978, S-index) and those of $H\alpha$ Gomes da Silva et al. (2011). For the other lines that are sensitive to stellar activity, we compute the ratio of the integrated flux in the line (C) over that in two control bands (V, R):

$$H\beta = \frac{C_\beta}{V_\beta + R_\beta}; \quad H\gamma = \frac{C_\gamma}{V_\gamma + R_\gamma}; \quad NaD = \frac{C_{Na} + C_{Na}}{V_{Na} + R_{Na}} \quad (1)$$

where the wavelength pass-bands are listed in Table 2.

3.2.2. Photometry

Since the contrast between spots and the rest of the photosphere increases at bluer wavelength, we use photometry in optical rather than near-infrared band, and retrieved photometric time series of the five targets from the All Sky Automated Survey (ASAS, Pojmanski 1997), available at <http://www.astrouw.edu.pl/asas>. Since M dwarfs are relatively faint objects in this band, the ASAS photometry through the smallest synthetic apertures provide the highest quality measurements by minimizing the sky background.

We systematically searched for spot induced periodicities for the whole photometric time-series as well as for each seasonal observations. The seasonal analysis helps to the detection of the stellar rotation period assuming that active regions evolves and lasts for an unknown lapse of time.

4. Data analysis

4.1. Methods

We apply the same method for the five stars, searching the time-series for variability and periodicities, and modeling the periodic

signals as Keplerian orbits. In an effort to disentangle activity signals from planets, we compare the detected periods with the stellar rotation period and we search all RV signals for a counterpart in the time-series of the activity indicators.

From the CCF computed by the HARPS DRS, we start by building a representative measurement uncertainty for each star which accounts for the photon noise (Bouchy et al. 2001) and the 0.60 m s^{-1} calibration error (see Fig. 6 in Fischer et al. 2016), but not for the stellar jitter. We quadratically add the two noise components for each epoch, and compute the typical expected error σ_i as a weighted average of these epoch uncertainties. Prior to the RV analysis, we subtract the secular acceleration (see Table 1). The observed dispersions of the pipeline RV measurements of GJ 3138, GJ 3323, GJ 273, GJ 628, and GJ 3293 stand above this expected error by factors of respectively 1.5, 1.5, 3.2, 3.7, and 3.1.

This motivated the extraction of the offline RVs described above, which we searched for periodicities by computing a Generalized Lomb-Scargle periodogram (Zechmeister & Kürster 2009). Our GLS normalization choice is such that a GLS power of 1.0 means that a sine wave is a perfect description of the data, while a power of 0.0 means that a constant model is an equally good fit. To translate GLS power values to false-alarm probabilities (FAP), we use bootstrap Monte-Carlo simulations, creating 10,000 synthetic time-series by shuffling the original velocity values between the observation dates. We compute a periodogram for each bootstrapped data set, and record the distribution of the maximum value of the bootstrapped periodograms. We obtain the FAP for a given GLS power as the fraction of the bootstrapped periodograms that had a higher maximum value. The window function of the data-sets is analyzed in order to identify aliasing or periodicities due to our temporal sampling.

When we identify a periodic signal with a FAP under 1%, we adjust a Keplerian to the velocities and look for additional periodic signals in the fit residuals, iterating until no significant signal is detected.

To protect against overfitting the data with a more complex model than they warrant, we compute the Bayesian Information Criterion (BIC: minus twice the Schwarz criterion, Schwarz 1978) for models with increasing numbers of Keplerian components. The BIC is widely used for model comparison because it is easily computed²; the BIC's reliability as an approximation of the logarithm of the (more rigorous but harder to derive) Bayes factor however depends on the sample size (Kass & Raftery 1995) and quantifies the evidence in favor (or not) of a model over the null hypothesis model H_0 (generally the simplest model).

We adjusted the (multi-)Keplerian models using the YORBIT (Ségransan et al. 2011) code, which efficiently explores the model parameter space through a genetic algorithm. After model convergence, we estimated the parameter uncertainties with a Markov Chain Monte Carlo algorithm. As noted above, all models include a free zero-point offset between the velocities acquired before and after the HARPS fibers upgrade (Lo Curto et al. 2015).

4.2. GJ 3138

4.2.1. Periodicity analysis

We acquired 199 radial velocities of GJ 3138, of which 156 were obtained prior to the mid-2015 HARPS fibers upgrade

² $\text{BIC} = -2 (\log \text{maximized likelihood}) + \text{number of parameters} (\log \text{number of measurements})$

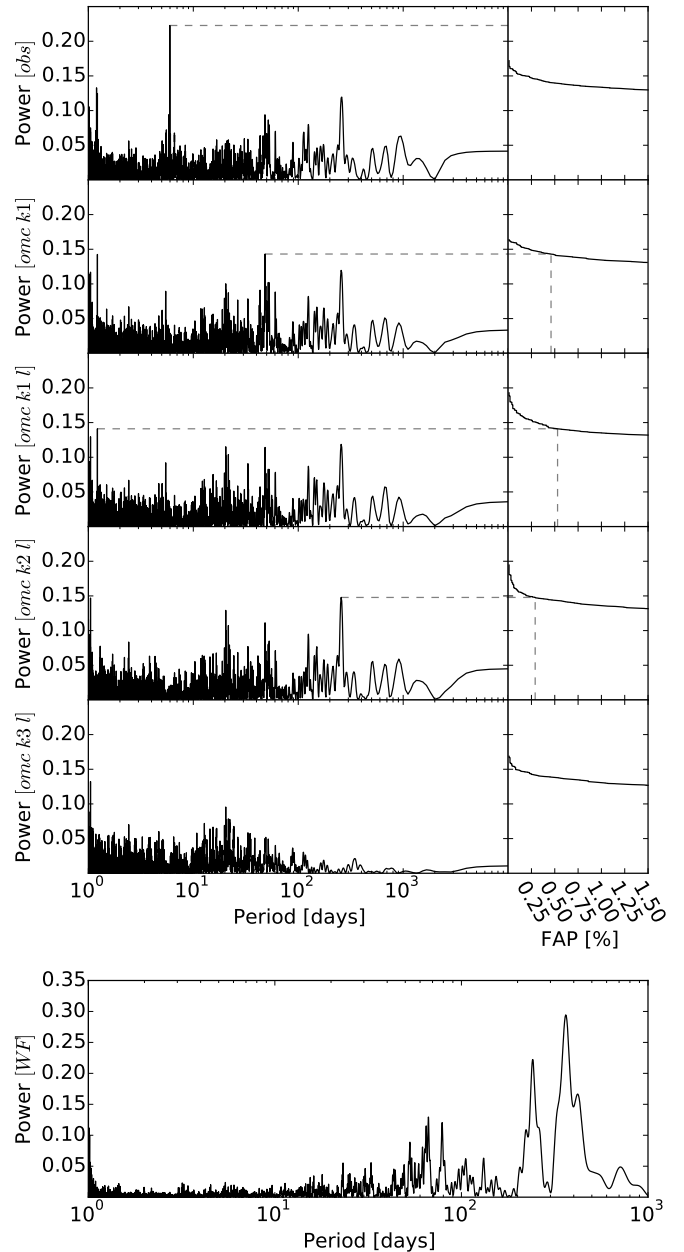


Fig. 1. *Top:* Periodograms (left columns) of the GJ 3138 radial velocities. We subsequently subtract a model to fit data (raw RVs on top) until no clear signal remains on the residues (bottom). The k in the y-axis label depicts a (single or multiple) Keplerian model while the l represents the linear model between RVs and $H\alpha$ (see text). In each step we modeled the signal highlighted with the horizontal dashed line. Right column represents the FAP derived from the bootstrap analysis. Each analyzed peak has a FAP under 0.75%. *Bottom:* The window function exhibits peaks located at 365 days, 240 days, 66 day, and 79 days.

and 43 afterwards. We discarded one measurement (epoch BJD=2457258.81) which is a strong outlier. The root-mean-square dispersion of these velocities is $\sigma_{(O-C)} = 2.87 \text{ m s}^{-1}$, well above their expected uncertainty of $\sigma_i = 1.82 \text{ m s}^{-1}$.

Our iterative periodogram analysis detects four significant periodicities (Fig. 1). The periodogram of the radial velocities shows a strong peak around a 6.0 days period, with a power much above any found in the 10'000 reshuffled data sets. Its

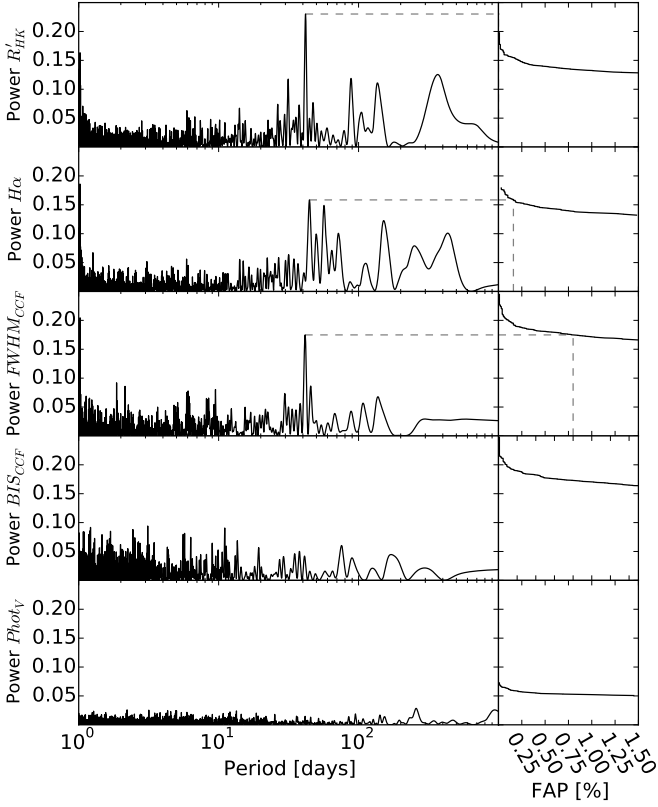


Fig. 2. Periodograms of the R'_{HK} , $H\alpha$, and $FWHM_{CCF}$ measurements of GJ 3138. Their low-FAP peaks at respectively 41.8 days, 44.6 days, and 41.2 days all reflect the stellar rotation period.

False Alarm Probability (FAP) is thus well below 0.01%. The residuals of a fit of the corresponding Keplerian model (model $k1$) have periodogram peaks at periods of 48.2, 1.2, and 257 days, with FAPs of respectively 0.46%, 0.49%, and 4.72%. In the next section, we show that the 48.2 days peak is likely due to stellar activity, since after subtraction of the other periodic radial velocity signals we observe a strong correlation with the $H\alpha$ flux. Instead of modeling this 48.2-day periodicity as a Keplerian signal, we use the RV- $H\alpha$ correlation derived in the next section to describe it. After subtraction of both that activity signal and the first planet, the strongest periodogram peak is at 1.2-day and has a 0.53% FAP. We adjust a 2-Keplerian model (model $k2$) to the activity-corrected radial velocity time-series (a RV time-series now corrected from the RV- $H\alpha$ correlation). In a fourth iteration, the periodogram of the residuals exhibits a significant power excess at period 257 days, with a FAP=0.29%. A fifth iteration finds two peaks at 1.05 and 20.4 days, which are 1 day⁻¹ aliases of each other. The strongest of the two has a 0.9% FAP that it just at our detection 1% FAP threshold. However, the BIC values of the models with three or four Keplerians ($\Delta BIC_{K3,K4} = 4.4$) do not favour this more complex model. In addition, a periodicity of 20.4 days is half the rotation of GJ 3138. We therefore interpret that this low RV signature is possibly provoked by stellar activity.

4.2.2. Validating the planet interpretation

The 48-days signal as stellar rotation

The stellar rotation period estimated from the average R'_{HK} is

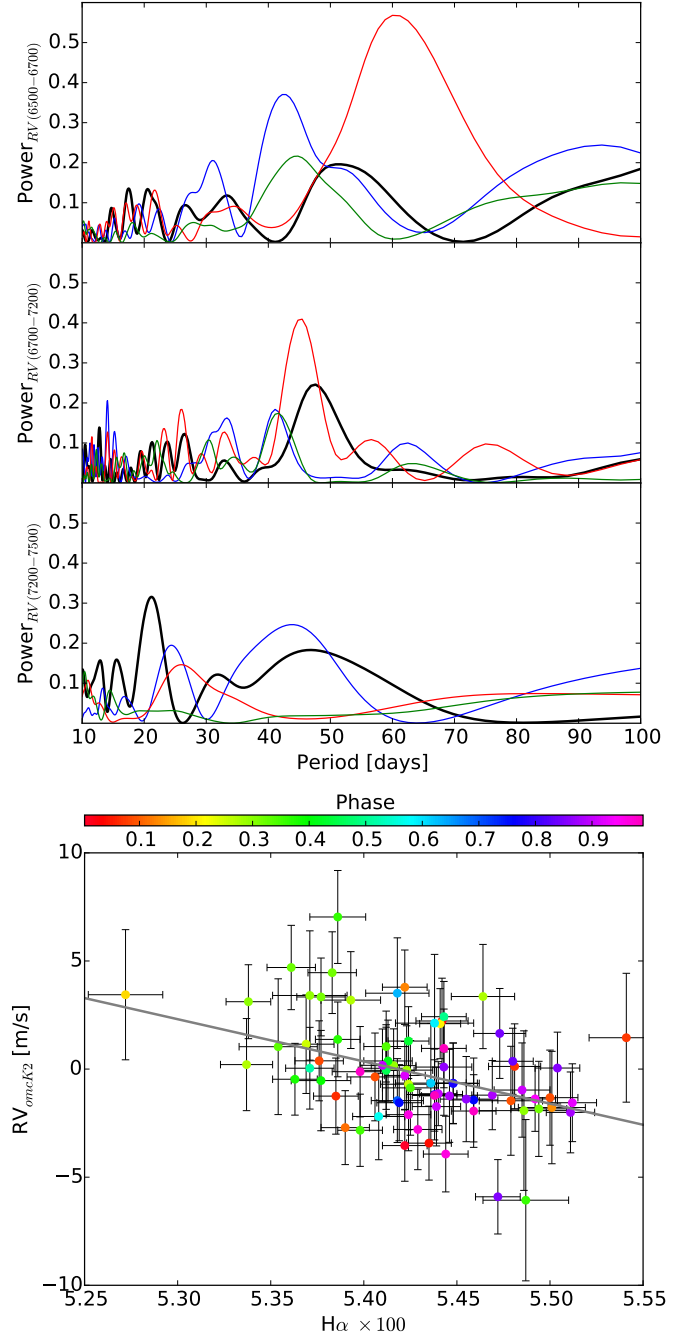


Fig. 3. Top panel: The black, red, blue and green curves depict the periodogram of the GJ 3138 RVs after removing the 1.22 and 6.0 days periodicities, $H\alpha$, R'_{HK} , and $FWHM_{CCF}$, respectively. First row shows periodograms for BJD-2450000 between 6500 and 6700, second row for 6700-7200, and third row for 7200-7500. Second row shows that RVs and $H\alpha$ have power excess at the same periodicity. RVs- $H\alpha$ anti-correlation is subtracted (see text). Bottom panel: The 77 radial velocities as a function of the $H\alpha$ for BJD from 2456700 to 2457200. Color represent the phase for a periodicity of 48.2 days. The linear fit is used to correct the RV interval.

34 days (Table 1). This is safely remote from the 1.2 day, 6.0 days, and 257 days periods, but within its likely errorbar of the 48 days period. We therefore search the time series of the activity indicators for periodicities (Fig. 2) and for correlation

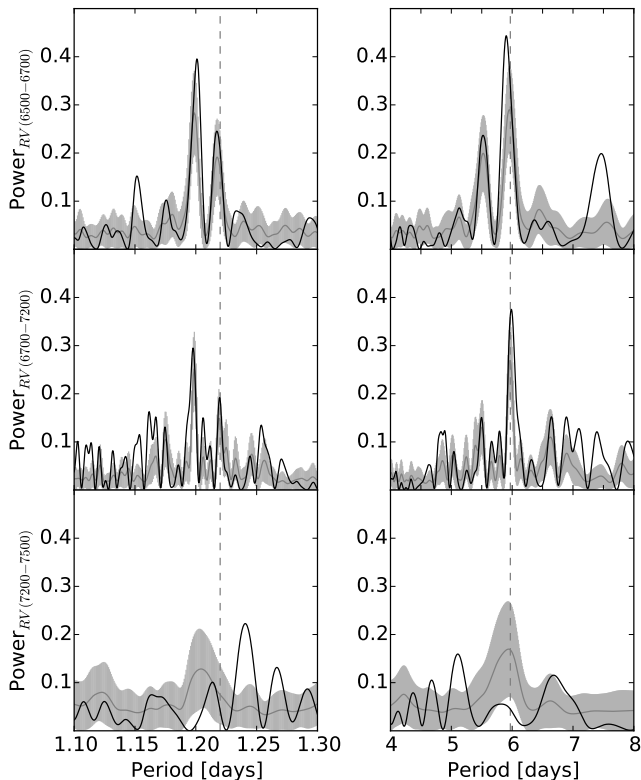


Fig. 4. Periodograms of the three subsets of RVs. Left and right columns are zooms around the 1.2 and 6 days zones of interest, respectively. Black curves depict the periodograms for the observed RVs (raw), the gray curves show the average periodograms of the 100 synthetic RVs, while the light gray areas represent the 1σ zones. The first and second rows of left column shows separately the one day alias of the 6.0 days peak (located at 1.20 days) and the 1.22 days signal (vertical dashed line). Third row in the right column shows that the lack of power for the sub-sample with BJD-2450000 between 7200 and 7500 is consistent (very close to the 1σ level) with the constrained coverage in phase of the 6.0 days signal.

with the measured radial velocity (Fig. 3, bottom). Since the fiber upgrade introduced an offset in both the FWHM_{CCF} and BIS_{CCF} timeseries, we restrict this analysis to the pre-upgrade measurements as those represent the bulk of the data-set. R'_{HK} , $H\alpha$ and FWHM_{CCF} show significant peaks at periods of respectively 41.8, 44.6 and 41.2 days, while neither the periodogram of the bisector nor that of the ASAS photometry (497 points over 9.0 years) show significant periodicities. The periodograms for the seasonal photometry do not show evidences of the stellar rotation. The three identified signals have similar periods, which are also close to the 34 days stellar rotation period estimate from R'_{HK} and to the 48.1-day periodicity in the RV time series. We surmise that these periods all reflect modulation of photospheric inhomogeneities by the stellar rotation, with their dispersion due to some combination of differential rotation and measurement noise.

We turn to sub-samples of the time series to confirm this suspicion. We subtract the 1.2 and 6.0 day signals from the RV series to focus on the 48 day signal, and divide the activity diagnostic and RV time series into three BJD-2450000 intervals: 6500–6700, 6700–7200 and 7200–7500, with 57, 77, and 41 measurements. Fig. 3 shows the corresponding periodograms.

The periodograms of the RV residuals and $H\alpha$ for the second epoch ([6700–7200]) are strikingly similar, with both having significant power excess around ~ 43 days. The RV residuals clearly anti-correlate with $H\alpha$ for that epoch (Fig. 3, bottom), with a Pearson coefficient of -0.42 . The same figure also shows $H\alpha$ phased to a 48.2-day period, with points for phases between 0.2-0.5 mostly in the upper left corner and points for phases between 0.7-0.9 mostly in the lower right part of the plot. We fit the anti-correlation and obtain :

$$RV = (-1.953 \pm 0.262) \times H\alpha + (0.106 \pm 0.001) \quad (2)$$

We use this relation to correct the activity effect over the central interval. Without evidence for a similar relation over the other two intervals, we do not correct the rest of the RV time series. This partial correction reduces the strength of the 48 days signal very significantly, as demonstrated by a comparison of the second and third periodograms of Figure 1. This adds to the evidence for stellar activity, and we classify the 48-day periodicity as an activity signal rather than a planet.

We inquire if the RV signals for the two shorter periodicities (1.22 and 6 days) are present along the entire data-set – favoring the scenario where RV variations are due to the presence of an exoplanet – or concentrate in a particular sub-sample – challenging the planetary interpretation. We thus divide in three our RV time-series, with sub-samples that satisfy BJD-2450000 in the ranges 6500-6700, 6700-7200, and 7200-7500 and compute their periodograms. Figure 4 shows those periodograms specifically around 1.22 and 6 days, where both the 1.22- and 6 - day signals seen as power excess in most epochs.

In parallel, we need to evaluate if the power excess are actually expected given the sampling of each one of the three sub-samples. To that intend, we make additional synthetic time-series (100) by drawing random RV points with a normal distribution centered around the best Keplerian fit and with a 2 m/s standard deviation. For each one of the synthetic time-series we make a new periodogram, and the gray areas in Fig 4 represent their ± 1 sigma power distribution.

Around both 1.22 and 6 days, the periodogram of the original time series (black lines in Fig 4) is never found below the ± 1 sigma region (gray areas). This means both signals are indeed detected every time the sampling allows so, which in turn means the signals seem coherent rather than transitory.

Overall, we conclude on the planetary nature of both the 1.22- and 6-day signals.

4.2.3. Orbital parameters

Considering the above analysis, we detect 4 periodicities and conclude to the detection of 3 planets and the stellar rotation. Our Keplerian solution is illustrated in Figure 5 and presented in Table 3, which reports separate noise estimates and rms residuals around the solution for the data acquired before and after the HARPS fibers upgrade. For the stellar mass reported in Table 1, the semi-amplitudes convert to minimum masses of 1.9, 4.4 and $10.9 M_{\oplus}$, in the regime of super-Earths and mini-Neptunes. Their irradiance are 116, 14, and 0.09 times the terrestrial one, which for extreme Bond albedos of 0.75 and 0.0 correspond to equilibrium temperatures ranges of respectively 640-900K, 375-530K, 107-150K.

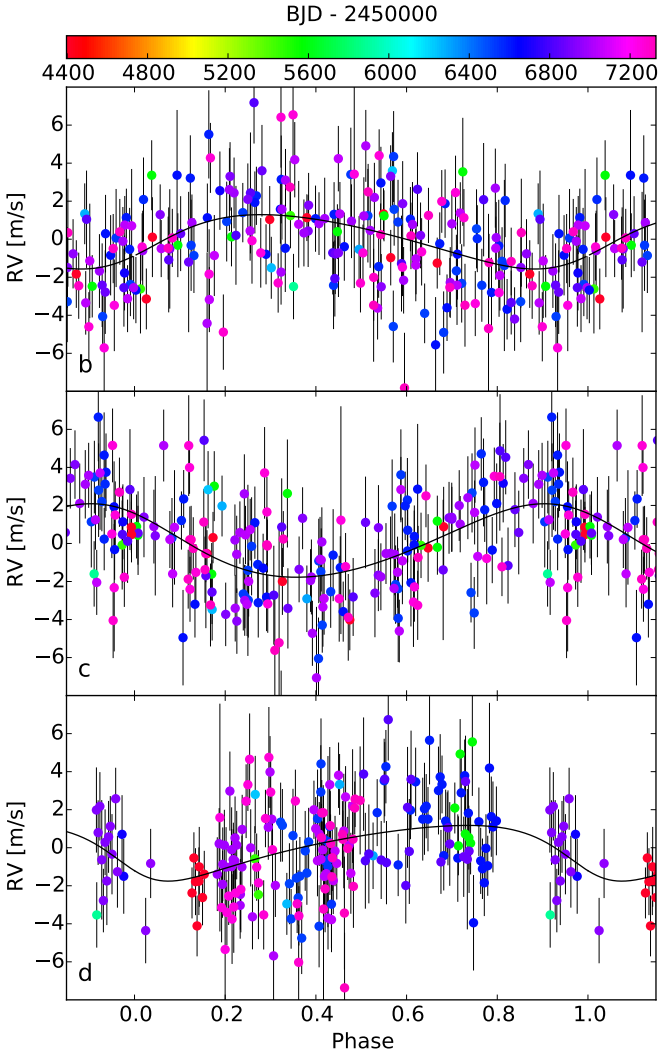


Fig. 5. Phase folded GJ 3138 RVs for the 1.22 day (top), 5.97 day (middle), and 258.5 day (bottom) orbits. Black solid curve and rainbow colors depict the Keplerian solution and BJD of observations, respectively.

4.3. GJ 3323

4.3.1. Periodicity analysis

We acquired 157 radial velocities on GJ 3323, including 132 before and 25 after the HARPS upgrade. We rejected three points because two have very low SNR (<3 at 550 nm; BJD=2456630.65, 2456926.86) and one is a $> 5\sigma$ outlier (BJD=2457258.92). The 154 remaining RVs show a standard deviation $\sigma_{(O-C)} = 2.85 \text{ m s}^{-1}$, in excess of estimated uncertainties $\sigma_i = 2.18 \text{ m s}^{-1}$. The periodogram of raw RVs (Fig. 6) shows a powerful peak around 5.4 days with FAP $\ll 0.01\%$. We fit a Keplerian to that first signal and compute the periodogram of the residuals. We found a second periodicity at around ~ 40 days with, again, a FAP $\ll 0.01\%$. We make a third iteration and found no more significant periodicity.

4.3.2. Challenging the planet interpretation

GJ 3323 b

Table 3. Parameters for the three Keplerian fitted to GJ 3138 RVs.

N_{Meas}		198		
σ_{ext}	[m/s]	0.39/1.37		
$\sigma_{(O-C)}$	[m/s]	2.05/2.60		
ΔV_{21}	[m/s]	$-0.16^{+0.52}_{-0.53}$		
BJD_{ref}	[days]	56684.6682638567		
γ	[km/s]	13.5973 ± 0.0002		
		GJ 3138c	GJ 3138b	GJ 3138d
P	[d]	$1.22003^{+0.00006}_{-0.00004}$	$5.974^{+0.001}_{-0.001}$	$257.8^{+3.6}_{-3.5}$
K_1	$[m s^{-1}]$	$1.43^{+0.27}_{-0.26}$	$1.93^{+0.26}_{-0.26}$	$1.47^{+0.35}_{-0.30}$
e		$0.19^{+0.18}_{-0.13}$	$0.11^{+0.11}_{-0.07}$	$0.32^{+0.20}_{-0.21}$
λ_0 at BJD_{ref}	[deg]	$239.4^{+10.5}_{-10.3}$	$42.5^{+7.2}_{-7.2}$	$128.8^{+13.0}_{-13.6}$
$m \sin(i)$	$[M_{\oplus}]$	$1.78^{+0.34}_{-0.33}$	$4.18^{+0.61}_{-0.59}$	$10.5^{+2.3}_{-2.1}$
a	[AU]	$0.0197^{+0.0005}_{-0.0005}$	$0.057^{+0.001}_{-0.001}$	$0.698^{+0.018}_{-0.019}$
S/S_{\oplus}		118.1	13.9	0.1
Transit prob.	[%]	10.5	3.7	0.3
$T_{\text{Trans}}-54000$	[days]	$2685.407^{+0.092}_{-0.072}$	$2685.47^{+0.25}_{-0.24}$	$2897.8^{+26.0}_{-27.0}$

GJ 3323 b is found with a period of 5.4 day that is significantly shorter than the 33-day period estimated for the stellar rotation (Table 1). We know that in some configurations, a spot coming in and out of view could produce a Doppler signal with significant power excess at half or a third of the stellar rotation period (Boisse et al. 2011). It is thus reassuring to know the 5.4 day period is also significantly different than any harmonic of the rotation.

Like for GJ 3138 RV analysis, we split the RV time series in three time intervals. They are chosen such that BJD-2450000 is in the ranges 6500-6800, 6800-7200, and 7200-7500, with 56, 67, and 24 points, respectively. Figure 8 show there periodograms with, on the left-hand side, a focus on period around 5 days. The signal is recovered at all epochs.

We can confidently accept that first signal as a planet.

GJ 3323 (c)

The periodicity around 40 day is close from our estimate of the stellar rotation. It therefore requires more attention to the different activity proxies.

Periodograms of R'_{HK} , FWHM_{CCF} , and $H\alpha$ present significant power excess in the period range around ~ 160 days (Fig. 7). The FWHM_{CCF} also shows additional power excess around 40 days. Conversely, in the same figure, the BIS_{CCF} index does not show any significant periodicity and the periodogram for the whole ASAS photometry time-series (654 points spanning 9.0 years) shows power excess at about 665 (2% FAP) and 88 days (10% FAP). From the seasonal analysis, a periodicity close to 88 days is detected for the ASAS seasons between BJD 2800–3200 (0.24%FAP) and 3500–4000 (0.42%FAP). Such a value is compatible with the 88.5 days reported by Kiraga (2012) for the rotational period. However, the reliability of the 88.5 days stellar rotation is questionable because only 2/10 of ASAS seasons shows the ~ 90 day periodicity despite that usually spots on M dwarfs are more stable over time (e.g. GJ 674, GJ 581, GJ 174, GJ 551) and the stellar rotation period estimated from the $\log(R'_{HK})$ is 33 days. Except for the less powerful power excess at 40 days in

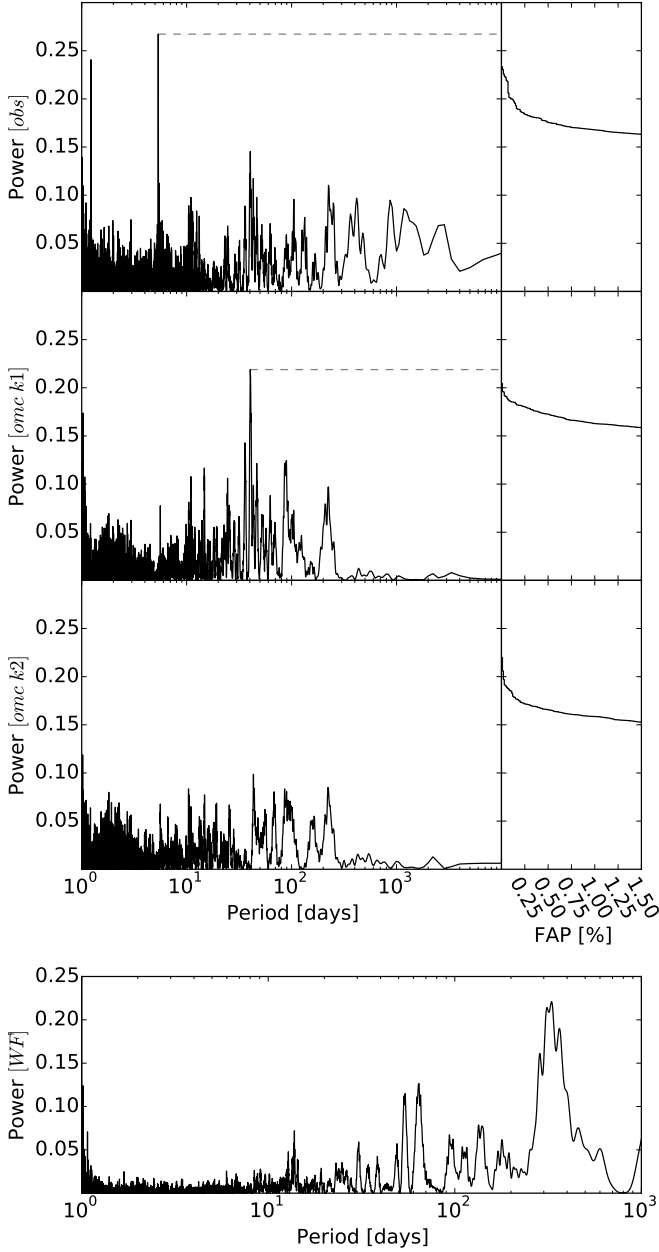


Fig. 6. *Top:* Top row shows the periodogram of GJ 3323 raw radial velocities, with a clear detection (FAP < 10⁻²%) of periodicity at 5.4 days. When subtracting the Keplerian adjusted to this signal, the periodogram of residuals exhibit a very significant peak (FAP < 10⁻²%) at 40 days (bottom row). *Bottom:* The window function shows peaks at one year, 64 days, and 54 days.

FWHM_{CCF}, the variability is thus seen in a period range much different than that of the 33-day period estimated for the stellar rotation by the $R'_{HK} - P_{rot}$ relation (Table 1). It is possible that such longer time-scale changes are related to magnetic cycles instead (Gomes da Silva et al. 2011).

As previously, we subdivide the time series of both RVs and activity proxies in the same three time intervals. We subtract the best Keplerian fit to RVs to focus on the 40 d periodicity (right-hand side of Fig. 8). Note that only the first two intervals have a meaningful sampling to probe the 40-day signal. The third interval only has 24 points spread on just one period and a half. Power

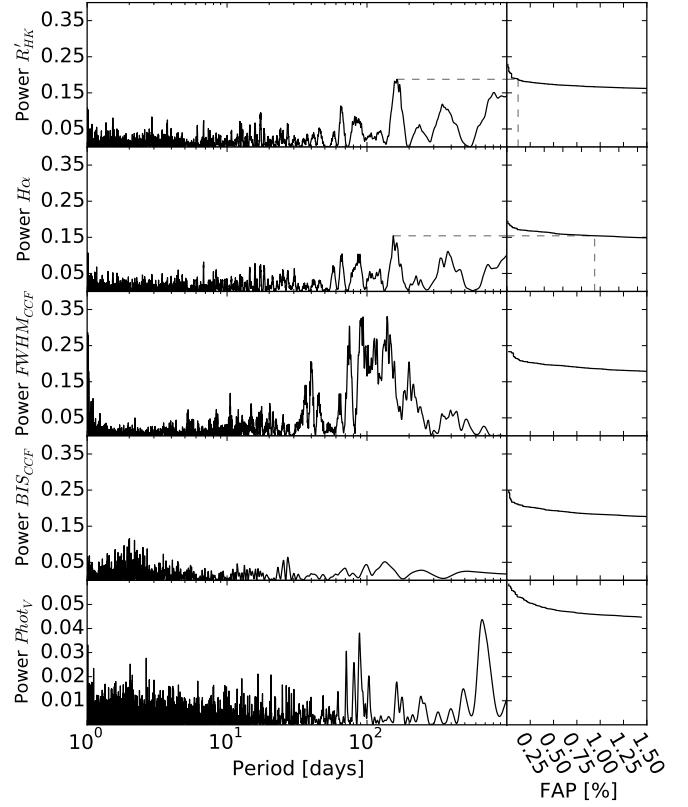


Fig. 7. Periodograms of the R'_{HK} , $H\alpha$, FWHM_{CCF}, and the BIS_{CCF} activity indices of GJ 3323. Significant peaks (FAP < 1%) are located at ~160 days for R'_{HK} and $H\alpha$. The FWHM_{CCF} periodograms is less clean at that periodicity and additionally shows power excess at ~40 days. No favored periodicity is present in the periodogram of BIS_{CCF} while the photometry periodogram shows power excess at about 665 and 88 days with 2% and 10.2% FAPs, respectively.

excess appears at about 40 days for both the RVs and FWHM_{CCF} periodograms in the 6500–6800 and 6800–7200 sub-samples.

In Figure 9, we further inspect RVs against FWHM_{CCF} for two time intervals and it is hard to exclude possible resemblances, in particular if we allow for a shift in phase. However, no other activity indicator shows evidences of stellar activity at about 40 days (Fig. 7) and today we have had no example of FWHM_{CCF} variation without Ca II H&K or $H\alpha$ variation); additionally, the FWHM_{CCF} periodograms for the 6500–6800 and 6800–7200 sub-samples show most of the power centered on periods 80–250. We therefore search for other possible origins of the power excess seen at about 40 days in the FWHM_{CCF} periodogram.

We show in Figure 10 the time-series for the FWHM_{CCF} sub-sample satisfying BJD-2450000 \in [6800–7200]. It is evident that this activity tracer is higher at about BJD-2450000=7050. In the same figure, we note that our sampling generates a peak at ~60 days in the window function. This translates in that the power excess at about 40 days is an alias of the strongest peak located at about 100 days ($1/37.5 = 1/100 + 1/60$); when subtracting a 100 days periodicity, no more power excess is present at about 40 days. However, this peak at ~100 days and its ~40 days alias remains unexplained because the others activity indicators show power excess concentrated at ~150 days – for the R'_{HK} and $H\alpha$ – and 665 days – for the photometry (Fig 7) while a stel-

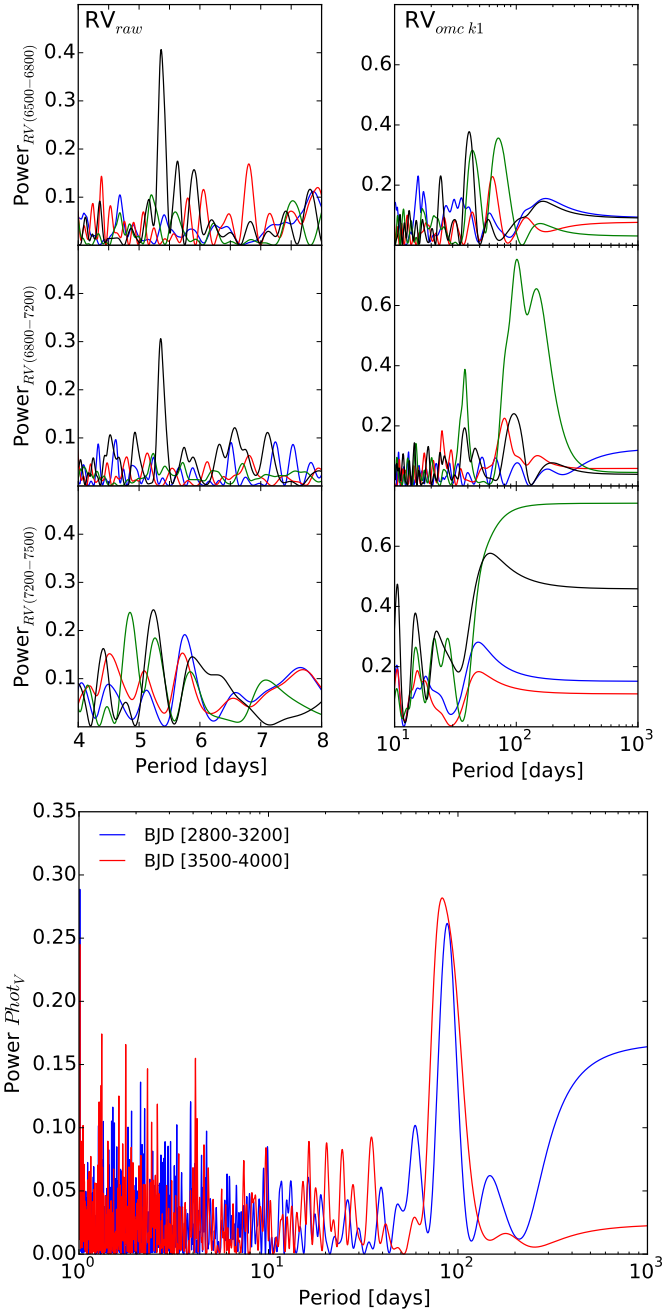


Fig. 8. *Top:* GJ 3323 periodograms of RVs (black curve), R'_{HK} (blue curve), $H\alpha$ (red curve), and $FWHM_{CCF}$ (green curve) for subsets satisfying BJD-2450000: 6500-6800, 6800-7200, and 7200-7500. Left column corresponds to raw RVs and the right column to the residues of subtract the Keplerian adjusted to the 5.4-days signal. We note the temporal stability of the shorter RV periodicity and that the one at 40 days also shows power excess in the $FWHM_{CCF}$ (first and second rows of right column). *Bottom:* Periodogram for the V-band ASAS photometry with BJD between 2800-3200 and 3500-4000. Significant power excess arises at about 90 days.

lar rotation period is expected to be at about 33 days (Table 1). All together and before more data could be acquired, we think GJ 3323c should be considered a planet candidate.

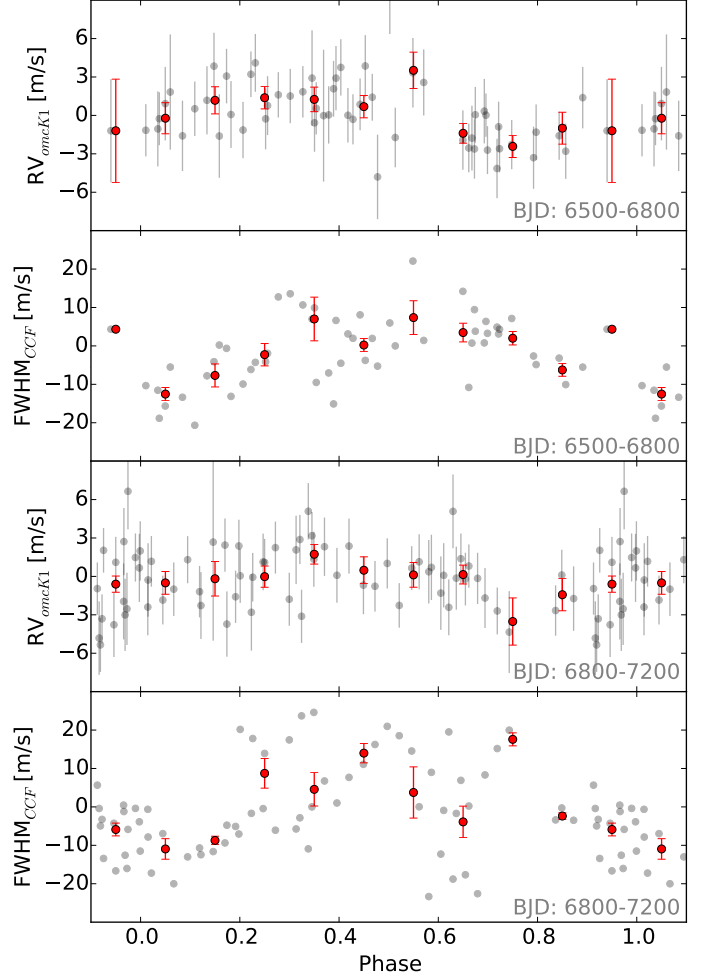


Fig. 9. GJ 3323 RV_{omck1} and $FWHM_{CCF}$ (the median value is subtracted) against the phase for the two different epochs where the variables show power excess at about 40 days in their periodograms (Fig. 8). Red points depict binned data to guide the eye, where a possible dependence arises for the BJD interval 6500-6800.

4.3.3. Keplerian analysis

We use YORBIT to fit a model with 2 Keplerians and converge on orbits with semi-amplitudes of 2.55 ± 0.32 and 1.49 ± 0.32 m/s. We estimated a stellar mass of $0.164 M_{\odot}$ (Table 1). This converts the semi-amplitudes to 2.02 ± 0.25 and $2.31 \pm 0.50 M_{\oplus}$ planets and makes GJ 3323 one of the lowest-mass star ($0.16 M_{\odot}$) known with planets discovered by radial velocity. GJ 3323b and GJ 3323(c) receive 2.51 and 0.17 times the Earth irradiance and have an equilibrium temperature in the range of 420-595K and 214-303K, respectively, if one assumes bond albedos between 0 and 0.75. Details of the derived parameters are given in Table 4 and Fig. 11 shows the phase folded RVs.

4.4. GJ 273

4.4.1. Periodicity analysis

We intensively monitored GJ 273, recording 280 spectra between December 2nd, 2003 and September 30th, 2016. From this 12.8 years RV monitoring, 43 of them were acquired after the HARPS fibers upgrade. The RVs have standard deviation

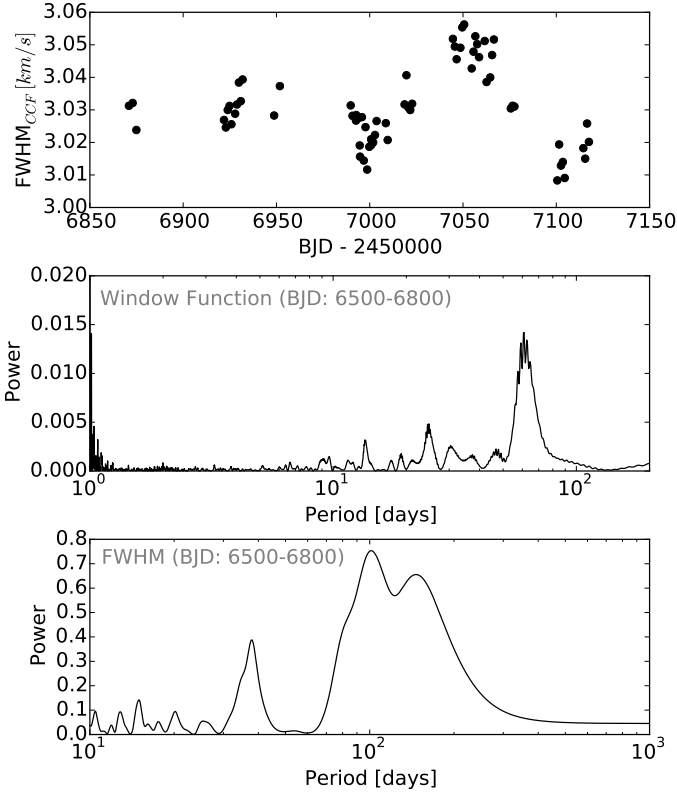


Fig. 10. When focusing on data with BJD between 6800 and 7200, we note that the FWHM_{CCF} increases at about BJD 7050, while at BJD 7000 and 7100 it is closer to the average value (upper panel) and produces the peak at ~ 100 days in its periodogram. The window function – with power excess at ~ 60 days (middle panel) – for this sub-sample shows that our sampling well explain that the 40 days peak is an alias of the stronger 100 days peak (bottom panel).

of $\sigma_{(O-C)} = 2.75 \text{ ms}^{-1}$, that are well above the estimated uncertainties of $\sigma_i = 0.94 \text{ ms}^{-1}$.

Figure 12 shows the periodograms, first, for the raw time series, and next, for the residuals of each iteration. Most of the power in the raw RV periodogram is concentrated at low frequencies with $\text{FAP} \ll 0.01$, and YORBIT converges to a solution with a periodicity of ~ 420 days. The periodogram of the residues shows a powerful peak largely above our 1%FAP threshold at about 20 days, modeled by a second Keplerian. After subtraction of this model, the two highest peaks in the periodogram of the residues are located at about 700 days and 5 days (both with $\text{FAP} \ll 0.01$). When adding a third Keplerian to the model, the favored solution contains the two previous periodicities plus the one at 700 days. Now the 5 day peak and its 1-day alias dominates the periodogram of the residues. Although the residues still have powers excess at about 100 days (0.5%FAP), our final model consists of four Keplerian because this periodicity is well explained by a signal generated by the stellar rotation (99 days; Table 2). As we will described below, we suspect that both the two longest periodicities (with $P \sim 420$ and ~ 700 days) also have a stellar origin.

4.4.2. Challenging the planet interpretation

GJ 273 b, c

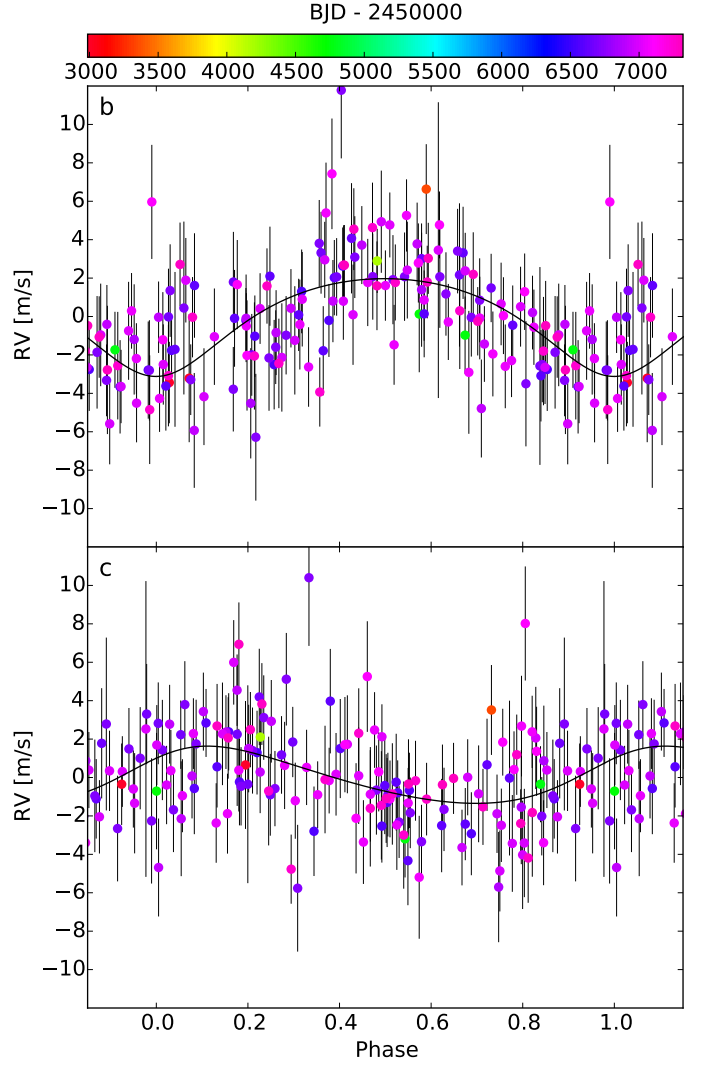


Fig. 11. Phase folded – 5.36 (top) and 40.5 days (bottom) – GJ 3323 RVs. Solid black curve and rainbow color-code represent the Keplerian solution and the BJD, respectively.

The two RV signals with the shortest periodicities (4.7 and 18.6 days) have periods that are well different than that estimated for the stellar rotation ($P_{\text{Rot}} \sim 99$ days, Table 1), well different than that measured for the two long-period RV signals (that we suspect to be caused by stellar activity), and well different than the harmonics of those periodicities ($\sim P/2$, $\sim P/3$, ...). They thus already appear as robust planet detections.

Yet, we want to check whether the signals are coherent across different epochs. We divide in four our RV time series, with sub-samples satisfying BJD-2450000 within the ranges 6200–6600, 6600–6800, 6800–7200, and 7200–7500. We compute the periodograms for each sub-sample. As we see in Figure 14, power excess is seen in almost all epochs.

As for GJ 3138, we need to understand whether the signal would be detected at each epoch. We proceed by making a 100 synthetic RV time-series with the same sampling as our observation, normally distributed ($\sigma = 2 \text{ m/s}$) and centered on the best Keplerian fit. The periodogram for each of the 100 time-series is computed, from which we derive the ± 1 power distribution. Because the periodogram of the original sub-samples fall inside the ± 1 region (gray zone in Fig 16), we conclude that there is no evidence that either the 5- or the 18-day signal are transitory.

Table 4. Parameters for the Keplerians fitted to GJ 3323 RVs.

		GJ 3323b	GJ 3323(c)
N_{Meas}		154	
σ_{ext}	[m/s]	0.31/0.88	
$\sigma_{(O-C)}$	[m/s]	2.10/2.19	
ΔV_{21}	[m/s]	$-2.82^{+0.63}_{-0.62}$	
BJD_{ref}	[days]	56800.0918533883	
γ	[km/s]	42.4508 ± 0.0002	
<hr/>			
P	[d]	$5.3636^{+0.0007}_{-0.0007}$	$40.54^{+0.21}_{-0.19}$
K_1	[$m s^{-1}$]	$2.55^{+0.33}_{-0.32}$	$1.49^{+0.33}_{-0.31}$
e		$0.23^{+0.11}_{-0.11}$	$0.17^{+0.12}_{-0.12}$
λ_0 at BJD_{ref}	[deg]	$180.4^{+7.1}_{-7.0}$	$305.3^{+13.0}_{-13.0}$
$m \sin(i)$	[M_{\oplus}]	$2.02^{+0.26}_{-0.25}$	$2.31^{+0.50}_{-0.49}$
a	[AU]	$0.03282^{+0.00054}_{-0.00056}$	$0.1264^{+0.0021}_{-0.0022}$
S/S_{\oplus}		2.58	0.17
Transit prob.	[%]	2.1	0.5
$T_{\text{Trans}} - 54000.0$	[days]	$2803.797^{+0.213}_{-0.218}$	$2816.39^{+2.54}_{-2.72}$

Overall, we accept both the 5- and 18-day signal as bona fide planet detections. Figure 16) shows the phase folded RVs.

Magnetic cycle and rotation

From Figure 12 we note that the raw RV periodogram exhibits power excess for periodicities from 300-4000 days, with peaks at 400-500 and 2000 days. Similarly, the periodograms of activity indicators show significant power excess in the same range of periodicities (Fig. 13). Time series for radial velocities and activity indicators are shown in Figure 15. The correlation and p-value are 0.18 and 0.002 respectively. However, the maximum RV corrections from this correlation are of few cm/s and too low for a noticeable improvement.

Another way to correct the RV-activity dependency is to proceed as in Dumusque et al. (2011). Analogously, they noticed that both RVs and Ca II H&K time series show remarkable resemblances. Dumusque et al. (2011) fit a Keplerian to the R'_{HK} and used the resulting parameters to fix a Keplerian model to RVs, but leaving the amplitude free. Proceeding this way we fix a model with $P \sim 2000$ days, then the periodogram of RV residues shows subsequently the signals from GJ 273 b and c. The periodogram from a third iteration exhibits a clear peak at ~ 100 days, the expected stellar rotation period (Table 1). Evidences of the stellar rotation appear in the periodograms of the R'_{HK} and the Na D-index measured between BJD 6200–6500 and 6500–6800, respectively.

The ~ 420 days peak in the RV periodogram could be explained as the 1 year alias of the longer period of ~ 2000 days seen in RVs and activity tracers (Figs. 12, 13, 15). The peak arising at ~ 700 days in the RV residues is close to the second harmonic ($P/3$) of the magnetic cycle. Because of that, we suspect this two RV signals ($P \sim 420, 700$ days) are the product of not well modeled stellar activity cycle.

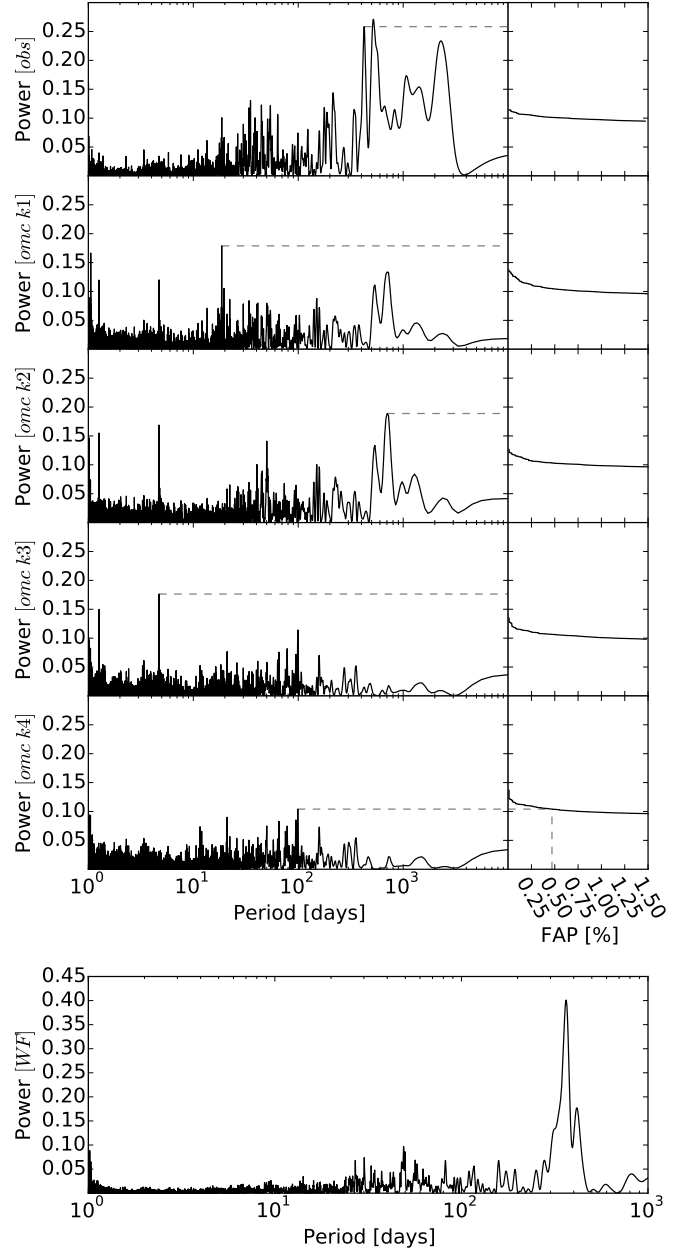


Fig. 12. Top: Periodograms for the radial velocities of GJ 273 and their residues after sequentially subtract the models accounting for the main periodicity. From top to bottom, up to four RV signals are seen with periodicities of 420, 20, 700, and 5 days. Bottom: The window function shows peaks located at one year and 49 days.

4.4.3. Keplerian analysis

GJ 273b is a super-Earth with a minimum mass of $2.89 \pm 0.26 M_{\oplus}$ with an orbital period of 18.650 ± 0.006 days. Orbiting at a distance of 0.09110 ± 0.00002 AU from its parent star, it is grazing the inner edge of the conservative habitable zone (Kopparapu et al. 2013), but with an incident flux of $1.06 S_{\oplus}$ it is well within the HZ if one assumes the planet is surrounded by an atmosphere and accounts for GCM (Kopparapu et al. 2016). It has an equilibrium temperature in the range 206-293 K (using albedos of 0.75 and 0, respectively). GJ 273c is among the less massive planets detected by radial velocities, with a minimum mass of $1.18 \pm 0.16 M_{\oplus}$. It complete one orbit in 4.7234 ± 0.0004 days.

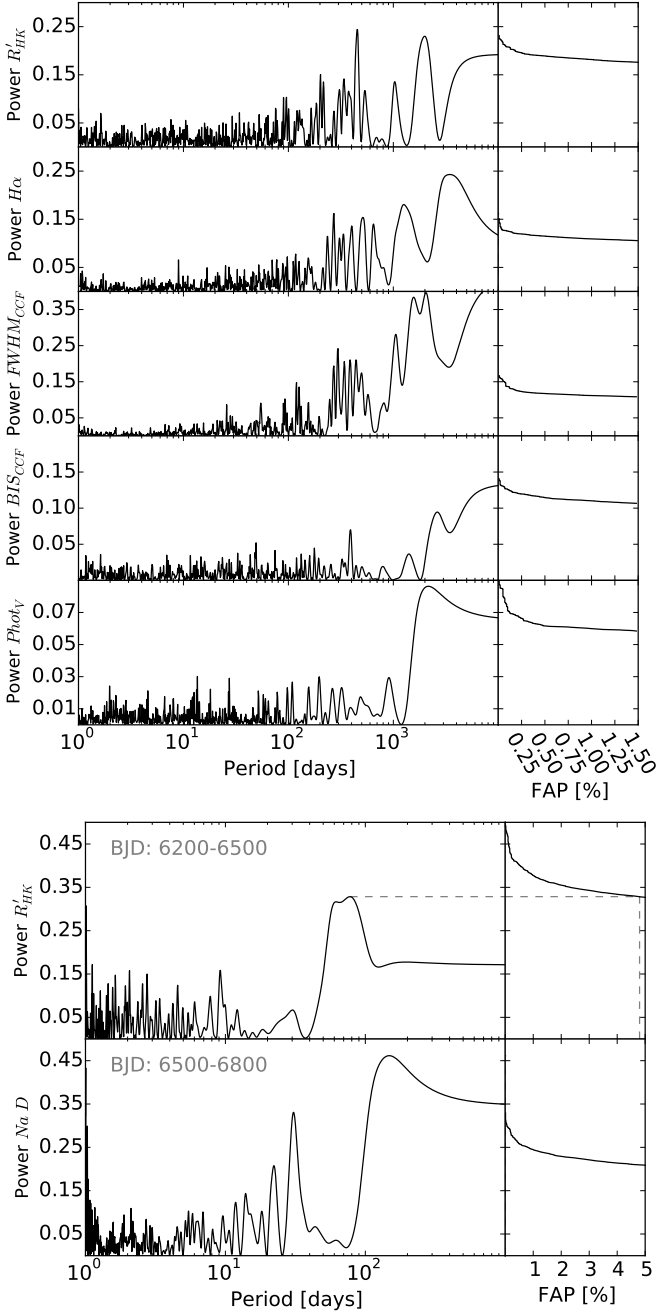


Fig. 13. *Top:* GJ 273 stellar activity indicators show a long-period modulation (~ 2000 days), and the periodogram of R'_{HK} has a prominent peak located at about 400 days. *Bottom:* Periodograms for seasonal R'_{HK} and Na D showing clues of the stellar rotation (estimated at about 100 days).

At the orbital distance of 0.036467 AU it receives almost $\times 7$ the stellar flux received at Earth and has an equilibrium temperature within 327–462 K, and thus much too close to the star to be considered in the circumstellar habitable zone.

4.5. GJ 628

Between June 2nd, 2004 and September 28rd, 2015 we collected 190 spectra of GJ 628. From these, 148 are publicly available and were previously analyzed by Wright et al. (2016). Three measures have the difference between GJ 628 systemic and the

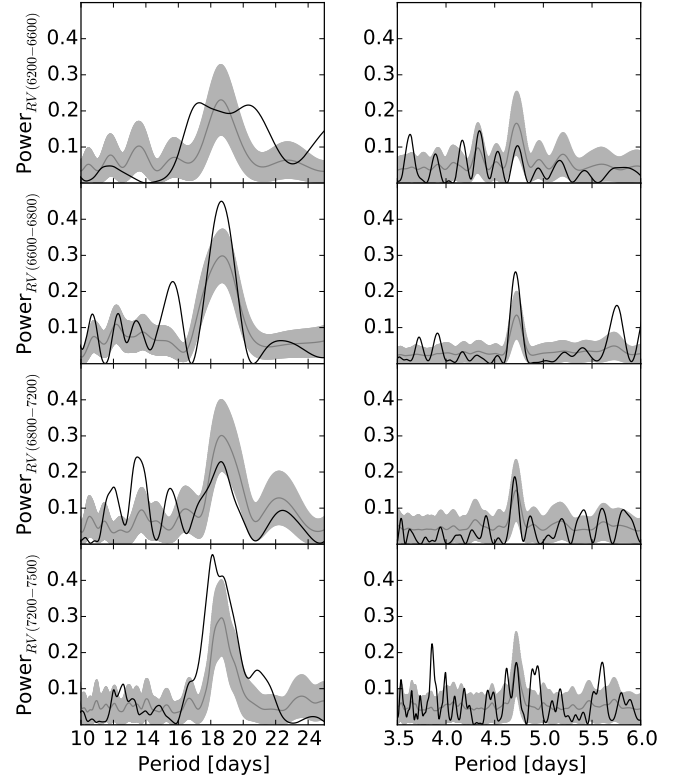


Fig. 14. Analysis for the stability of the two shorter RV signals of GJ 273. Black curves are the periodograms of the isolated RV signals with a periodicity of 18 days (left panel) and 4.7 days (right panel). The gray curves correspond to the average periodograms of the synthetic RVs and the 1σ zones are shown in light gray zones.

Moon RVs $< 1 \text{ km s}^{-1}$ and the angle between objects $< 25^\circ$. We considered these measures (BJD=2454661.6, 2454662.6, and 2454663.7) contaminated by Moon and are rejected for the subsequent analysis. As we will see below, we come to the same conclusions for the RV signals at shorter periodicity (4.9 and 17.9 days) but a different one for the periodicity at 67 days. Here we detect a third RV signal at a longer periodicity and identify a stellar activity cycle.

GJ 628 RVs have a dispersion of $\sigma_{(O-C)} = 2.72 \text{ ms}^{-1}$ and a mean internal error of $\sigma_i = 1.02 \text{ ms}^{-1}$. The dispersion excess comes from several periodic variations as is shown in Fig. 17. The periodogram of raw RVs exhibits two narrow spikes at 4.9 and 17.9 days, with FAP $< 10^{-2}\%$ and 0.46%, respectively, and a third one at about 205 days with a 0.29% FAP. After subtracting a two Keplerian model to the 4.9 and 17.9 days periods, the periodogram of resulting residues (third row in Fig 17) shows several peaks located at 217, 48, 454, 115 days, detected with FAPs $< 0.01\%$, 0.02%, 0.07%, and 0.17%, respectively. We added a third Keplerian to each period with power excess (one at time) and found that the solution including the 217 days signal results in significantly lower χ^2_v and BIC (see Table 8). We note that the 67 days RV signature discussed in Wright et al. is not significant here, as the weak peak located at this periodicity has a 2.5% FAP. After include the 217 days signal in our model the highest peak in the periodogram of RVs residues (P \sim 380 days) has a FAP of 6.3%, and therefore no more signatures are detected.

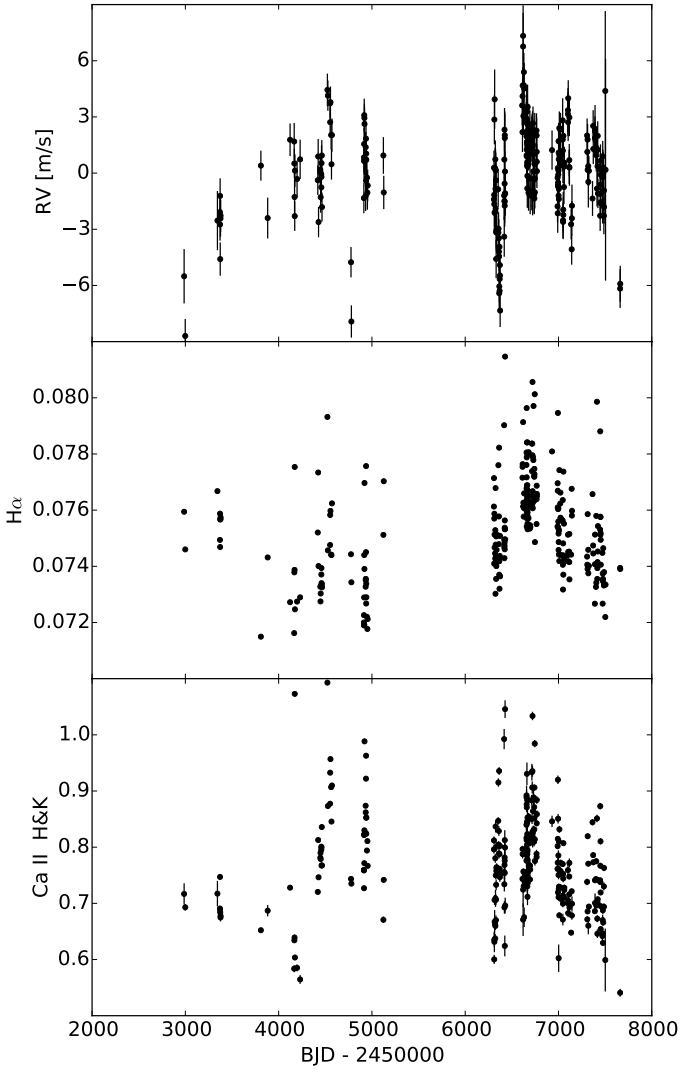


Fig. 15. GJ 273 radial velocities and activity indicator showing resemblances, suggesting that RVs are impacted by a stellar activity cycle.

Stellar activity and orbital solution

The Ca II H&K chromospheric emission reveals that GJ 628 presents an activity cycle (Fig. 18). We combine literature Ca II H&K measurements (Wright et al. 2004; Isaacson & Fischer 2010) to better understand the cycle identified with HARPS data alone. Although the data time span is increased by about 4 years, the combined data does not cover a complete activity cycle, which is at least of about 19 years. Figure 18 also shows one flare event detected in both R'_{HK} and $H\alpha$ (BJD=2456481.55). Concerning the $FWHM_{CCF}$, in addition to the expected offset due to the HARPS fiber upgrade, this activity index – computed through the DRS – presents other unexplained offsets of about 1 km/s (too large to be from stellar origin) and its analysis is omitted here.

The stellar rotation period of GJ 628 is estimated to be 93 days (Table 1) and the $H\alpha$ periodogram (Fig. 18) presents significant power excess at 64 days, however we can not assert that this periodicity is linked to a yearly alias of the stellar rotation. We do not identify any periodicity linked to the stellar rotation neither from the seasonal $H\alpha$ nor from the seasonal R'_{HK} mea-

Table 5. Parameters for the Keplerian fitted to GJ 273 RVs.

		GJ 273b	GJ 273c
N_{Meas}		280	
σ_{ext}	[m/s]	0.76/0.44	
$\sigma_{(O-C)}$	[m/s]	1.59/1.36	
ΔV_{21}	[m/s]	$-1.98^{+0.40}_{-0.38}$	
BJD_{ref}	[days]	56238.2123938802	
γ	[km/s]	18.4086 ± 0.0002	
		GJ 273b	GJ 273c
P	[d]	$18.6498^{+0.0059}_{-0.0052}$	$4.7234^{+0.0004}_{-0.0004}$
K_1	[$m s^{-1}$]	$1.61^{+0.15}_{-0.15}$	$1.06^{+0.15}_{-0.15}$
e		$0.10^{+0.09}_{-0.07}$	$0.17^{+0.13}_{-0.12}$
λ_0 at BJD_{ref}	[deg]	$229.6^{+5.3}_{-5.5}$	$75.60^{+8.1}_{-8.4}$
$m \sin(i)$	[M_{\oplus}]	$2.89^{+0.27}_{-0.26}$	$1.18^{+0.16}_{-0.16}$
a	[AU]	$0.091101^{+0.000019}_{-0.000017}$	$0.036467^{+0.000002}_{-0.000002}$
S/S_{\oplus}		1.06	6.66
Transit prob.	[%]	1.6	4.3
$T_{\text{Trans}}-54000.0$	[days]	$2249.295^{+0.489}_{-0.573}$	$2238.58^{+0.26}_{-0.19}$

surements. The peak at about 64 days in the $H\alpha$ periodogram and the 67 days RV signal reported in Wright et al. (2016) are worryingly close. The HARPS only R'_{HK} periodogram presents power excess at 120 days that can be explained as the yearly alias of the stellar rotation period. Considering the possible aliases, and unlike Wright et al. (2016), we do not regard the 67 days signal as a planet detection. The ASAS photometry, which consists in 600 points spread over 8.7 years, shows hints of the stellar rotation. The periodogram for the photometry satisfying BJD between 2452650 and 2452950 shows a strong peak at about 100 days, and the entire data set shows two peaks at near this periodicity: one peak with 0.95% FAP at 129 days and another with a FAP slightly greater at about 86 days.

Additionally, the third strongest peak of the window function data-set is located at the 66-days periodicity (bottom panel in Fig. 17), hence, we can not discard that the 67-days signal seen in RVs in Wright et al. and $H\alpha$ are generated by the data temporal sampling itself. From the same figure we note the strong peak located at one year, translating that one year aliases are highly expected.

Stellar differential rotation could be inferred from the APT photometry (spanning 6 years) presented in Kane et al. (2016) plus the ASAS photometry. Minimum and maximum periods from the photometry are $P_{\text{min}} = 84.2 \pm 3.0$ and $P_{\text{min}} = 106.3 \pm 7.3$. Well determined periodicities from the APT photometry shows no evidences of $P_{\text{Rot.}} \geq 120$ days, and we interpret the 120 days and 129 days peaks in Figures 18 and 19, respectively, as aliases of the true stellar rotation period.

4.5.1. Keplerian analysis

When adjusting a Keplerian to the 48 days periodicity (second highest peak in the $RV_{\text{ome } k2}$ periodogram) the resulting orbit eccentricity is relatively high ($e \sim 0.7$). Then, the periodogram of the residues shows the 217 days peak with high significance. Regarding the stability of the orbits, a solution including this periodicity is uncomfortable because it crosses the orbits with 17.9 and 217 days periodicities – if assuming coplanar orbits.

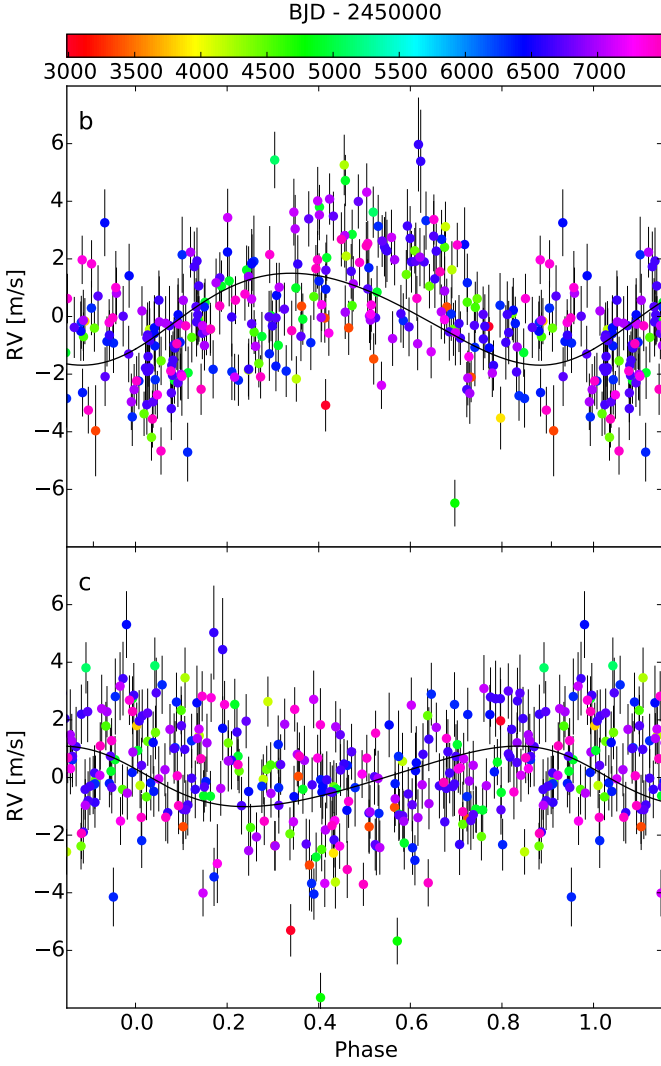


Fig. 16. GJ 273 radial velocities phase folded to 18.7 (top) and 4.7 days (bottom). Black curve and rainbow colors represent the Keplerian solution and BJD of observations, respectively.

The more conservative solution and that preferred by both minimum χ^2 or BIC consists in three Keplerian adjusting the 4.9, 17.9 and 217 days periodicities. The orbital parameters for such a solution are tabulated in Table 6 and Fig. 20 depicts the phase folded RVs with the model. GJ 628c falls outside the conservative HZ (Kopparapu et al. 2013), however, if considering the GCM in synchronous rotating planets (Kopparapu et al. 2016), the incident radiation translates in that planet lies within the circumstellar HZ of its parent star.

4.6. GJ 3293

Astudillo-Defru et al. (2015) reported the detection of two Neptune-like companions orbiting GJ 3293 with periodicities 30.6 and 124 days, and a possible super-Earth orbiting with 48.1 days periodicity. To shed light on the nature of the 48.1 days signal we gathered 61 new RVs from 13th October, 2014 to 4th April, 2015. In this work we measure a RV dispersion of $\sigma_{(O-C)} = 7.73 \text{ m s}^{-1}$ and a mean internal error of $\sigma_i = 2.33 \text{ m s}^{-1}$.

Astudillo-Defru et al. $H\alpha$ analysis suggested that the stellar rotation of GJ 3293 period is 41 days, and from RVs

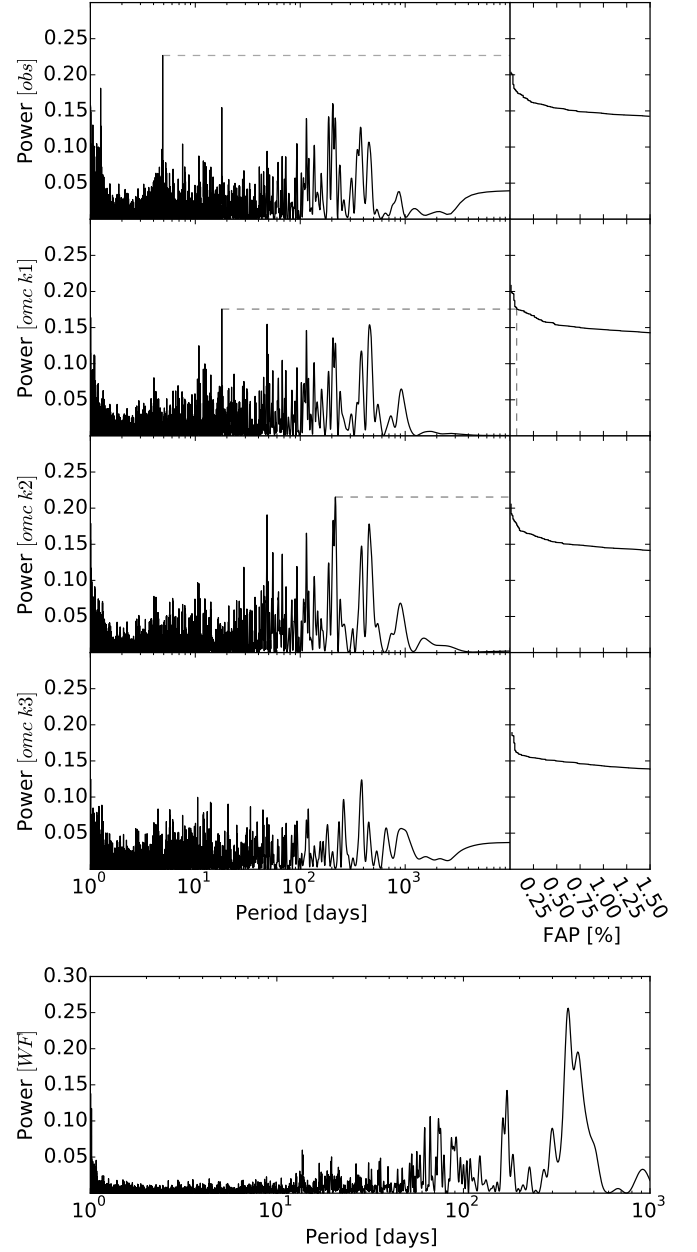


Fig. 17. Top panel: GJ 628 periodograms of RVs. First row shows the periodogram of raw RVs and the rest of rows depicts the periodograms of RV residues after subtracting the Keplerian adjusted to the periodicity marked with horizontal shaded line. Bottom panel: The window function showing peaks at one year, half-year, 66 days, 73 days, and 62 days.

they argued about an uncertain nature of the 48.1 days signal. This is because 48.1 days is close to the stellar rotation and because the lack of such a signal in the 2010-2011 data set. By using several chromospheric activity indicators ($H\beta$, $H\gamma$, $Na D$, R'_{HK} , $FWHM_{CCF}$), and improving the $H\alpha$ detection, we confirm the 41.0 day value for the stellar rotation. The ASAS photometry (599 points spanning 8.7 yr) does not show periodic variability compatible with stellar rotation. However, the Moon synodic period is evident in the photometry periodogram. The synodic periodicity appears with 2.3%FAP for the photometry acquired between BJD 1500 and 2020. Neither a 41.0 days signal, nor its yearly aliases at 36.9 and 46.2 days ap-

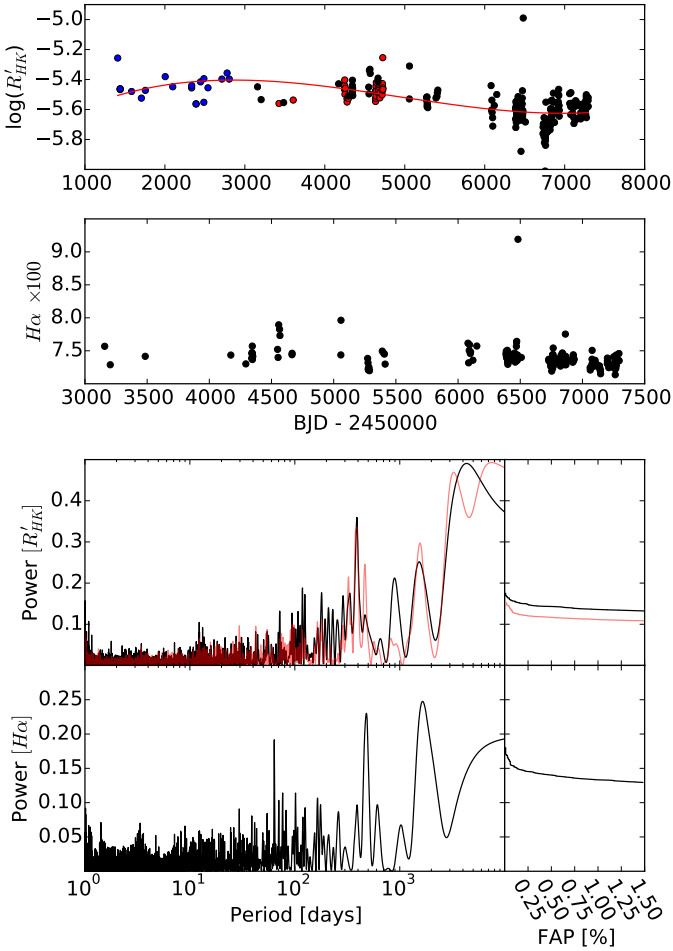


Fig. 18. *Top panel:* GJ 628 measures of the $\log(R'_{HK})$ and the $H\alpha$ activity indices against BJD, where the presence of an activity cycle becomes evident: the red curve in top row helps to guide eyes. Black points represent our HARPS measurements, while blue and red points depict measurements from Wright et al. (2004) and Isaacson & Fischer (2010), respectively, acquired with HRES. A flare event occurs at BJD 2456481.6. *Bottom panel* depicts the R'_{HK} and $H\alpha$ periodograms. The R'_{HK} periodogram for HARPS+HRES data (red curve) shows the activity cycle of ≥ 7000 days and a peak at about 400 days compatible with its yearly alias. Periodogram of the only HARPS R'_{HK} – black curve – shows power excess at about 120 days while the one for $H\alpha$ shows a clear peak at 64 days.

pears affecting the 48.1 days RV signature in the periodogram. Today, the 41-day period of the stellar rotation and the 48.1-day period seen in RVs seem distinct enough to interpret the 48.1-day signal as due to a planetary companion. Moreover, after subtraction of both the 30.6 and 124 days signals and after analyzing the RV residues ($RV_{omc\ k2}$), we found that the 48.1 days periodicity is temporally stable when splitting the sample in a more optimal way (target seasonal visibility instead of calendar year). The four RV subsets used for the present analysis satisfies BJD between 4790 and 5750, 5750 and 6100, 6100 and 6350, 6900 and 7150. Figure 21 shows such a stability of the 48.1 days signal and the periodograms of a set of activity indicators. This planet is within the habitable zone of its parent star, with an equilibrium temperature between 171 K and 241 K.

When modeling the 30.6, 48.1, and 124 days RV periodicities by three Keplerian, a fourth signal appears in the residues.

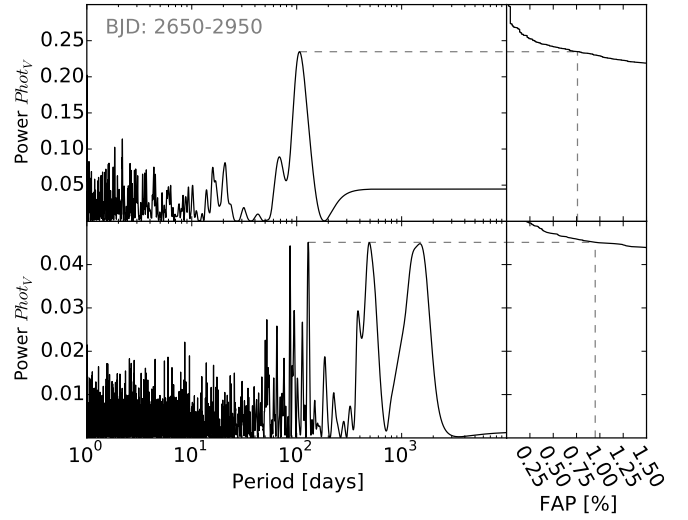


Fig. 19. Periodogram of the photometry for GJ 628. First row shows the periodogram using data for BJD between 2452650 and 2452950, where we see a clear peak associated to the stellar rotation. The periodogram using the whole date-set is shown in the second row.

Table 6. Parameters for the three Keplerian fitted to GJ 628 RVs.

N_{Meas}		187		
σ_{ext}	[m/s]	0.86/ 2.01		
$\sigma_{(O-C)}$	[m/s]	1.71/ 2.34		
ΔV_{21}	[m/s]	$0.5093^{+0.5348}_{-0.5267}$		
BJD_{ref}	[days]	56309.9363933752		
γ	[km/s]	$-21.03738^{+0.00015}_{-0.00015}$		
		GJ 628b	GJ 628c	GJ 628d
P	[d]	$4.8869^{+0.0005}_{-0.0005}$	$17.8719^{+0.0059}_{-0.0059}$	$217.21^{+0.55}_{-0.52}$
K_1	[$m s^{-1}$]	$1.67^{+0.20}_{-0.19}$	$1.92^{+0.19}_{-0.19}$	$2.23^{+0.31}_{-0.29}$
e		$0.15^{+0.13}_{-0.10}$	$0.11^{+0.10}_{-0.07}$	$0.55^{+0.08}_{-0.09}$
λ_0 at BJD_{ref}	[deg]	$333.6^{+7.0}_{-6.9}$	$141.5^{+5.9}_{-5.9}$	$129.0^{+7.7}_{-7.8}$
$m \sin(i)$	[M_{\oplus}]	$1.91^{+0.26}_{-0.25}$	$3.41^{+0.43}_{-0.41}$	$7.70^{+1.12}_{-1.06}$
a	[AU]	$0.0375^{+0.0012}_{-0.0013}$	$0.0890^{+0.0029}_{-0.0031}$	$0.470^{+0.015}_{-0.017}$
S/S_{\oplus}		7.34	1.30	0.06
Transit prob.	[%]	3.3	1.4	0.2
$T_{\text{Trans}}-54000$	[days]	$2311.498^{+0.191}_{-0.204}$	$2325.333^{+0.584}_{-0.597}$	$2501.7^{+16.6}_{-16.6}$

The periodogram (Fig. 22) shows power excess at a periodicity of 13.3 days. Such a peak was also present in Astudillo-Defru et al. (2015, see their Fig.4) but without enough significance (1σ). Here the corresponding peak is clearly visible despite its weakness, and the FAP decreases to 3.4% (2σ). Furthermore, a model consisting of four Keplerian is significantly favored over the three Keplerian model (see the BIC difference in Table 8). Accordingly, our solution for GJ 3293 consists in two super-Earths (P=13.3, 48.1 days) and two Neptune-mass planets (P=30.6, 122.6 days) with minimum masses of $3.3 M_{\oplus}$, $7.6 M_{\oplus}$ and $23.5 M_{\oplus}$, $21.1 M_{\oplus}$. At their separation from GJ 3293, the Neptune-mass planet b and the super-Earth planet b are within the circumstellar habitable zone. Figure 23 shows

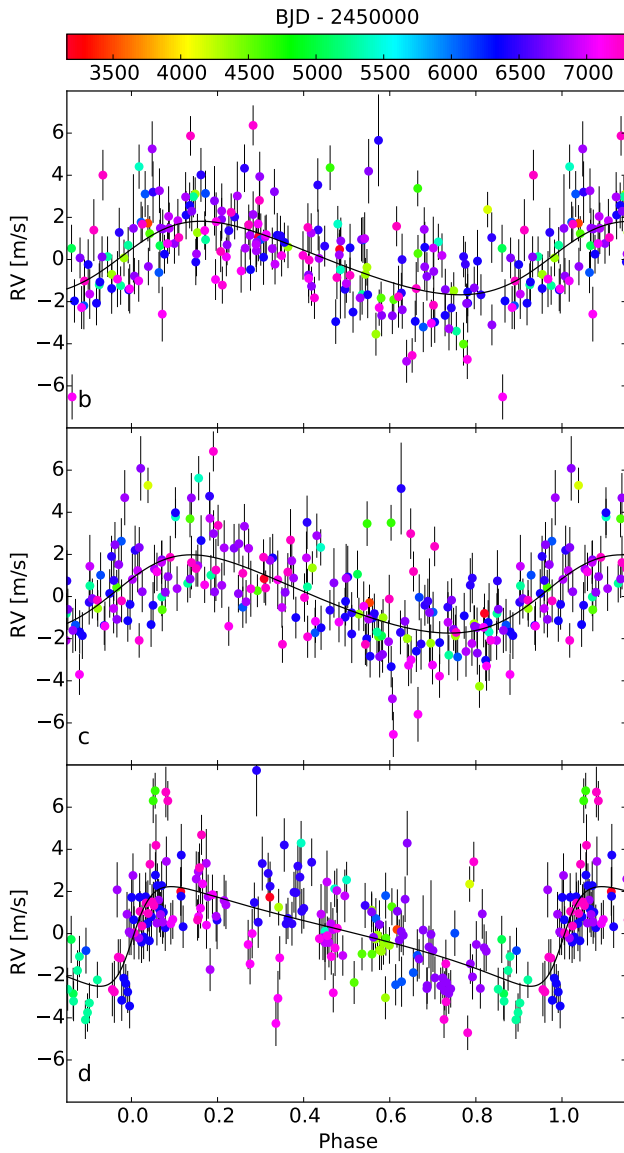


Fig. 20. Radial velocities of GJ 628 folded to 4.89 (top row), 17.87 (middle row), and 217.2 days (bottom row). Our solution consisting of three Keplerian is showed as the black solid curve while the BJD is represented by color.

the phase folded RVs with the four Keplerian and Table 7 gives the orbital parameters.

In comparison to Astudillo-Defru et al. (2015), where a model with three Keplerian was used, GJ 3293 RVs are modeled here with four Keplerian. This may involve changes in some of the orbital parameters. The only significant (2σ) change comes from the eccentricity of the orbit with a 122.7 days periodicity, where we found $e=0.11\pm 0.09$ instead of the 0.37 ± 0.06 reported in Astudillo-Defru et al.. The other orbital parameters remain unchanged.

We performed an additional test to our GJ 3293 solution by running a N-body integrator. We ran *GENGA* (Grimm & Stadel 2014) through the Data and Analysis Center for Exoplanets (DACE³). The initial conditions in Table 7 are used and our simulation lasts for 10^6 yr. Figure 24 shows the stability of the sys-

³ <https://dace.unige.ch/>

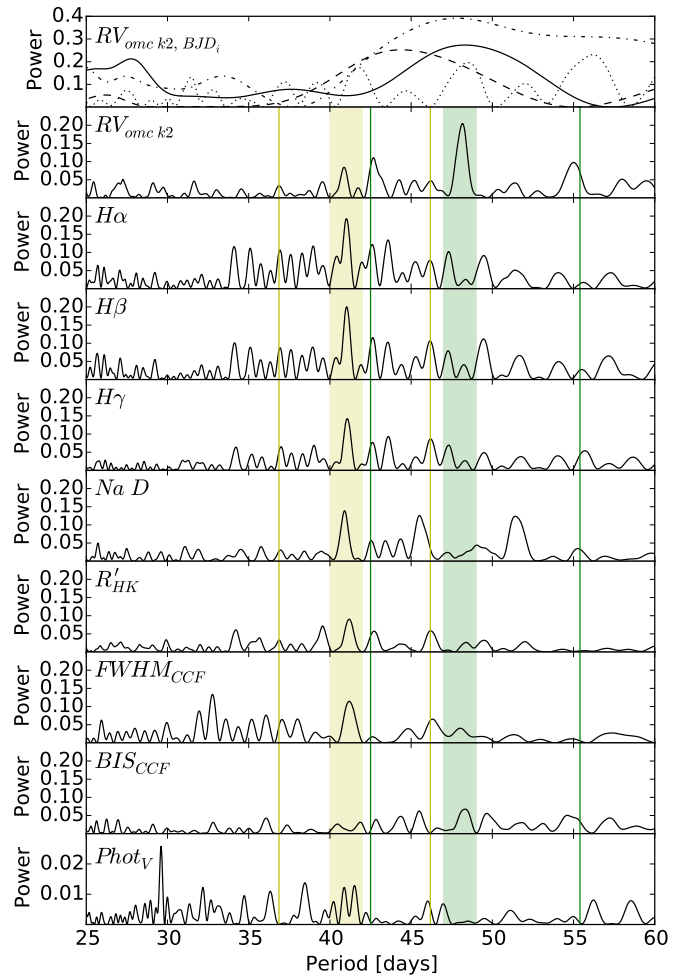


Fig. 21. From top to bottom: First row shows the periodogram of $RV_{omc\ k2}$ for different RVs subset where BJD is within 4790-5750 (dotted), 5750-6100 (solid), 6100-6350 (dash-dotted), and 6900-7150 (dashed). There is power excess about 48 days for all the subsets. Second row depicts the $RV_{omc\ k2}$ periodogram for the entire sample. Third to ninth rows display the periodograms of different stellar activity indicators. The green and yellow shaded area represent the planetary and stellar signals, respectively. The same color code is used for the thin vertical lines depicting the yearly aliases. Periodicity of both signals are clearly separated.

tem over this time span as well as the secular variation of the eccentricity.

5. Summary and conclusions

We have analyzed between 150 and 280 RVs of GJ 3138, GJ 3323, GJ 273, GJ 628, and GJ 3293. To fully exploit the Doppler information contained in M dwarf spectra, the RVs extraction from HARPS data was done by maximizing the likelihood. For each star, a high signal-to-noise reference spectrum was built out of all observed spectra. The RV analysis includes a careful monitoring of several spectroscopic activity indicators and photometry, from where we measure stellar rotation periods for three stars, except for GJ 3323. For GJ 628 Ca II H&K chromospheric emission reveals a long term variation compatible to a Sun-like magnetic cycle.

Conditioned to a knowledge on the orbital inclination, our analysis results in the detection of 12 planets (9 new), includ-

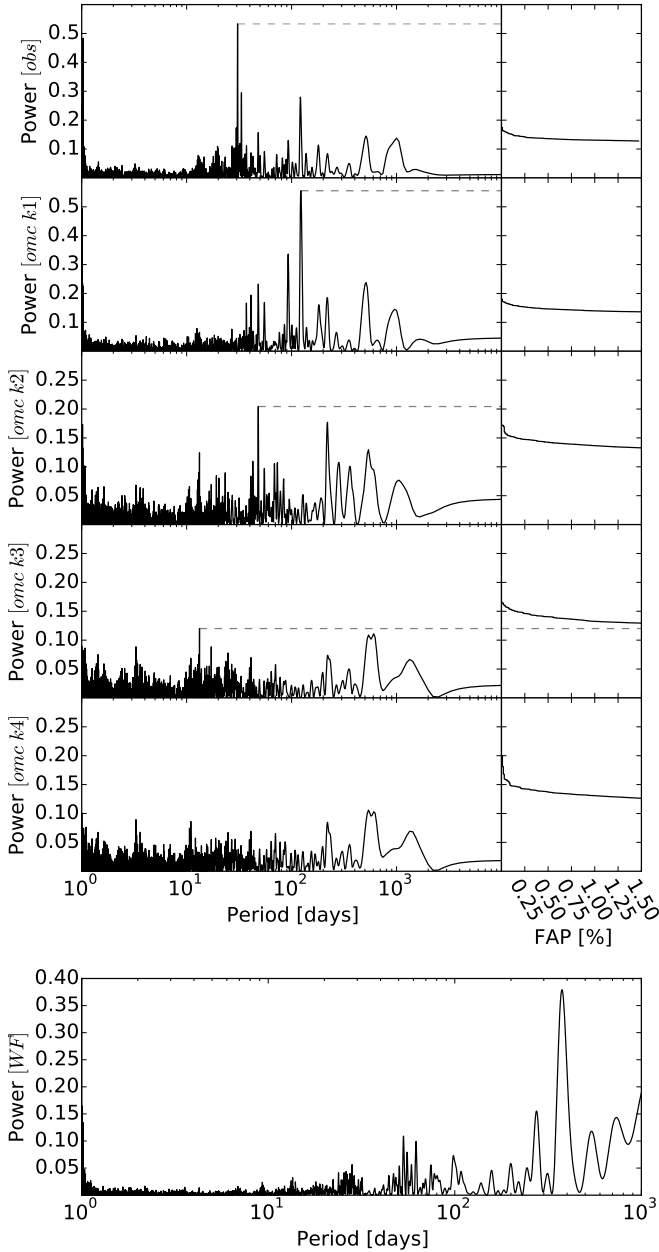


Fig. 22. *Top:* Periodograms of GJ 3293 of RVs showing the successive signals. Since Astudillo-Defru et al. (2015, see their Fig.4), the $RV_{omc\ k3}$ periodogram shows a rising of the 13.3 days by adding new RV measurements. *Bottom:* The window function exhibits peaks at one year, 275 days, 53 days, and 62 days.

ing Earth-mass planets and super-Earths. GJ 3138 radial velocities reveal four signals: three of them are compatible with planets having minimum masses of 1.8, 4.2, and 10.5 Earth-masses, orbiting with periods of 1.22, 5.97, and 258 days, respectively, while a signal with 48 days periodicity is more related to stellar activity as it shows dependence with $H\alpha$. We recall that the $RV-H\alpha$ dependence was subtracted and that more RVs of this star are needed because the phase for the 258 days signal is not fully covered. These orbits are located outside the habitable zone of GJ 3138.

We interpret the RV variations of the fully convective star GJ 3323 as the signal coming from two low-mass planets. These have minimum masses of 2.0 and 2.3 Earth-masses M_{\oplus} and are

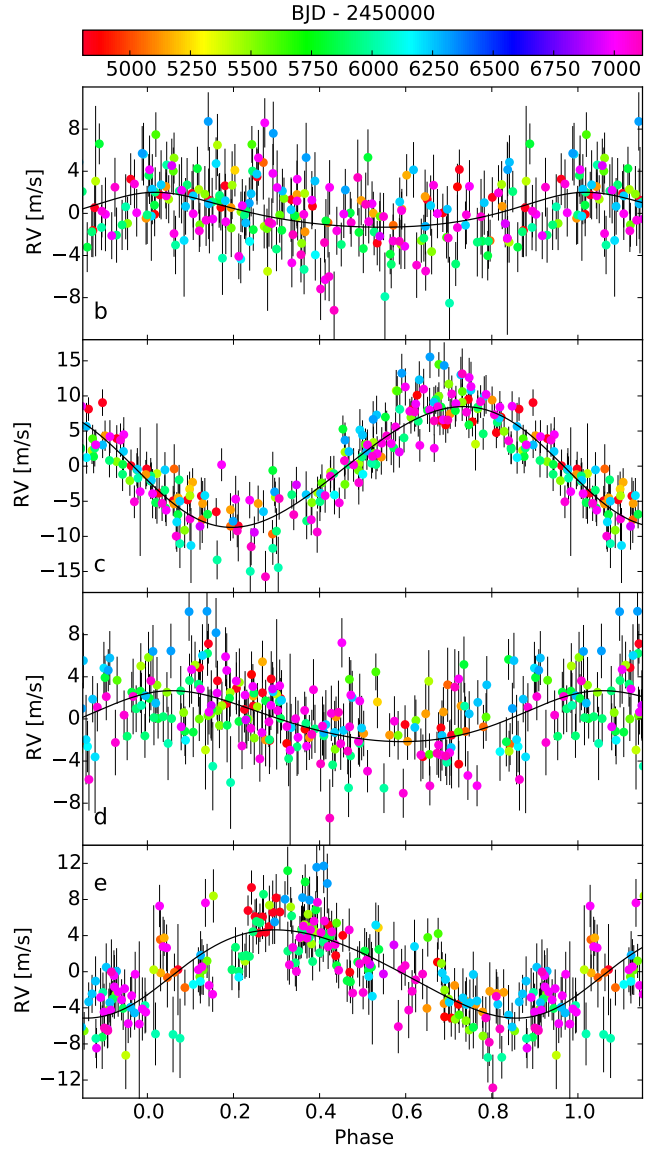


Fig. 23. From top to bottom: Radial velocities of GJ 3293 folded to 13.3 (first row), 30.6 (second row), 48.1 (third row), and 122.6 days (fourth row). The Keplerian solution is represented by the solid black curve and the BJD of observations by the rainbow color-code.

orbiting with periodicities of 5.36 and 40.5 days, respectively. The planets are orbiting outside the conservative boundaries of the HZ. GJ 3323b and GJ 3323c receive 2.5 and 0.17 times stellar flux compared to the Sun, respectively.

The M dwarf GJ 273 is orbited by both a super-Earth and an Earth-mass planets. They have minimum masses of 2.89 and 1.18 M_{\oplus} and orbital periods of 18.65 and 4.72 days, respectively. GJ 273b receives 1.06 times as much radiation as our Earth does from our Sun. It thus lies well within the habitable zone (Kopparapu et al. 2016) and water (if any) may flow on its surface. Located at only 3.8 parsec, GJ 273 is also the closest known planetary system with a planet in the HZ after Proxima Centauri (Anglada-Escudé et al. 2016). Compared to the flaring star Proxima Centauri, we highlight the quietness of GJ 273. This makes GJ 273b even more attractive because its lower atmospheric erosion, which translates into a more favorable environment for habitability.

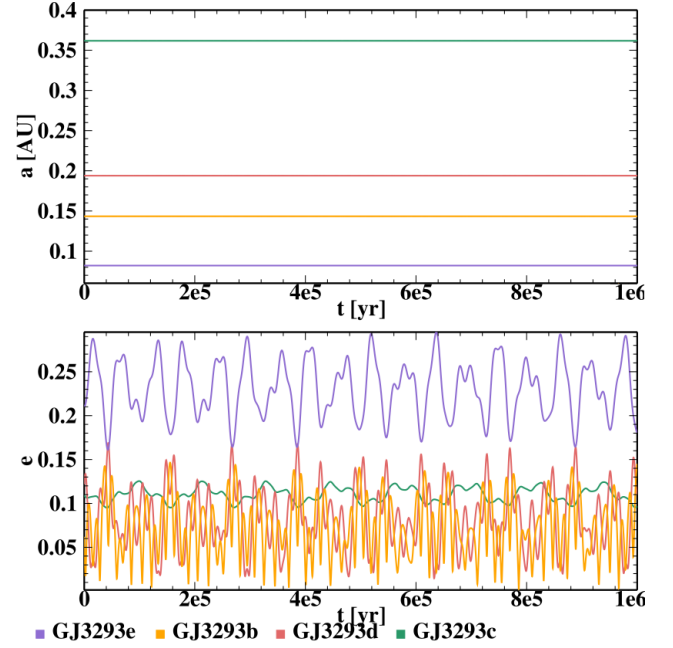
Table 7. Parameters for the four Keplerian fitted to GJ 3293 RVs.

		GJ 3293e	GJ 3293b
N_{Meas}		207	
σ_{ext}	[m/s]	1.02	
$\sigma_{(O-C)}$	[m/s]	2.78	
BJD_{ref}	[days]	56023.1731538393	
γ	[km/s]	13.29558 \pm 0.00023	
		GJ 3293d	GJ 3293c
P	[d]	13.2543 $^{+0.0078}_{-0.0104}$	30.5987 $^{+0.0083}_{-0.0084}$
K_1	[$m s^{-1}$]	1.658 $^{+0.328}_{-0.321}$	8.603 $^{+0.320}_{-0.323}$
e		0.21 $^{+0.20}_{-0.14}$	0.06 $^{+0.04}_{-0.04}$
λ_0 at BJD_{ref}	[deg]	349.5 $^{+11.9}_{-12.5}$	102.7 $^{+2.0}_{-2.0}$
$m \sin(i)$	[M_{\oplus}]	3.28 $^{+0.64}_{-0.64}$	23.54 $^{+0.88}_{-0.89}$
a	[AU]	0.08208 $^{+0.00003}_{-0.00004}$	0.14339 $^{+0.00003}_{-0.00003}$
S/S_{\oplus}		3.34	1.07
Transit prob.	[%]	2.3	1.3
$T_{\text{Trans-54000}}$	[days]	2026.847 $^{+0.538}_{-0.664}$	2052.320 $^{+0.384}_{-0.436}$
		GJ 3293d	GJ 3293c
P	[d]	48.1345 $^{+0.0628}_{-0.0661}$	122.6196 $^{+0.2429}_{-0.2371}$
K_1	[$m s^{-1}$]	2.420 $^{+0.338}_{-0.334}$	4.891 $^{+0.300}_{-0.295}$
e		0.12 $^{+0.13}_{-0.09}$	0.11 $^{+0.10}_{-0.08}$
λ_0 at BJD_{ref}	[deg]	333.7 $^{+7.5}_{-7.6}$	242.0 $^{+4.0}_{-4.1}$
$m \sin(i)$	[M_{\oplus}]	7.60 $^{+1.05}_{-1.05}$	21.09 $^{+1.24}_{-1.26}$
a	[AU]	0.19394 $^{+0.00017}_{-0.00018}$	0.36175 $^{+0.00048}_{-0.00047}$
S/S_{\oplus}		0.59	0.17
Transit prob.	[%]	1.0	0.5
$T_{\text{Trans-54000}}$	[days]	2038.471 $^{+1.883}_{-1.827}$	2090.855 $^{+3.682}_{-4.681}$

We found GJ 628 is orbited by at least 3 planets. We found a Sun-like magnetic cycle and clues that the stellar rotation is about 128 days. From this, it follows that the 67 days RV signal is more likely produced by stellar activity, not by a planetary companion as reported by Wright et al.. Here we found that a model including three Keplerian with $P=4.89, 17.87, 217.2$ days is favored. This solution corresponds to planets with $m \sin(i)=1.9, 3.4, 7.7 M_{\oplus}$. For GJ 628c we derive a mean orbital distance slightly larger than Wright et al. (using our uncertainty we differ 1.67σ – their uncertainty for a is disturbingly low). At this distance and compared to the Sun-Earth system, GJ 628c receives 1.29 the flux received at Earth.

New radial velocities of GJ 3293 allow us to confirm the detection of the planet previously suggested in Astudillo-Defru et al. (2015). Additionally, we report the detection of an extra RV signal. The planet we confirm has a minimum mass of $7.6 M_{\oplus}$ and orbital period of 48.1 days, it is therefore inside the habitable zone of GJ 3293. The additional planet is a super-Earth with $m \sin(i)=3.3 M_{\oplus}$ and an orbit with $P=13.25$ days. The previously detected planets are at $P=30.6, 122.6$ days with $m \sin(i)=23.5, 21.1 M_{\oplus}$; here we report a slightly lower eccentricity for the farthest one.

Acknowledgements. This publication makes use of data products from the Two Micron All Sky Survey, which is a joint project of the University of Massachusetts and the Infrared Processing and Analysis Center/California Institute of Technology, funded by the National Aeronautics and Space Administration and the National Science Foundation. X. B., X. D., and T. F. acknowledge the support of the French Agence Nationale de la Recherche (ANR),


Fig. 24. Results from the *GENGA* simulation showing the stability of the GJ 3293 system over 10^6 years.

under the program ANR-12-BS05-0012 Exo-atmos and of PNP (Programme nationale de planétologie). This work has been partially supported by the Labex OSUG@2020. X.B. acknowledges funding from the European Research Council under the ERC Grant Agreement n. 337591-ExTra.

NCS acknowledges the support by Fundação para a Ciência e a Tecnologia (FCT) (project ref. PTDC/FIS-AST/1526/2014) through national funds and by FEDER through COMPETE2020 (ref. POCI-01-0145-FEDER-016886), as well as through grant UID/FIS/04434/2013 (POCI-01-0145-FEDER-007672). NCS was also supported by FCT through the Investigador FCT contract reference IF/00169/2012 and POPH/FSE (EC) by FEDER funding through the program "Programa Operacional de Factores de Competitividade - COMPETE".

We are very thankful to Jean-Baptiste Delisle for his precious comments about dynamics of planetary systems. We appreciate the anonymous referee for her/his comments that improves the manuscript.

This research made use of the databases at the Centre de Données astronomiques de Strasbourg (<http://cds.u-strasbg.fr>), NASA's Astrophysics Data System Service (http://adsabs.harvard.edu/abstract_service.html) and the <http://arXiv.org> paper repositories. This work made use of SCIPY (Jones et al. 2001–), IPYTHON (Perez & Granger 2007), and MATPLOTLIB (Hunter 2007).

References

- Almenara, J. M., Astudillo-Defru, N., Bonfils, X., et al. 2015, *A&A*, 581, L7
 Anglada-Escudé, G., Amado, P. J., Barnes, J., et al. 2016, *Nature*, 536, 437
 Anglada-Escudé, G. & Butler, R. P. 2012, *ApJS*, 200, 15
 Astudillo-Defru, N., Bonfils, X., Delfosse, X., et al. 2015, *A&A*, 575, A119
 Astudillo-Defru, N., Delfosse, X., Bonfils, X., et al. 2016, *ArXiv e-prints*
 Baranne, A., Mayor, M., & Poncet, J. L. 1979, *Vistas in Astronomy*, 23, 279
 Berta-Thompson, Z. K., Irwin, J., Charbonneau, D., et al. 2015, *Nature*, 527, 204
 Boisse, I., Bouchy, F., Hébrard, G., et al. 2011, *A&A*, 528, A4
 Bonfils, X., Delfosse, X., Udry, S., et al. 2013, *A&A*, 549, A109
 Bonfils, X., Gillon, M., Udry, S., et al. 2012, *A&A*, 546, A27
 Bouchy, F., Pepe, F., & Queloz, D. 2001, *A&A*, 374, 733
 Boyajian, T. S., von Braun, K., van Belle, G., et al. 2012, *ApJ*, 757, 112
 Butler, R. P., Vogt, S. S., Marcy, G. W., et al. 2004, *ApJ*, 617, 580
 Charbonneau, D., Berta, Z. K., Irwin, J., et al. 2009, *Nature*, 462, 891
 Chelli, A. 2000, *A&A*, 358, L59
 Crossfield, I. J. M., Petigura, E., Schlieder, J. E., et al. 2015, *ApJ*, 804, 10
 Cutri, R. M., Skrutskie, M. F., van Dyk, S., et al. 2003, *VizieR Online Data Catalog*, 2246, 0
 Delfosse, X., Forveille, T., Ségransan, D., et al. 2000, *A&A*, 364, 217
 Dumusque, X., Lovis, C., Ségransan, D., et al. 2011, *A&A*, 535, A55
 Fischer, D. A., Anglada-Escudé, G., Arriagada, P., et al. 2016, *PASP*, 128, 066001

Table 8. Statistical factors for the models where we gradually (according to the peak strength in the periodogram) add a Keplerian to the simplest constant model.

Model	Added period [days]	FAP [%]	BIC	$\sigma_{(O-C)}$ [$m s^{-1}$]	χ^2_ν
GJ 3138					
Const.	–	–	459.93	2.87	2.39
K1	5.97	$<10^{-2}$	379.26	2.45	1.79
K2	1.22	0.29	349.08	2.24	1.54
K3	258	0.17	326.52	2.04	1.31
K4	20.4	0.9	322.17	1.90	1.17
GJ 3323					
Const.	–	–	293.04	2.85	1.66
K1	5.4	$<10^{-2}$	196.02	2.27	1.09
K2	40	$<10^{-2}$	184.62	2.00	0.87
GJ 273					
Const.	–	–	2388.48	2.75	8.52
K1	424	$<10^{-2}$	1552.96	2.21	5.54
K2	18.6	$<10^{-2}$	1292.05	1.99	4.57
K3	700	$<10^{-2}$	952.43	1.67	3.26
K4	4.7	$<10^{-2}$	817.24	1.50	2.69
GJ 628					
Const.	–	–	1346.63	2.72	7.00
K1	4.9	$<10^{-2}$	1034.37	2.39	5.54
K2	17.9	0.07	854.03	2.13	4.52
K3	217	$<10^{-2}$	599.18	1.71	3.00
K3	48	0.02	691.44	1.86	3.54
K3	454	0.07	645.82	1.78	3.28
K3	115	0.17	710.05	1.88	3.65
GJ 3293					
Const.	–	–	2193.79	7.73	10.62
K1	30.6	$<10^{-2}$	1025.97	5.21	4.95
K2	122.7	$<10^{-2}$	456.62	3.3	2.03
K3	48.1	$<10^{-2}$	380.80	2.84	1.55
K4	13.3	3.4	361.43	2.61	1.34

Gaidos, E., Mann, A. W., Lépine, S., et al. 2014, *MNRAS*, 443, 2561
Galland, F., Lagrange, A.-M., Udry, S., et al. 2005, *A&A*, 443, 337
Giampapa, M. S., Schneeberger, T. J., Linsky, J. L., & Worden, S. P. 1978, *ApJ*, 226, 144
Gillon, M., Demory, B.-O., Barman, T., et al. 2007, *A&A*, 471, L51
Gomes da Silva, J., Santos, N. C., Bonfils, X., et al. 2011, *A&A*, 534, A30
Grimm, S. L. & Stadel, J. G. 2014, *ApJ*, 796, 23
Hawley, S. L., Gizis, J. E., & Reid, I. N. 1996, *AJ*, 112, 2799
Henry, T. J., Jao, W.-C., Subasavage, J. P., et al. 2006, *AJ*, 132, 2360
Hosey, A. D., Henry, T. J., Jao, W.-C., et al. 2015, *AJ*, 150, 6
Howarth, I. D., Siebert, K. W., Hussain, G. A. J., & Prinja, R. K. 1997, *MNRAS*, 284, 265
Hunter, J. D. 2007, *Computing in Science Engineering*, 9, 90
Isaacson, H. & Fischer, D. 2010, *ApJ*, 725, 875
Johnson, D. R. H. & Soderblom, D. R. 1987, *AJ*, 93, 864
Jones, E., Oliphant, T., Peterson, P., et al. 2001–, *SciPy: Open source scientific tools for Python*, [Online; accessed 2016-06-16]
Kane, S. R., von Braun, K., Henry, G. W., et al. 2016, *ArXiv e-prints*
Kass, R. E. & Raftery, A. E. 1995, *Journal of the American Statistical Association*, 90, 773
Kiraga, M. 2012, *Acta Astron.*, 62, 67
Kopparapu, R. K., Ramirez, R., Kasting, J. F., et al. 2013, *ApJ*, 765, 131
Kopparapu, R. K., Ramirez, R. M., SchottelKotte, J., et al. 2014, *ApJ*, 787, L29
Kopparapu, R. k., Wolf, E. T., Haqq-Misra, J., et al. 2016, *ApJ*, 819, 84
Kordopatis, G., Gilmore, G., Steinmetz, M., et al. 2013, *AJ*, 146, 134

Leggett, S. K. 1992, *ApJS*, 82, 351
Leggett, S. K., Allard, F., Geballe, T. R., Hauschildt, P. H., & Schweitzer, A. 2001, *ApJ*, 548, 908
Linsky, J. L., Bornmann, P. L., Carpenter, K. G., et al. 1982, *ApJ*, 260, 670
Lo Curto, G., Pepe, F., Avila, G., et al. 2015, *The Messenger*, 162, 9
Lovis, C. & Pepe, F. 2007, *A&A*, 468, 1115
Mayor, M., Pepe, F., Queloz, D., et al. 2003, *The Messenger*, 114, 20
Nakajima, T. & Morino, J.-I. 2012, *AJ*, 143, 2
Neves, V., Bonfils, X., Santos, N. C., et al. 2013, *A&A*, 551, A36
Nidever, D. L., Marcy, G. W., Butler, R. P., Fischer, D. A., & Vogt, S. S. 2002, *ApJS*, 141, 503
Pepe, F., Mayor, M., Galland, F., et al. 2002, *A&A*, 388, 632
Perez, F. & Granger, B. E. 2007, *Computing in Science Engineering*, 9, 21
Perruchot, S., Bouchy, F., Chazelas, B., et al. 2011, in *Proc. SPIE*, Vol. 8151, Techniques and Instrumentation for Detection of Exoplanets V, 815115
Pojmanski, G. 1997, *Acta Astron.*, 47, 467
Queloz, D., Henry, G. W., Sivan, J. P., et al. 2001, *A&A*, 379, 279
Rodriguez, D. R., Duchêne, G., Tom, H., et al. 2015, *MNRAS*, 449, 3160
Schwarz, G. 1978, *Ann. Statist.*, 6, 461
Ségransan, D., Mayor, M., Udry, S., et al. 2011, *A&A*, 535, A54
Snellen, I., de Kok, R., Birkby, J. L., et al. 2015, *A&A*, 576, A59
Suárez Mascareño, A., Rebolo, R., González Hernández, J. I., & Esposito, M. 2015, *MNRAS*, 452, 2745
van Leeuwen, F. 2007, *A&A*, 474, 653
Vaughan, A. H., Preston, G. W., & Wilson, O. C. 1978, *PASP*, 90, 267
Ward-Duong, K., Patience, J., De Rosa, R. J., et al. 2015, *MNRAS*, 449, 2618
Wildi, F., Pepe, F., Chazelas, B., Lo Curto, G., & Lovis, C. 2010, in *Proc. SPIE*, Vol. 7735, Ground-based and Airborne Instrumentation for Astronomy III, 77354X
Wilson, O. C. 1968, *ApJ*, 153, 221
Wright, D. J., Wittenmyer, R. A., Tinney, C. G., Bentley, J. S., & Zhao, J. 2016, *ApJ*, 817, L20
Wright, J. T., Marcy, G. W., Butler, R. P., & Vogt, S. S. 2004, *ApJS*, 152, 261
Zacharias, N., Finch, C. T., Girard, T. M., et al. 2012, *VizieR Online Data Catalog*, 1322
Zechmeister, M. & Kürster, M. 2009, *A&A*, 496, 577
Zechmeister, M., Kürster, M., & Endl, M. 2009, *A&A*, 505, 859
Zucker, S. & Mazeh, T. 2006, *MNRAS*, 371, 1513

Appendix A: RVs

We list here the radial velocities in the barycentric frame – without subtracting the secular acceleration – and activity indicators. RV uncertainties accounts for an instrumental error of $0.60 m s^{-1}$ (added quadratically). A maximum likelihood approach is used to compute RVs, using a high signal-to-noise stellar template.

Table 1. Radial velocities – not corrected for activity (Eq. 2) – time series for GJ 3138.

BJD - 2400000	RV [km s^{-1}]	σ_{RV} [km s^{-1}]	FWHM [km s^{-1}]	Contrast	BIS [km s^{-1}]	S-index	$H\alpha$
54396.706036	13.59614	0.00134	3.35441	13.46537	-16.61000	0.94071	0.05333
54397.781533	13.59639	0.00135	3.35775	13.56172	-9.54700	0.94202	0.05302
54398.695400	13.59508	0.00176	3.35078	13.53711	-17.41900	0.96591	0.05326
54399.583478	13.59125	0.00160	3.35057	13.43478	-6.81600	0.84540	0.05318
54400.615060	13.59404	0.00178	3.34159	13.45599	-12.88400	0.90862	0.05344
54400.819836	13.59635	0.00210	3.35177	13.31886	-14.07400	0.95901	0.05329
54402.681054	13.59657	0.00146	3.35578	13.70179	-8.18600	0.87283	0.05305
54403.675525	13.59650	0.00123	3.35096	13.66022	-9.63700	0.90260	0.05309
55463.837566	13.59838	0.00172	3.35700	13.25050	-17.06400	1.04321	0.05465
55465.874088	13.59653	0.00234	3.34506	13.16562	-7.80700	0.91799	0.05445
55577.552114	13.60058	0.00134	3.34789	13.35279	-13.86800	0.97692	0.05313
55579.581782	13.60073	0.00155	3.34387	13.25734	-14.98500	0.89117	0.05306
55580.587109	13.60173	0.00184	3.33436	13.18216	-10.28500	0.91336	0.05308
55583.526836	13.59976	0.00144	3.35161	13.28745	-10.43500	0.94103	0.05363
55585.537572	13.60033	0.00168	3.34494	13.40263	-12.01500	0.98060	0.05281
55586.527265	13.59596	0.00164	3.34740	13.19095	-13.19900	1.03679	0.05251
55587.524342	13.60089	0.00284	3.34129	13.13059	-2.92000	1.09265	0.05264
55889.636369	13.59785	0.00172	3.33717	13.40663	-19.49400	0.91264	0.05448
56237.611076	13.60069	0.00203	3.34103	13.11140	1.70900	1.06400	0.05479
56255.585618	13.59593	0.00163	3.34440	13.26795	-17.90400	0.90603	0.05445
56285.584393	13.59913	0.00160	3.35720	13.15232	-14.79600	0.88034	0.05396
56304.623043	13.59674	0.00175	3.33418	13.23627	-4.19700	0.86622	0.05383
56509.904138	13.59978	0.00208	3.36974	13.17619	-1.30200	0.95357	0.05428
56510.902530	13.60185	0.00191	3.36890	13.33130	-11.70200	0.98885	0.05440
56514.903036	13.59438	0.00213	3.37009	13.25634	-17.38700	0.90003	0.05508
56515.864675	13.59545	0.00157	3.35629	13.34831	-11.04300	0.97035	0.05473
56516.932027	13.60164	0.00246	3.35920	13.23328	-8.69200	0.88516	0.05456
56518.904008	13.59608	0.00197	3.36052	13.33960	-16.62600	0.90217	0.05505
56519.878411	13.59264	0.00145	3.35914	13.39045	-7.39300	0.84260	0.05467
56520.844456	13.59543	0.00206	3.34764	13.40402	-5.72900	0.90343	0.05451
56521.880494	13.59497	0.00189	3.36013	13.37710	-5.69600	0.91711	0.05399
56523.872284	13.59993	0.00210	3.35285	13.48317	-8.62500	0.91189	0.05426
56524.833222	13.59475	0.00167	3.34643	13.40957	-11.75800	0.81014	0.05419
56525.833178	13.59567	0.00179	3.35012	13.37366	-5.80200	0.86719	0.05438
56530.894893	13.59721	0.00258	3.35678	13.31493	-6.55100	0.62715	0.05502
56531.776178	13.59203	0.00216	3.34475	13.25105	-10.61900	0.77320	0.05477
56532.746473	13.60133	0.00246	3.33048	13.25151	2.41100	0.59093	0.05431
56532.861608	13.60245	0.00239	3.35024	13.34839	-9.00600	0.69872	0.05474
56534.756799	13.60047	0.00240	3.34890	13.39694	-13.56200	0.83002	0.05451
56534.895882	13.60216	0.00156	3.36834	13.59934	-9.99800	0.82805	0.05478
56536.759053	13.59496	0.00192	3.35056	13.32355	-15.90900	0.83666	0.05457
56536.819705	13.59593	0.00450	3.36516	13.26975	-37.53300	0.73041	0.05465
56537.753615	13.59795	0.00222	3.34719	13.26488	-9.68600	0.73181	0.05474
56537.910627	13.59547	0.00190	3.34726	13.39337	-9.74700	0.79346	0.05462
56538.800136	13.59573	0.00230	3.34523	13.32618	-18.82500	0.71612	0.05468
56564.807535	13.60127	0.00176	3.36573	13.33620	-7.97700	0.96767	0.05388
56568.789558	13.60092	0.00221	3.34630	13.25064	-10.06900	0.80642	0.05369
56569.762689	13.60258	0.00193	3.35098	13.24308	-12.49200	0.75308	0.05392
56576.742456	13.59996	0.00164	3.35228	13.46891	-8.18200	0.86235	0.05378
56583.733688	13.60194	0.00153	3.36412	13.40071	-8.76100	0.86312	0.05434
56586.681427	13.60087	0.00180	3.35304	13.29600	-11.94000	0.88140	0.05461
56590.712809	13.59742	0.00218	3.35655	13.33438	-7.28300	0.87488	0.05462
56591.705931	13.59757	0.00242	3.36698	13.19955	-14.68800	0.68016	0.05457
56592.688300	13.60016	0.00169	3.35104	13.24054	-23.21400	0.85770	0.05468
56593.702924	13.60219	0.00169	3.35882	13.39924	-10.13900	0.97983	0.05510
56594.585928	13.60713	0.00232	3.35817	13.12117	-14.11600	0.87429	0.05450
56599.660938	13.60405	0.00231	3.36132	13.29721	-5.68900	0.79001	0.05444
56600.636339	13.60485	0.00225	3.36415	13.15658	-8.64600	0.88781	0.05417
56601.684283	13.60088	0.00152	3.37446	13.32202	-17.50800	0.98138	0.05438
56602.666683	13.59524	0.00183	3.36256	13.33914	-12.31800	0.91074	0.05482
56603.747517	13.59784	0.00165	3.34900	13.27602	-8.43200	1.02521	0.05465
56604.633309	13.60027	0.00174	3.35197	13.23647	-15.58300	0.94345	0.05394
56610.652082	13.59881	0.00230	3.36290	13.33974	-16.68400	0.95143	0.05349
56612.608512	13.60196	0.00204	3.35558	13.14563	-11.49600	0.81723	0.05319
56614.569439	13.60108	0.00190	3.34075	13.19132	-13.13100	0.83782	0.05333
56616.670354	13.60130	0.00163	3.34856	13.26269	-18.76900	0.88723	0.05331

Table 1. continued.

BJD - 2400000	RV [km s^{-1}]	σ_{RV} [km s^{-1}]	FWHM [km s^{-1}]	Contrast	BIS [km s^{-1}]	S-index	$H\alpha$
56619.596705	13.59426	0.00251	3.36542	13.35203	-25.06000	0.58304	0.05328
56622.642703	13.60049	0.00180	3.35582	13.44265	-13.47500	0.91147	0.05384
56623.670455	13.59846	0.00174	3.35424	13.30237	-13.50100	0.89734	0.05433
56624.669203	13.59789	0.00159	3.37057	13.43783	-8.43000	0.83262	0.05394
56625.727611	13.59582	0.00175	3.34020	13.23279	-13.87500	0.80004	0.05359
56626.671291	13.59758	0.00179	3.35228	13.32172	-18.83800	0.79012	0.05422
56627.680694	13.59732	0.00158	3.35017	13.36101	-20.40800	0.88258	0.05417
56628.661349	13.60277	0.00343	3.34891	13.16246	0.30700	0.72993	0.05372
56629.702623	13.60034	0.00211	3.35180	13.27514	-10.80800	0.81146	0.05438
56630.635744	13.60075	0.00239	3.36774	13.33310	-5.39000	0.85869	0.05421
56632.599453	13.59953	0.00181	3.35079	13.30917	-24.09100	0.94877	0.05394
56677.577795	13.60200	0.00206	3.35544	13.30769	-11.57500	0.96870	0.05322
56678.541285	13.59772	0.00197	3.35753	13.34667	-8.36600	1.05591	0.05347
56814.930748	13.60061	0.00298	3.35791	13.18471	-25.39900	0.72350	0.05538
56815.929855	13.59863	0.00252	3.34379	13.21359	-8.00600	0.77898	0.05477
56817.924473	13.59621	0.00260	3.34730	13.13517	4.32200	0.79434	0.05498
56824.943215	13.59538	0.00205	3.34246	13.15784	-21.71300	0.81050	0.05421
56826.953102	13.60491	0.00195	3.34567	12.89205	-20.22300	0.76136	0.05359
56827.945124	13.60032	0.00219	3.35574	13.09369	-14.01500	0.75502	0.05423
56828.953374	13.60680	0.00215	3.34510	12.94325	-10.50700	0.62083	0.05384
56838.931070	13.59950	0.00200	3.36076	13.10607	-19.10500	0.96543	0.05406
56839.924059	13.60332	0.00318	3.34831	13.00040	1.45100	0.63773	0.05436
56840.924120	13.59765	0.00276	3.36374	13.11286	-20.14200	0.85377	0.05434
56841.923070	13.59892	0.00256	3.34584	13.05790	-17.02300	0.78629	0.05416
56858.926050	13.59495	0.00168	3.34875	13.32961	-10.40200	0.79011	0.05457
56862.916777	13.60073	0.00197	3.34532	13.32598	-7.45100	0.77904	0.05479
56863.925602	13.59727	0.00220	3.34959	13.25051	-18.79000	0.68462	0.05498
56871.873011	13.59718	0.00211	3.35209	13.29239	-10.12700	0.79041	0.05421
56872.895827	13.60134	0.00241	3.36758	13.25786	-19.92400	0.74436	0.05461
56873.918585	13.59768	0.00369	3.34955	13.20321	2.20800	0.54650	0.05484
56874.914258	13.59749	0.00220	3.35747	13.29366	-2.30400	0.80458	0.05492
56920.855587	13.60022	0.00224	3.36390	13.23916	-11.66300	0.92315	0.05390
56921.822521	13.60122	0.00170	3.35931	13.29958	-18.82800	0.92555	0.05413
56922.831215	13.60485	0.00180	3.35492	13.32503	-15.54900	0.93628	0.05375
56923.889018	13.60045	0.00314	3.35785	13.12486	-16.37100	0.79852	0.05351
56924.816816	13.59378	0.00167	3.37286	13.41404	-13.54300	0.90286	0.05396
56925.783814	13.59760	0.00173	3.35673	13.33992	-8.63500	0.90032	0.05384
56926.782931	13.59751	0.00232	3.37004	13.32315	-14.07600	0.81767	0.05375
56927.759163	13.60114	0.00189	3.36259	13.22574	-6.61400	0.89326	0.05411
56928.743357	13.60152	0.00159	3.35201	13.22369	-10.70900	0.91943	0.05422
56929.713846	13.59828	0.00211	3.34470	13.13957	-8.53000	0.85622	0.05410
56931.803538	13.59921	0.00163	3.36410	13.26887	-16.62100	0.92559	0.05441
56932.801581	13.59845	0.00189	3.37338	13.21400	-10.49300	0.91977	0.05369
56948.858596	13.59238	0.00172	3.33358	13.23405	-15.49000	0.86050	0.05470
56951.689543	13.59649	0.00182	3.35502	13.35604	-8.37600	0.83554	0.05437
56989.581458	13.59690	0.00194	3.34790	13.34840	-10.61400	0.94289	0.05416
56990.648986	13.59585	0.00187	3.37350	13.41220	-11.07500	0.90680	0.05445
56992.571667	13.59697	0.00176	3.35805	13.28010	-11.79900	0.87009	0.05416
56992.699714	13.59697	0.00194	3.35498	13.18169	-19.21400	0.87696	0.05457
56993.603765	13.60024	0.00186	3.37146	13.35763	-12.37600	0.84628	0.05446
56994.577938	13.59871	0.00210	3.36050	13.38463	-12.02200	0.86180	0.05436
56996.746809	13.59795	0.00208	3.33857	13.08755	-18.77300	0.81647	0.05471
56997.630082	13.59573	0.00197	3.36212	13.30026	-17.89200	0.83561	0.05453
56997.743894	13.59632	0.00223	3.34635	13.13081	-15.16400	0.70666	0.05441
56998.612607	13.59749	0.00160	3.35813	13.39541	-3.20300	0.89622	0.05467
56998.727726	13.59763	0.00215	3.33984	13.15415	-10.34200	0.71759	0.05443
56999.590548	13.59904	0.00148	3.35834	13.39013	-10.43900	0.86654	0.05437
56999.691408	13.60006	0.00218	3.34688	13.19096	-13.43500	0.82198	0.05483
57000.624733	13.59798	0.00180	3.35532	13.26103	-21.57400	0.86571	0.05509
57002.600134	13.59399	0.00175	3.35963	13.30760	-14.83400	0.88429	0.05442
57002.725622	13.59403	0.00186	3.35006	13.20158	-13.93800	0.86299	0.05426
57003.592537	13.59658	0.00165	3.37124	13.41869	-11.20200	0.92886	0.05436
57003.741542	13.59792	0.00182	3.34774	13.08552	-25.21500	0.77343	0.05441
57008.593347	13.59829	0.00203	3.36301	13.38047	2.93000	0.85301	0.05403
57009.590606	13.59517	0.00171	3.37979	13.50938	-17.60300	0.93733	0.05387
57018.590364	13.60278	0.00171	3.37837	13.27469	-2.01900	1.00588	0.05335

Table 1. continued.

BJD - 2400000	RV [km s^{-1}]	σ_{RV} [km s^{-1}]	FWHM [km s^{-1}]	Contrast	BIS [km s^{-1}]	S-index	$H\alpha$
57019.578810	13.60469	0.00189	3.37391	13.18844	-3.66200	0.97577	0.05381
57020.582798	13.60028	0.00164	3.37259	13.29449	-12.53700	0.97766	0.05410
57021.591889	13.59090	0.00373	3.32291	12.78210	-11.03100	1.03731	0.05484
57022.614220	13.59623	0.00166	3.35418	13.21407	-12.69400	1.00566	0.05361
57044.550952	13.59706	0.00153	3.36711	13.28446	-15.80700	0.99978	0.05477
57045.549162	13.59507	0.00166	3.35588	13.23429	-7.13200	0.91933	0.05502
57046.554652	13.59548	0.00187	3.34107	13.15156	-2.81900	0.89711	0.05508
57047.569887	13.60157	0.00168	3.35764	13.23505	-8.67300	0.89177	0.05408
57048.548319	13.60142	0.00157	3.35951	13.28153	-8.77500	1.00030	0.05420
57049.529101	13.59764	0.00150	3.37323	13.35810	-13.89900	0.93609	0.05490
57050.546027	13.59415	0.00167	3.36208	13.22924	-14.20600	0.92692	0.05421
57051.545060	13.59532	0.00209	3.36858	13.25684	-0.12100	0.92287	0.05396
57052.551385	13.59477	0.00165	3.36786	13.36550	-8.02200	0.95279	0.05419
57053.548499	13.60393	0.00198	3.36492	13.33053	-6.70300	0.77403	0.05439
57054.538773	13.59766	0.00171	3.37347	13.32750	-10.44900	0.87384	0.05433
57055.538746	13.59712	0.00176	3.36113	13.25527	-11.96000	0.87020	0.05383
57056.540513	13.59660	0.00185	3.36280	13.24985	-10.88700	0.94694	0.05374
57057.534272	13.59622	0.00190	3.36615	13.24590	-10.45400	0.84554	0.05410
57058.545935	13.60277	0.00172	3.35166	13.22015	-11.76700	0.85241	0.05419
57061.537194	13.60135	0.00301	3.36111	13.12634	-14.76200	0.95794	0.05270
57062.534138	13.59869	0.00162	3.34155	13.11857	-15.24800	0.95880	0.05439
57064.539394	13.60048	0.00228	3.34619	13.03379	-2.65100	0.76377	0.05367
57065.532395	13.60120	0.00213	3.33874	13.12294	-14.90000	0.83799	0.05335
57066.529979	13.60299	0.00299	3.35416	13.04852	-13.60000	0.63750	0.05369
57248.913436	13.59953	0.00599	3.42099	13.28269	32.04900	0.34144	0.05396
57249.881901	13.59667	0.00183	3.39164	13.20601	-7.67400	0.80189	0.05425
57251.900642	13.59395	0.00335	3.40118	13.20227	-2.82900	0.57011	0.05441
57252.899165	13.59431	0.00171	3.39151	13.16291	0.50400	0.84095	0.05450
57253.923291	13.59465	0.00152	3.38929	13.21238	1.80100	0.86602	0.05417
57255.843118	13.59570	0.00236	3.42720	13.34035	0.40200	0.75318	0.05373
57256.808083	13.59577	0.00241	3.40688	13.25737	-10.34300	0.80660	0.05386
57257.843294	13.59706	0.00127	3.39323	13.20139	-0.31700	0.94394	0.05512
57258.811082	13.58263	0.00167	3.41246	13.33552	-7.59100	0.84434	0.05462
57260.838593	13.59636	0.00226	3.40873	13.34329	-3.93500	0.80614	0.05437
57263.826312	13.60248	0.00194	3.40278	13.37434	-8.95000	0.92533	0.05426
57264.840822	13.60245	0.00138	3.39402	13.25265	-3.28400	0.87470	0.05423
57265.829183	13.60303	0.00241	3.40305	13.40610	-9.67400	0.81586	0.05452
57269.835246	13.59949	0.00177	3.39712	13.28066	-2.78400	0.89602	0.05436
57270.897448	13.59730	0.00149	3.38652	13.15002	3.01700	0.89227	0.05444
57273.820018	13.59352	0.00182	3.40733	13.26877	1.71600	0.76721	0.05428
57274.829134	13.60102	0.00151	3.39878	13.20592	4.82800	0.86925	0.05451
57276.776977	13.60480	0.00265	3.39867	13.27314	8.64900	0.76571	0.05378
57277.807167	13.60106	0.00184	3.39619	13.31228	1.64500	0.87513	0.05396
57278.843490	13.59658	0.00177	3.39789	13.33575	-1.01400	0.78305	0.05399
57291.849971	13.60073	0.00165	3.38654	13.20899	-6.33700	0.87905	0.05437
57292.851251	13.59815	0.00154	3.39029	13.19300	6.23800	0.81225	0.05472
57293.702352	13.59587	0.00198	3.39639	13.25714	-0.93600	0.79322	0.05533
57293.849809	13.59829	0.00156	3.38711	13.05976	-3.96900	0.77868	0.05456
57306.677126	13.59781	0.00178	3.40989	13.42505	4.93200	0.87638	0.05419
57306.844106	13.59900	0.00173	3.39117	13.20205	1.45300	0.92928	0.05446
57307.674587	13.59869	0.00145	3.39457	13.34392	-3.35300	0.90137	0.05391
57307.836139	13.59266	0.00603	3.38783	13.16774	9.08000	99.00000	0.05344
57308.747244	13.59566	0.00228	3.40634	13.30861	-10.78500	0.96410	0.05496
57311.706421	13.60054	0.00182	3.40188	13.35921	-4.51400	0.92338	0.05451
57311.865483	13.60088	0.00153	3.37142	13.11247	0.22900	0.81339	0.05432
57312.612196	13.59665	0.00155	3.40356	13.42444	-2.64400	0.95504	0.05439
57312.833689	13.59624	0.00174	3.38019	13.22558	0.30500	0.91122	0.05436
57318.607733	13.59942	0.00175	3.39599	13.34035	-3.50100	0.93871	0.05477
57318.817847	13.59755	0.00151	3.38780	13.17087	-6.42600	0.91751	0.05448
57319.727316	13.59413	0.00297	3.41124	13.37541	4.55200	0.74901	0.05437
57319.810394	13.58975	0.00290	3.40478	13.19515	-12.58000	0.76969	0.05414
57321.614538	13.59868	0.00166	3.40100	13.26734	5.52100	0.83963	0.05418
57324.626352	13.59948	0.00164	3.40719	13.31540	-1.43000	0.90288	0.05454
57324.853234	13.59528	0.00218	3.37680	12.94524	-0.08700	0.69849	0.05471
57325.602745	13.60049	0.00139	3.40115	13.29440	0.93500	0.87488	0.05415
57325.812706	13.60015	0.00147	3.36939	12.95619	-3.60000	0.86889	0.05427

Table 1. continued.

BJD - 2400000	RV [$km s^{-1}$]	σ_{RV} [$km s^{-1}$]	FWHM [$km s^{-1}$]	Contrast	BIS [$km s^{-1}$]	S-index	$H\alpha$
57328.664922	13.60144	0.00284	3.41158	13.20892	8.73500	0.79694	0.05431

Table 2. Radial velocities time series for GJ 3323.

BJD - 2400000	RV [$km\,s^{-1}$]	σ_{RV} [$km\,s^{-1}$]	FWHM [$km\,s^{-1}$]	Contrast	BIS [$km\,s^{-1}$]	S-index	$H\alpha$
52986.721748	42.44749	0.00212	3.03195	27.57384	-12.03000	5.92003	0.13107
52997.681842	42.44901	0.00333	3.03125	26.59910	-21.51800	3.46817	0.11630
53343.728670	42.45623	0.00234	3.01471	27.21297	-10.98700	4.29847	0.15122
54174.512651	42.45516	0.00167	3.00959	27.37128	-10.46400	3.26599	0.09855
54732.819933	42.45234	0.00303	3.02512	26.90758	-12.95900	4.35294	0.17680
54754.811111	42.44929	0.00201	3.00958	27.20065	-11.52400	3.37133	0.12970
54766.801860	42.44864	0.00198	3.01873	27.12191	-21.09000	6.14713	0.15387
56565.795415	42.45409	0.00218	3.01656	26.85931	-10.35200	2.83963	0.09553
56570.836787	42.44937	0.00233	3.03166	26.94122	-9.68400	3.91838	0.10323
56576.841993	42.45069	0.00190	3.02085	27.06002	-9.13200	3.94609	0.10746
56584.761943	42.44747	0.00216	3.02159	26.78650	-11.79500	3.10963	0.10419
56600.778992	42.45008	0.00238	3.02753	26.91700	-9.07400	7.61343	0.15610
56601.817070	42.45144	0.00177	3.04441	26.95606	-16.35700	4.99883	0.11961
56602.792355	42.45216	0.00212	3.04523	26.73436	-12.29800	6.90819	0.17352
56603.821170	42.45574	0.00201	3.04232	26.51181	-17.37500	8.87299	0.20934
56604.775155	42.45315	0.00226	3.04157	26.83680	-5.38700	5.35839	0.13033
56612.812718	42.45324	0.00272	3.05374	26.76979	-10.05900	4.61655	0.11861
56613.696400	42.45357	0.00258	3.03309	26.64906	-11.26200	4.27667	0.13637
56617.634769	42.44807	0.00253	3.03239	26.75526	-19.01600	5.33530	0.13905
56617.841163	42.44721	0.00232	3.04110	26.62875	-15.95500	5.39541	0.13746
56618.645450	42.45063	0.00252	3.03244	26.70015	-0.44400	4.11711	0.12330
56618.778925	42.45050	0.00169	3.03803	26.81231	-9.35800	4.59152	0.11912
56619.684023	42.44882	0.00232	3.03655	26.91732	-11.73600	4.57863	0.12259
56619.813875	42.45261	0.00196	3.03477	26.88971	-22.59700	3.92350	0.11426
56622.668584	42.44667	0.00243	3.02903	26.93606	-12.33200	3.95254	0.11610
56624.759813	42.45033	0.00188	3.02848	27.07112	-14.93800	3.45599	0.10139
56626.685328	42.45356	0.00240	3.02614	26.98093	-7.60700	5.19341	0.12041
56628.675398	42.44865	0.00403	3.03600	27.28278	-11.50500	4.91216	0.14017
56632.630276	42.45057	0.00207	3.01282	26.94317	-12.59800	3.61569	0.10276
56673.651468	42.45523	0.00287	3.01601	26.81051	-15.69500	4.42763	0.11691
56677.631561	42.45415	0.00261	3.02755	26.91094	-13.20200	7.26449	0.12450
56678.658208	42.45596	0.00213	3.03102	26.81393	-8.55200	10.46576	0.16895
56680.649872	42.45454	0.00178	3.02552	26.83146	-4.14500	7.05664	0.14347
56685.642839	42.45522	0.00373	3.03865	27.02553	-13.66400	99.00000	0.12933
56686.584936	42.45036	0.00515	3.07861	27.31724	-22.15800	99.00000	0.12237
56687.598566	42.45276	0.00251	3.03829	26.81024	-17.88100	6.53281	0.11442
56688.573923	42.45062	0.00213	3.03478	26.80212	-8.76200	5.10013	0.11997
56689.567831	42.45450	0.00202	3.03974	26.82334	-19.78700	5.66139	0.12735
56690.562340	42.45527	0.00183	3.03361	26.75467	-12.31800	6.21175	0.13824
56712.599508	42.45074	0.00204	3.02132	26.94356	-15.56800	5.00668	0.12034
56713.580419	42.44914	0.00293	3.02012	26.78505	-11.76900	8.47570	0.18884
56714.597055	42.45171	0.00450	3.02615	27.04759	-16.52500	99.00000	0.12934
56715.594110	42.44940	0.00275	3.01829	26.80705	-12.82300	99.00000	0.12947
56716.598560	42.45496	0.00213	3.01100	26.47187	-10.15600	10.73077	0.16105
56717.594399	42.45425	0.00266	3.02387	26.88679	-14.35100	99.00000	0.12205
56718.602587	42.44898	0.00326	3.03188	26.71433	-9.77100	99.00000	0.16543
56719.556589	42.44993	0.00261	3.01852	26.96195	-22.58300	5.76872	0.12135
56720.539212	42.44916	0.00220	3.02173	26.86998	-11.11600	6.66546	0.16313
56721.545640	42.45691	0.00226	3.02737	26.77884	-11.00200	5.50469	0.13528
56722.544893	42.45527	0.00230	3.02972	26.74868	-16.29000	5.48195	0.12432
56726.521319	42.45205	0.00204	3.02215	26.77266	-17.22400	4.95211	0.11917
56727.536346	42.45496	0.00224	3.02462	26.83641	-4.77700	7.17295	0.14186
56728.529663	42.45613	0.00220	3.02714	26.79498	-9.45500	5.64943	0.12029
56729.521210	42.45005	0.00196	3.03364	26.78799	-14.52200	5.99571	0.13819
56730.526772	42.45372	0.00241	3.02789	26.56001	-14.91500	9.33756	0.22614
56731.530320	42.44590	0.00330	3.02639	26.52288	-1.60800	13.50073	0.25413
56732.530836	42.46378	0.00355	3.03763	26.91276	-19.24600	4.59163	0.11915
56738.499859	42.45291	0.00232	3.04586	26.41703	-8.78500	8.18078	0.16036
56739.515319	42.45170	0.00218	3.03547	26.65952	-17.10300	8.22501	0.18019
56740.509415	42.44740	0.00187	3.03493	26.61684	-15.95600	6.51177	0.14450
56741.495341	42.44732	0.00184	3.03599	26.73245	-19.67900	4.35802	0.11381
56742.490642	42.44891	0.00192	3.03880	26.68653	-15.02200	4.15929	0.10661
56744.484058	42.45152	0.00217	3.02680	26.51695	-12.17400	5.92758	0.11680
56870.924563	42.44581	0.00287	3.03125	26.89367	-2.26600	99.00000	0.10342
56872.925377	42.45191	0.00297	3.03212	26.87111	-19.56100	99.00000	0.11124
56874.922884	42.44967	0.00287	3.02382	26.82361	-13.62000	6.32269	0.11975

Table 2. continued.

BJD - 2400000	RV [$km\ s^{-1}$]	σ_{RV} [$km\ s^{-1}$]	FWHM [$km\ s^{-1}$]	Contrast	BIS [$km\ s^{-1}$]	S-index	$H\alpha$
56921.897450	42.44790	0.00255	3.02690	26.58869	-13.29900	8.19231	0.16855
56922.875992	42.45251	0.00205	3.02460	26.61812	-6.61800	9.63730	0.17528
56923.898993	42.44718	0.00299	3.02998	26.77558	-13.91500	99.00000	0.12803
56924.857312	42.45238	0.00221	3.03122	26.69998	-8.93400	5.09481	0.11120
56925.861283	42.45699	0.00203	3.02559	26.71634	-13.40100	3.97774	0.10912
56927.860321	42.45341	0.00192	3.02882	26.75171	-5.74700	4.60635	0.11302
56928.844949	42.45307	0.00186	3.03166	26.76994	-10.04800	4.59136	0.11445
56929.869637	42.45288	0.00228	3.03841	26.79223	-8.42100	4.03027	0.10654
56930.886592	42.45362	0.00214	3.03268	26.74449	-16.52800	4.87371	0.11421
56931.872653	42.45643	0.00215	3.03935	26.76873	-7.94500	4.33513	0.10876
56948.750957	42.44888	0.00197	3.02827	26.79248	-14.92500	4.48373	0.10852
56951.849404	42.45077	0.00204	3.03732	26.83374	-10.69300	4.57496	0.12370
56989.790387	42.45326	0.00198	3.03138	26.54151	-15.20300	10.53923	0.22973
56990.757202	42.45272	0.00252	3.02818	27.16364	-11.42300	4.71697	0.11603
56992.635759	42.44478	0.00211	3.02671	27.00290	-13.41000	4.13695	0.10839
56992.768584	42.44673	0.00191	3.02841	27.06829	-13.18000	4.46629	0.11292
56993.739665	42.44628	0.00252	3.02740	27.10374	-21.49600	4.93673	0.12452
56994.651671	42.44843	0.00282	3.01908	27.12602	-9.02600	7.09488	0.13760
56994.803535	42.44934	0.00282	3.01563	27.29166	-22.54800	3.64991	0.10550
56995.816269	42.45568	0.00266	3.02778	27.07691	-9.07500	6.37225	0.12840
56996.799071	42.45332	0.00198	3.01443	27.00867	-16.97700	3.73728	0.10596
56997.733561	42.44852	0.00191	3.02470	26.93109	-7.96400	4.20719	0.11578
56998.626707	42.44891	0.00209	3.01165	26.96193	-17.44900	3.22215	0.10679
56999.760234	42.45216	0.00184	3.01865	26.75831	-5.51900	5.17269	0.13483
57000.735344	42.45285	0.00201	3.02097	27.07056	-7.38600	3.89649	0.10650
57000.848839	42.45218	0.00261	3.01921	26.68982	-11.75200	7.23123	0.15774
57001.847744	42.45585	0.00770	3.02003	25.99693	-1.04300	99.00000	0.11058
57002.810838	42.45318	0.00208	3.02228	27.06454	-16.21200	6.15651	0.14547
57003.677519	42.44837	0.00204	3.02657	27.10628	-15.89900	3.65714	0.10455
57008.621130	42.45228	0.00267	3.02592	27.14088	-13.32100	5.72693	0.12168
57009.617987	42.45504	0.00220	3.02074	26.96758	-10.68500	10.01146	0.22623
57018.673653	42.45227	0.00215	3.03169	26.96673	-17.69600	3.98294	0.10638
57019.675020	42.45070	0.00255	3.04065	27.04299	-12.74500	4.19530	0.10488
57020.679580	42.45023	0.00251	3.03075	27.02071	-23.00200	5.30918	0.12293
57021.708327	42.45202	0.00246	3.02996	26.87971	-10.22800	5.59343	0.11555
57022.733914	42.45574	0.00169	3.03188	26.91211	-12.08900	4.22832	0.11114
57044.589980	42.45383	0.00212	3.05183	26.70695	-10.81700	5.01399	0.12208
57045.613929	42.45085	0.00190	3.04946	26.56700	-7.22600	6.52547	0.13492
57046.584408	42.45106	0.00184	3.04557	26.55651	-6.22000	4.53634	0.11074
57048.600868	42.45065	0.00207	3.04910	26.52619	-16.38000	7.51700	0.15292
57049.602037	42.45174	0.00208	3.05536	26.70474	-8.37700	5.29797	0.12615
57050.605485	42.45303	0.00215	3.05626	26.44869	-4.94000	6.95242	0.15623
57054.657263	42.45423	0.00227	3.04274	26.45172	-9.04400	5.24030	0.12697
57055.600699	42.45200	0.00198	3.04790	26.51987	-12.06500	5.13271	0.12470
57056.603008	42.45154	0.00196	3.05263	26.38498	-5.54700	7.27745	0.15494
57057.582899	42.44765	0.00174	3.05020	26.43003	-6.60500	7.62359	0.17333
57058.599013	42.45124	0.00171	3.04621	26.52568	-11.16700	4.63561	0.12599
57061.631194	42.44863	0.00218	3.05118	26.13830	-3.42300	14.43350	0.24713
57062.618407	42.45137	0.00197	3.03857	26.34971	-8.81600	3.60780	0.12653
57064.589290	42.45039	0.00234	3.03998	26.31927	-9.15500	14.31762	0.22802
57065.591072	42.45230	0.00183	3.04685	26.54224	-12.44600	4.51633	0.13864
57066.568296	42.44768	0.00320	3.05164	26.59044	-11.33400	99.00000	0.17211
57075.622812	42.45596	0.00262	3.03045	26.75335	-14.30100	99.00000	0.12346
57076.565867	42.45597	0.00188	3.03127	26.77617	-9.71200	6.17672	0.13056
57077.576810	42.44895	0.00221	3.03103	26.87372	-10.17600	4.04438	0.10297
57100.530151	42.45029	0.00248	3.00832	27.04720	-13.82100	2.47301	0.10192
57101.515855	42.44931	0.00287	3.01937	27.11657	-24.69300	3.82175	0.09569
57102.510471	42.45861	0.00288	3.01287	27.13715	-2.92600	3.95899	0.09801
57103.522319	42.45382	0.00206	3.01399	27.04052	-17.38700	2.44009	0.09374
57104.518730	42.45094	0.00200	3.00907	26.95793	-14.01700	2.24153	0.09155
57114.496914	42.45517	0.00174	3.01824	26.95194	-13.73400	3.13566	0.11033
57115.494349	42.45178	0.00199	3.01501	26.91208	-9.10000	2.38081	0.10703
57116.491808	42.45658	0.00297	3.02581	26.87620	-10.41200	4.44457	0.11642
57117.492370	42.45244	0.00232	3.02016	27.02400	-14.25800	3.39793	0.09847
57255.920787	42.44508	0.00283	3.07751	26.62114	-8.15400	4.55698	0.11517
57257.912527	42.44564	0.00180	3.06616	26.41662	-0.03900	4.17049	0.12276

Table 2. continued.

BJD - 2400000	RV [$km\ s^{-1}$]	σ_{RV} [$km\ s^{-1}$]	FWHM [$km\ s^{-1}$]	Contrast	BIS [$km\ s^{-1}$]	S-index	$H\alpha$
57260.910428	42.44646	0.00280	3.08167	26.65100	-7.89100	4.31529	0.10218
57263.893389	42.45314	0.00234	3.05696	26.52060	1.69000	2.87060	0.09636
57264.915432	42.44865	0.00303	3.06034	26.65941	-4.05900	3.31521	0.09064
57265.895515	42.44641	0.00282	3.06453	26.61076	3.07400	3.97297	0.11188
57266.867288	42.44500	0.00264	3.05921	26.57073	-7.73000	2.85168	0.09573
57267.874110	42.44590	0.00279	3.06358	26.47948	-1.23700	9.38917	0.20066
57268.918713	42.45051	0.00208	3.05386	26.58609	-0.65500	2.74130	0.09311
57269.897918	42.44954	0.00189	3.05721	26.64630	0.71400	4.15007	0.10939
57274.887720	42.44932	0.00198	3.05182	26.76491	0.54000	3.02397	0.09190
57277.876610	42.44770	0.00209	3.04926	26.91096	0.68300	2.81730	0.09380
57278.887738	42.44543	0.00233	3.04976	26.86071	-2.13800	2.83683	0.08874
57291.891056	42.45270	0.00219	3.04941	26.89322	-2.59500	2.89947	0.09316
57292.874295	42.44937	0.00212	3.05005	26.75245	-1.86000	2.09830	0.08878
57293.821211	42.45305	0.00218	3.04502	26.79655	-5.76300	2.29726	0.09064
57294.839359	42.45179	0.00196	3.05161	26.78458	-2.70300	2.47311	0.09274
57295.856488	42.45459	0.00213	3.04900	26.72952	-0.62600	2.49787	0.09036
57306.854547	42.44976	0.00231	3.05623	26.70083	0.77000	4.52554	0.10946
57308.829964	42.44744	0.00233	3.06362	26.43556	-5.96100	6.33133	0.12470
57311.836394	42.45032	0.00209	3.05935	26.51989	-1.65500	3.90944	0.10560
57312.818948	42.45062	0.00185	3.05321	26.53567	2.89700	4.93102	0.11964
57318.761715	42.44753	0.00178	3.06888	26.42995	0.15800	3.65978	0.10654
57319.788535	42.44515	0.00334	3.06425	26.69174	2.48600	4.60485	0.11292

Table 3. Radial velocities time series for GJ 273.

BJD - 2400000	RV [km s^{-1}]	σ_{RV} [km s^{-1}]	FWHM [km s^{-1}]	Contrast	BIS [km s^{-1}]	S-index	$H\alpha$
52986.769625	18.40354	0.00145	2.97871	27.91234	-5.50100	0.71683	0.07591
52998.774768	18.40073	0.00091	2.96841	27.67013	-8.65700	0.69299	0.07457
53343.769216	18.40549	0.00158	2.96227	27.41423	-3.31700	0.71733	0.07665
53370.806664	18.40891	0.00081	2.97153	27.80775	-7.43500	0.69075	0.07491
53371.752065	18.40807	0.00086	2.97149	27.63837	-6.45600	0.74705	0.07585
53372.725047	18.40842	0.00094	2.97386	27.85808	-6.11400	0.68818	0.07466
53373.743236	18.40827	0.00089	2.97169	27.65849	-7.64800	0.67819	0.07563
53376.718116	18.40813	0.00098	2.96720	27.49864	-8.93000	0.67491	0.07565
53377.709863	18.40650	0.00087	2.96360	27.50865	-7.33500	0.67755	0.07571
53809.594622	18.41105	0.00080	2.96783	27.49974	-6.61500	0.65216	0.07147
53882.473921	18.40764	0.00109	2.96130	27.37236	-5.86100	0.68695	0.07429
54122.685331	18.41518	0.00087	2.97262	27.49480	-9.79400	0.72792	0.07269
54166.583084	18.41272	0.00099	2.96946	27.49043	-8.18600	0.58368	0.07159
54168.600417	18.41310	0.00079	2.96766	27.48976	-8.47200	0.63281	0.07376
54170.614529	18.41061	0.00092	2.96487	27.43003	-6.81000	0.63916	0.07385
54172.565182	18.41187	0.00079	2.97010	27.50964	-8.03100	1.07294	0.07751
54174.594089	18.41405	0.00087	2.96549	27.42195	-6.62800	0.60356	0.07244
54197.549776	18.41348	0.00099	2.96903	27.43340	-8.08100	0.58522	0.07272
54230.466669	18.41524	0.00105	2.96439	27.27798	-8.35100	0.56453	0.07287
54419.844384	18.41500	0.00079	2.97079	27.44220	-7.72100	0.72035	0.07517
54423.817207	18.41377	0.00093	2.97237	27.39786	-8.68200	0.81272	0.07731
54427.772699	18.41067	0.00081	2.97297	27.42915	-6.40300	0.74641	0.07398
54446.814818	18.41354	0.00084	2.97430	27.46432	-8.41100	0.78126	0.07325
54448.820568	18.41290	0.00092	2.96878	27.34758	-11.83500	0.78982	0.07272
54450.794968	18.41356	0.00083	2.96941	27.42271	-9.30800	0.77884	0.07300
54456.800705	18.41588	0.00085	2.97306	27.41704	-6.01500	0.79515	0.07329
54457.742892	18.41444	0.00077	2.97840	27.55179	-8.81600	0.80089	0.07368
54458.719732	18.41345	0.00092	2.97291	27.38615	-9.36500	0.79903	0.07391
54459.686929	18.41551	0.00094	2.97549	27.35758	-10.61300	0.76741	0.07337
54462.750494	18.41313	0.00082	2.97351	27.46356	-7.21700	0.83587	0.07333
54464.772398	18.41199	0.00077	2.97555	27.57515	-6.63300	0.76749	0.07323
54522.666754	18.41822	0.00087	2.97449	27.39866	-7.02700	1.09295	0.07929
54527.636909	18.41938	0.00081	2.96887	27.36354	-7.62800	0.87327	0.07454
54551.611043	18.41909	0.00083	2.96562	27.25632	-7.68100	0.87736	0.07473
54552.534316	18.41671	0.00079	2.97377	27.39810	-10.67700	0.93035	0.07580
54555.557823	18.41710	0.00084	2.97139	27.39465	-9.35700	0.95685	0.07595
54562.506663	18.41551	0.00076	2.97380	27.55625	-9.16500	0.90692	0.07439
54566.496586	18.41588	0.00082	2.97502	27.45266	-5.07500	0.84561	0.07437
54571.512198	18.41573	0.00089	2.97230	27.33479	-7.52100	0.90975	0.07621
54775.834894	18.40781	0.00081	2.97232	27.41756	-7.99000	0.74350	0.07440
54779.766792	18.40491	0.00086	2.96747	27.36679	-6.70200	0.73511	0.07340
54913.620769	18.41416	0.00081	2.96945	27.30984	-8.73200	0.75956	0.07197
54914.582072	18.41606	0.00083	2.97324	27.38906	-9.80900	0.75860	0.07223
54915.536500	18.41571	0.00089	2.97266	27.39146	-8.60900	0.72696	0.07187
54916.560737	18.41632	0.00085	2.97484	27.33991	-5.70000	0.82153	0.07286
54917.554628	18.41566	0.00088	2.97738	27.45931	-8.92200	0.82321	0.07437
54918.566086	18.41753	0.00080	2.97559	27.38583	-6.49100	0.77145	0.07188
54919.526993	18.41965	0.00077	2.97608	27.45001	-7.53900	0.82998	0.07388
54920.581410	18.41922	0.00089	2.96923	27.26817	-7.67200	0.98593	0.07694
54932.518355	18.41439	0.00080	2.97660	27.50431	-7.15700	0.87377	0.07324
54933.516720	18.41673	0.00082	2.97174	27.34351	-7.31500	0.86197	0.07348
54934.500192	18.41593	0.00088	2.97730	27.39382	-6.72200	0.82492	0.07353
54936.499261	18.41480	0.00092	2.98095	27.48114	-8.41100	0.92199	0.07448
54937.498854	18.41656	0.00089	2.97770	27.43184	-9.30700	0.96283	0.07754
54938.473356	18.41789	0.00080	2.97801	27.46918	-4.88000	0.85261	0.07265
54939.508305	18.41745	0.00086	2.97539	27.38930	-9.29600	0.82382	0.07335
54940.521623	18.41596	0.00091	2.97912	27.40799	-8.87600	0.85259	0.07287
54946.492672	18.41514	0.00084	2.97712	27.53571	-8.00900	0.79404	0.07217
54951.477885	18.41467	0.00091	2.97771	27.47824	-4.47200	0.81075	0.07174
54954.483482	18.41431	0.00085	2.97367	27.34189	-7.22500	0.76680	0.07209
55122.858861	18.41760	0.00098	2.97412	27.25748	-6.46300	0.67073	0.07509
55126.872125	18.41732	0.00089	2.97089	27.31362	-5.52700	0.74178	0.07700
56307.789125	18.41806	0.00087	2.96365	26.90067	-9.98100	0.79608	0.07610
56308.615950	18.41922	0.00092	2.96689	27.03197	-10.16100	0.81205	0.07711
56310.691665	18.41627	0.00101	2.97277	27.15207	-10.03900	0.60028	0.07407
56311.626008	18.41848	0.00121	2.97077	27.07558	-9.52400	0.63524	0.07567

Table 3. continued.

BJD - 2400000	RV [kms^{-1}]	σ_{RV} [kms^{-1}]	FWHM [kms^{-1}]	Contrast	BIS [kms^{-1}]	S-index	$H\alpha$
56312.722975	18.42262	0.00132	2.97100	26.95121	-12.09500	0.63145	0.07584
56314.747090	18.41715	0.00098	2.97155	27.01433	-9.97800	0.70596	0.07510
56315.643754	18.42183	0.00159	2.97562	26.87110	-5.74100	0.66735	0.07464
56320.705129	18.42329	0.00109	2.97289	27.12021	-9.95100	0.65926	0.07443
56321.727093	18.42057	0.00095	2.97194	27.00527	-7.66300	0.63755	0.07425
56322.652346	18.42272	0.00101	2.97706	27.08939	-9.45400	0.78030	0.07526
56323.680892	18.41868	0.00093	2.97552	27.10722	-10.48400	0.65977	0.07409
56324.642159	18.41818	0.00135	2.97519	27.02004	-9.18800	0.70878	0.07299
56325.667508	18.42065	0.00112	2.97410	27.03004	-11.05800	0.83674	0.07675
56326.664511	18.41759	0.00101	2.97576	27.06155	-10.55400	0.70539	0.07474
56327.679718	18.41907	0.00094	2.97379	27.10307	-5.65000	0.74982	0.07411
56328.577254	18.41759	0.00104	2.97186	27.02428	-9.50100	0.70617	0.07415
56329.611068	18.41709	0.00098	2.96910	27.03097	-4.86500	0.67021	0.07429
56331.596277	18.41530	0.00102	2.96925	26.99218	-8.31500	0.73301	0.07352
56332.634450	18.41653	0.00101	2.97108	27.08036	-10.26500	0.80076	0.07504
56333.664010	18.41633	0.00089	2.97091	27.05878	-9.03300	0.75565	0.07398
56335.610169	18.41830	0.00090	2.97273	27.03220	-8.34400	0.76330	0.07510
56336.611555	18.41835	0.00095	2.97421	27.06045	-7.16600	0.76420	0.07456
56353.574676	18.41641	0.00094	2.97788	27.15281	-7.35000	0.84678	0.07507
56355.598545	18.41828	0.00096	2.97911	27.06661	-8.40900	0.91356	0.07757
56357.625292	18.41795	0.00087	2.97698	27.11178	-10.12400	0.80462	0.07431
56360.586627	18.41817	0.00102	2.97657	27.11530	-9.50200	0.82882	0.07476
56361.635838	18.41594	0.00101	2.97542	27.04491	-8.45500	0.78718	0.07575
56363.590519	18.41579	0.00093	2.97614	27.11070	-8.14800	0.93563	0.07819
56364.618328	18.41301	0.00083	2.97139	27.07778	-9.27100	0.75810	0.07367
56365.612876	18.41293	0.00087	2.97410	27.03863	-10.51800	0.75463	0.07415
56367.564391	18.41325	0.00089	2.97691	27.15100	-7.81600	0.78785	0.07317
56368.588297	18.41407	0.00093	2.97466	27.07103	-8.07200	1.24303	0.08467
56369.576870	18.41445	0.00084	2.97546	27.09786	-8.59200	0.76154	0.07428
56371.520139	18.41472	0.00098	2.97706	27.10259	-9.35000	0.74660	0.07434
56372.492218	18.41202	0.00087	2.97199	27.04659	-10.12800	0.80217	0.07505
56374.522768	18.41426	0.00088	2.97565	27.10369	-6.13600	0.75164	0.07362
56417.477216	18.41967	0.00129	2.97562	27.03488	-7.69000	0.99242	0.07899
56418.478552	18.41605	0.00107	2.97659	27.08375	-8.32000	0.75176	0.07493
56419.459612	18.41829	0.00112	2.97559	27.02741	-7.68900	0.73400	0.07465
56420.498121	18.41858	0.00103	2.97255	27.08891	-8.57100	0.69084	0.07426
56421.474125	18.42185	0.00116	2.97014	26.99157	-11.16500	0.76845	0.07471
56422.466135	18.41863	0.00111	2.97150	26.97360	-8.99800	0.78171	0.07482
56423.489475	18.41701	0.00112	2.97317	26.91271	-9.17200	0.77221	0.07534
56423.497460	18.41722	0.00113	2.96843	26.90973	-7.62300	0.75399	0.07458
56424.454475	18.41839	0.00132	2.97777	27.04158	-9.23900	0.62420	0.07530
56424.462807	18.41867	0.00127	2.97982	27.07076	-9.59000	0.80737	0.07560
56426.472363	18.42055	0.00108	2.97604	27.00307	-7.14300	0.79949	0.07529
56427.457075	18.41922	0.00121	2.97666	27.06062	-8.58100	1.04264	0.08144
56428.470454	18.41878	0.00113	2.97582	27.03144	-9.46800	0.69616	0.07493
56610.831488	18.42406	0.00107	2.98131	27.04939	-8.37400	2.59384	0.10773
56613.841040	18.42442	0.00106	2.97992	27.13775	-9.65000	0.74361	0.07713
56614.804104	18.42605	0.00088	2.97456	27.06685	-11.22900	0.79348	0.07751
56615.838827	18.42650	0.00100	2.97814	27.13785	-8.12200	0.78398	0.07761
56620.753324	18.43021	0.00163	2.97664	26.77291	-10.40000	0.67104	0.07610
56620.844245	18.42957	0.00179	2.98472	26.80123	-9.13600	0.71579	0.07910
56623.807504	18.42432	0.00087	2.97834	27.10346	-9.45100	0.75283	0.07623
56626.819020	18.42365	0.00087	2.98048	27.08189	-9.13500	0.73041	0.07574
56628.834118	18.42617	0.00103	2.98121	27.08271	-9.03000	0.74205	0.07605
56631.799826	18.42419	0.00137	2.98024	27.12018	-9.49900	0.67527	0.07657
56656.669846	18.42672	0.00103	2.98211	27.07660	-8.24500	0.83979	0.07758
56656.722196	18.42664	0.00132	2.97594	27.08608	-7.11900	0.81231	0.07595
56656.771225	18.42662	0.00108	2.98121	27.10948	-9.01300	0.77594	0.07631
56657.603189	18.42693	0.00128	2.97133	27.00131	-10.95500	0.88886	0.07675
56657.714187	18.42630	0.00112	2.98241	27.10089	-7.40700	0.75567	0.07610
56657.769732	18.42538	0.00107	2.98399	27.17700	-8.81900	0.89221	0.07802
56658.721928	18.42354	0.00101	2.98381	27.22623	-9.30500	0.87310	0.07960
56658.778341	18.42449	0.00096	2.98258	27.14501	-10.31200	0.81257	0.07714
56659.704378	18.42238	0.00099	2.97717	27.08212	-9.13300	0.87088	0.07785
56659.761300	18.42192	0.00093	2.98224	27.16126	-8.64300	0.74960	0.07539
56660.697093	18.42281	0.00108	2.97756	27.04225	-8.15200	0.80352	0.07685

Table 3. continued.

BJD - 2400000	RV [km s^{-1}]	σ_{RV} [km s^{-1}]	FWHM [km s^{-1}]	Contrast	BIS [km s^{-1}]	S-index	$H\alpha$
56660.756920	18.42331	0.00111	2.97818	27.06647	-5.37500	0.77711	0.07568
56661.611471	18.42334	0.00129	2.97042	26.92812	-11.78100	0.93060	0.07838
56661.670986	18.42431	0.00115	2.97478	27.00618	-8.37200	0.84249	0.07653
56661.728197	18.42368	0.00110	2.97836	27.07417	-9.88100	0.78919	0.07613
56665.589518	18.42186	0.00113	2.96536	26.95037	-8.35700	0.77399	0.07576
56665.644958	18.42064	0.00104	2.97680	27.07766	-7.98100	0.73009	0.07581
56665.660988	18.42181	0.00104	2.97717	27.09266	-7.39300	0.77634	0.07606
56665.677099	18.42309	0.00113	2.98068	27.10987	-11.31800	0.81854	0.07644
56665.695144	18.42236	0.00105	2.97889	27.15043	-7.40400	0.84316	0.07686
56665.728824	18.42191	0.00104	2.98117	27.09528	-9.33000	0.78768	0.07632
56665.744438	18.42201	0.00111	2.98341	27.13004	-8.53800	0.74551	0.07655
56665.760306	18.42297	0.00112	2.97943	27.13761	-7.26300	0.82329	0.07645
56666.566157	18.42378	0.00138	2.96803	26.92621	-8.70800	0.73704	0.07591
56666.640521	18.42086	0.00109	2.97469	27.01870	-9.00500	0.75083	0.07574
56666.658658	18.42235	0.00105	2.97860	27.06970	-10.50300	0.84603	0.07668
56666.689654	18.42198	0.00102	2.98225	27.14704	-8.51000	0.88474	0.07795
56666.708300	18.42249	0.00100	2.97973	27.15594	-4.27400	0.79223	0.07588
56666.756494	18.42298	0.00096	2.98170	27.16000	-7.67200	0.88312	0.07838
56667.576801	18.42431	0.00122	2.97011	26.94702	-6.18400	0.85257	0.07668
56667.668560	18.42225	0.00120	2.98068	27.07410	-10.58200	0.71160	0.07529
56667.686211	18.42434	0.00116	2.98042	27.08515	-9.78100	0.73523	0.07599
56667.717704	18.42243	0.00106	2.98077	27.12256	-8.72100	0.77189	0.07549
56667.757982	18.42338	0.00101	2.98186	27.09978	-8.13900	0.79554	0.07616
56678.672904	18.41976	0.00096	2.98548	27.16012	-8.06400	0.75813	0.07568
56680.698488	18.42193	0.00091	2.98198	27.13006	-9.45900	0.84131	0.07803
56692.616462	18.42347	0.00095	2.97682	27.03478	-10.66600	0.76736	0.07531
56693.608046	18.42280	0.00093	2.97939	27.03419	-8.84200	0.76693	0.07626
56694.640530	18.42375	0.00100	2.98407	27.17169	-9.88300	0.74258	0.07544
56695.587749	18.42463	0.00092	2.97942	27.09086	-8.48600	0.81514	0.07625
56696.611862	18.42101	0.00100	2.98392	27.16551	-9.71500	0.76006	0.07537
56697.632848	18.42177	0.00090	2.97879	27.09092	-7.97900	0.80790	0.07536
56713.621163	18.42306	0.00102	2.97826	27.04741	-7.72300	0.88327	0.07647
56714.625345	18.42499	0.00122	2.98228	27.01296	-9.23600	0.93354	0.07834
56716.639607	18.42201	0.00097	2.97838	27.01615	-7.81400	0.85034	0.07736
56718.641538	18.42286	0.00106	2.97951	27.00431	-10.47600	0.90624	0.07834
56719.608402	18.42240	0.00107	2.98385	27.15640	-10.96800	0.82686	0.07608
56720.631533	18.42132	0.00105	2.98209	27.07022	-8.26300	0.93539	0.07792
56721.599367	18.42135	0.00097	2.98282	27.12918	-9.77000	1.03358	0.08053
56722.593170	18.42042	0.00102	2.97889	27.10865	-7.93300	0.80845	0.07665
56723.599297	18.42325	0.00099	2.97855	27.07863	-8.26200	0.82447	0.07604
56724.567973	18.42267	0.00089	2.97582	27.09457	-9.65200	0.81793	0.07623
56726.574112	18.42227	0.00090	2.97801	27.06370	-8.47900	0.86438	0.07786
56730.589864	18.42246	0.00103	2.98157	27.07677	-3.91500	0.82973	0.07775
56732.546171	18.42503	0.00134	2.98544	27.07257	-7.43900	0.88872	0.07968
56738.546949	18.41919	0.00102	2.98313	27.13458	-6.90700	0.80967	0.07631
56739.506008	18.41964	0.00098	2.98346	27.06977	-10.96200	0.87134	0.07718
56740.500445	18.41878	0.00090	2.98407	27.17593	-8.73400	0.83157	0.07716
56741.511280	18.42041	0.00084	2.98289	27.16678	-8.36700	0.84686	0.07744
56742.506595	18.42192	0.00090	2.98676	27.21100	-8.81800	0.90616	0.07725
56744.512026	18.42073	0.00088	2.98119	27.07626	-9.45400	0.88500	0.07633
56745.507004	18.42185	0.00094	2.97943	27.07962	-9.27900	0.98439	0.08010
56746.520209	18.42205	0.00086	2.98191	27.11604	-9.24300	0.81397	0.07641
56747.537465	18.42343	0.00096	2.97715	26.99298	-12.55900	0.77535	0.07483
56764.497762	18.42137	0.00092	2.97709	27.01861	-10.87600	0.78813	0.07548
56765.489138	18.42521	0.00096	2.97676	27.06104	-12.37600	0.78247	0.07636
56766.493187	18.42420	0.00085	2.98071	27.07011	-9.07100	0.84207	0.07684
56767.508959	18.42356	0.00094	2.98391	27.14851	-9.39700	0.88020	0.07655
56768.479111	18.42265	0.00090	2.97972	27.02908	-9.77900	0.85882	0.07647
56930.895481	18.42412	0.00105	2.97412	26.98234	-8.76000	0.84599	0.07806
56989.802327	18.42124	0.00086	2.98202	27.13837	-9.70800	0.76132	0.07539
56990.781226	18.42221	0.00093	2.98506	27.21792	-9.75800	0.80189	0.07693
56991.805092	18.42297	0.00104	2.98753	27.21207	-6.44900	0.76935	0.07607
56992.792265	18.42499	0.00089	2.98412	27.14827	-8.84300	0.81131	0.07666
56993.823236	18.42345	0.00101	2.98670	27.11611	-8.24500	0.92000	0.07943
56994.828439	18.42238	0.00120	2.98649	27.11593	-10.05300	0.71950	0.07536
56995.853064	18.41980	0.00106	2.98602	27.17976	-7.58300	0.69423	0.07399

Table 3. continued.

BJD - 2400000	RV [kms^{-1}]	σ_{RV} [kms^{-1}]	FWHM [kms^{-1}]	Contrast	BIS [kms^{-1}]	S-index	$H\alpha$
56997.783090	18.42157	0.00084	2.98484	27.12983	-8.68100	0.76022	0.07556
56998.766401	18.42117	0.00106	2.98294	27.05534	-9.32400	0.78519	0.07603
57000.722254	18.41970	0.00098	2.97982	27.01306	-10.60500	0.75043	0.07514
57000.835999	18.42024	0.00089	2.98364	27.12950	-6.76500	0.71090	0.07455
57001.860419	18.42320	0.00158	2.98533	26.60969	-9.83500	0.59964	0.07484
57002.836675	18.42260	0.00092	2.98452	27.16886	-9.65100	0.72577	0.07528
57003.699730	18.42031	0.00087	2.97453	27.01878	-11.40800	0.72948	0.07439
57003.780741	18.42083	0.00085	2.98362	27.16208	-8.29900	0.81035	0.07524
57008.794664	18.42554	0.00089	2.98483	27.23691	-8.47600	0.67870	0.07416
57009.758282	18.42343	0.00096	2.98417	27.23776	-9.52000	0.82957	0.07739
57018.767659	18.42274	0.00089	2.98080	27.15568	-7.75000	0.74996	0.07620
57019.805281	18.42318	0.00086	2.98292	27.12674	-9.91000	0.72861	0.07438
57020.768848	18.42328	0.00094	2.98391	27.14113	-9.21900	0.70647	0.07659
57021.781778	18.42432	0.00088	2.98855	27.17832	-8.35500	0.77245	0.07570
57022.823157	18.42267	0.00084	2.97704	27.11455	-7.85900	0.75755	0.07568
57044.693905	18.42648	0.00118	2.98442	27.09853	-11.64000	0.71069	0.07560
57045.680325	18.42537	0.00088	2.98023	27.07829	-10.33400	0.77001	0.07633
57046.711419	18.42460	0.00111	2.98142	27.04414	-7.86200	0.67113	0.07403
57047.720844	18.42274	0.00094	2.98188	27.09602	-11.19900	0.69951	0.07436
57048.661080	18.42284	0.00095	2.98506	27.13972	-6.11600	0.71390	0.07314
57049.681451	18.42213	0.00092	2.98576	27.21182	-10.53600	0.75232	0.07479
57050.644993	18.42184	0.00095	2.98385	27.08475	-9.47200	0.74432	0.07436
57051.724850	18.41991	0.00095	2.97985	27.07808	-9.89400	0.71017	0.07367
57052.722463	18.42108	0.00083	2.98022	27.03200	-8.91900	0.80395	0.07734
57058.694989	18.42167	0.00091	2.98065	27.03456	-9.71100	0.71058	0.07549
57061.731883	18.42160	0.00094	2.98047	27.04682	-7.45800	0.72385	0.07426
57062.695315	18.42460	0.00085	2.97379	26.99258	-6.76100	0.72778	0.07414
57100.592199	18.42745	0.00116	2.98244	26.99822	-11.25900	0.70007	0.07437
57101.563018	18.42745	0.00118	2.98060	27.00319	-10.54000	0.75914	0.07510
57103.559591	18.42649	0.00100	2.98365	27.07202	-7.17300	0.68253	0.07415
57104.566632	18.42590	0.00096	2.98320	27.12200	-9.43300	0.70296	0.07449
57114.553001	18.42345	0.00090	2.98290	27.14434	-6.43800	0.71577	0.07449
57115.524461	18.42345	0.00086	2.98384	27.12692	-9.32500	0.74772	0.07412
57116.547039	18.42555	0.00100	2.98480	27.00897	-8.79500	0.77198	0.07512
57117.520686	18.42267	0.00097	2.98074	27.13717	-8.97800	0.69275	0.07351
57135.481637	18.41998	0.00081	2.98086	27.09210	-11.50000	0.64780	0.07439
57141.460481	18.41990	0.00082	2.97932	26.96584	-10.79200	0.72150	0.07673
57143.483399	18.42274	0.00092	2.97784	26.95689	-10.37900	0.67834	0.07578
57144.471666	18.42215	0.00113	2.97483	26.96636	-9.34700	0.69936	0.07595
57306.879470	18.42413	0.00091	3.01023	26.78015	0.50000	0.73823	0.07432
57308.876373	18.42539	0.00089	3.01356	26.83116	2.71400	0.67152	0.07403
57311.884138	18.42380	0.00083	3.00876	26.67166	-0.72300	0.68565	0.07388
57312.876246	18.42351	0.00083	3.01130	26.72934	0.47000	0.81954	0.07583
57318.839512	18.42174	0.00083	3.01256	26.79415	0.63200	0.77057	0.07456
57319.838136	18.42068	0.00137	3.01486	26.81770	2.76100	0.66017	0.07372
57325.822378	18.42236	0.00079	3.01386	26.75967	2.09900	0.69423	0.07399
57364.853322	18.42358	0.00093	3.02330	27.03307	1.19300	99.00000	99.00000
57371.730133	18.42336	0.00084	3.01605	26.86124	-0.91000	0.78297	0.07471
57372.828553	18.42151	0.00081	3.00668	26.62447	0.86700	0.77043	0.07443
57389.781072	18.42324	0.00086	3.00784	26.76121	2.35600	0.68386	0.07264
57390.762202	18.42303	0.00082	3.01606	26.88903	2.51500	0.74108	0.07404
57391.750483	18.42265	0.00127	3.00874	26.70419	-1.45100	0.70061	0.07510
57401.675203	18.42379	0.00081	3.00824	26.74595	-0.08800	0.74325	0.07324
57404.700923	18.42473	0.00087	3.00930	26.78715	0.31800	0.77504	0.07577
57405.655072	18.42384	0.00077	3.01032	26.77887	-0.15600	0.69604	0.07339
57412.639032	18.42132	0.00095	3.00941	26.75819	0.15600	0.85110	0.07983
57415.657416	18.42256	0.00092	3.00947	26.83194	0.62900	0.67273	0.07352
57416.667010	18.42500	0.00099	3.00849	26.80937	-0.70400	0.64594	0.07391
57418.614654	18.42373	0.00100	3.01311	26.91735	3.32700	0.70182	0.07412
57420.659199	18.42461	0.00078	3.00621	26.69475	1.52300	0.70735	0.07450
57422.660081	18.42347	0.00078	3.00409	26.62487	0.67900	0.74120	0.07540
57446.582774	18.41912	0.00081	3.00464	26.65581	0.66600	0.74112	0.07528
57447.579846	18.42115	0.00088	3.00525	26.67549	1.23500	0.87298	0.07878
57448.549767	18.41938	0.00086	3.00722	26.71020	1.63700	0.76699	0.07574
57449.541826	18.41805	0.00082	3.00723	26.76689	1.60700	0.73777	0.07510
57450.547159	18.42301	0.00088	3.00487	26.74095	0.91900	0.81040	0.07572

Table 3. continued.

BJD - 2400000	RV [$km\ s^{-1}$]	σ_{RV} [$km\ s^{-1}$]	FWHM [$km\ s^{-1}$]	Contrast	BIS [$km\ s^{-1}$]	S-index	$H\alpha$
57451.558509	18.42152	0.00083	3.00372	26.69255	0.68100	0.71935	0.07515
57452.574371	18.42187	0.00083	3.00346	26.63638	-0.21800	0.65426	0.07492
57453.596667	18.41989	0.00075	2.99797	26.54464	0.34800	0.69501	0.07403
57470.583554	18.42202	0.00099	3.00924	26.83953	2.96000	0.64179	0.07445
57473.515142	18.42253	0.00104	3.00591	26.71376	1.49300	0.67017	0.07264
57474.499335	18.42479	0.00082	3.00373	26.71959	0.02300	0.64658	0.07371
57475.537342	18.42411	0.00094	3.00878	26.82267	-0.49700	0.68541	0.07345
57476.553290	18.42390	0.00083	3.00050	26.57438	-0.42700	0.62957	0.07352
57479.555674	18.42417	0.00079	3.00004	26.50052	-0.28100	0.66590	0.07462
57486.493274	18.41831	0.00099	3.00740	26.74996	-1.63700	0.73018	0.07329
57487.487937	18.42197	0.00091	3.00202	26.71092	0.40600	0.69389	0.07334
57488.475204	18.42076	0.00089	3.00307	26.65701	0.50000	0.76105	0.07377
57501.505489	18.42417	0.00427	2.99388	24.86092	-14.65300	0.59399	0.07217
57504.519884	18.42134	0.00592	2.99889	26.70189	1.53800	0.39360	0.07265
57660.904333	18.41722	0.00103	3.01042	26.44238	1.14700	0.54085	0.07392
57661.897769	18.41612	0.00096	2.94915	25.04482	0.75300	-0.58547	0.07387

Table 4. Radial velocities time series for GJ 628.

BJD - 2400000	RV [km s^{-1}]	σ_{RV} [km s^{-1}]	FWHM [km s^{-1}]	Contrast	BIS [km s^{-1}]	S-index	$H\alpha$
53158.680215	-21.03311	0.00115	3.77357	28.86726	-15.36500	0.88246	0.07568
53203.583611	-21.03738	0.00094	3.81234	30.43251	-9.57700	0.78018	0.07288
53484.842215	-21.03704	0.00086	3.80200	30.29858	-9.77500	0.75919	0.07416
54172.850539	-21.03481	0.00084	3.80888	30.15304	-11.23400	0.90972	0.07435
54293.651400	-21.03805	0.00087	3.81178	30.19980	-14.18100	0.80749	0.07301
54340.569879	-21.03397	0.00079	3.80503	30.14626	-10.29200	0.84268	0.07387
54342.501740	-21.03870	0.00078	3.80672	30.18799	-11.28300	0.87879	0.07457
54343.504502	-21.03988	0.00088	3.81453	30.20132	-10.13400	0.88025	0.07472
54344.510226	-21.03943	0.00094	3.81459	30.25547	-10.49900	0.89484	0.07462
54345.481995	-21.03766	0.00089	3.81554	30.21907	-12.10100	0.94368	0.07571
54346.509962	-21.03841	0.00101	3.81745	30.00185	-12.24300	0.83292	0.07367
54347.508071	-21.04242	0.00102	3.81419	30.04039	-12.24700	0.87048	0.07437
54349.535398	-21.03769	0.00087	3.80740	30.05646	-10.54300	0.81023	0.07414
54548.860872	-21.03915	0.00102	3.81674	30.03333	-11.77900	0.87996	0.07521
54552.812644	-21.03760	0.00078	3.81413	30.02749	-11.79600	0.82369	0.07399
54557.843093	-21.04009	0.00083	3.81349	30.08027	-12.22100	1.04762	0.07894
54564.846724	-21.03570	0.00083	3.81050	30.07118	-12.60700	1.06001	0.07826
54567.891484	-21.03503	0.00088	3.81884	30.11524	-11.14300	1.01326	0.07731
54664.630369	-21.03152	0.00106	3.82678	29.91111	-12.39700	0.92988	0.07440
54665.624951	-21.03277	0.00085	3.81687	30.03701	-13.36100	0.96453	0.07462
55057.526605	-21.03906	0.00112	3.81389	30.16290	-13.85200	0.78500	0.07437
55058.530042	-21.03935	0.00123	3.81207	29.87786	-10.00300	1.09812	0.07963
55272.860710	-21.04096	0.00102	3.81202	30.01395	-9.81000	0.79604	0.07384
55275.844206	-21.04216	0.00095	3.81440	29.94381	-12.33700	0.77009	0.07318
55277.841634	-21.03998	0.00096	3.80994	30.06281	-11.44900	0.80042	0.07230
55278.816074	-21.03655	0.00098	3.80894	29.90328	-12.07900	0.73271	0.07208
55281.801051	-21.04065	0.00091	3.81377	29.92160	-12.13000	0.75111	0.07232
55282.876735	-21.03825	0.00091	3.80962	30.00568	-10.53600	0.74660	0.07253
55283.840835	-21.03619	0.00096	3.81627	30.03624	-12.78600	0.73850	0.07211
55287.849125	-21.03825	0.00086	3.81205	29.94184	-10.68900	0.72549	0.07198
55390.596107	-21.02953	0.00105	3.81045	30.01475	-12.47500	0.79180	0.07495
55402.654669	-21.03811	0.00232	3.82308	29.65733	-15.84300	0.80413	0.07462
55407.511916	-21.03270	0.00086	3.81126	29.85419	-13.04800	0.83126	0.07450
55413.540186	-21.03570	0.00086	3.81589	29.98588	-13.10600	0.85442	0.07298
56079.658291	-21.03645	0.00097	3.81233	29.81635	-13.22400	0.89336	0.07615
56084.591155	-21.03307	0.00109	3.81420	29.73539	-14.29600	0.71014	0.07317
56089.634904	-21.03594	0.00098	3.81309	29.79900	-10.36700	0.77615	0.07504
56092.634963	-21.04004	0.00119	3.81779	29.70432	-12.53000	0.69601	0.07591
56098.555990	-21.04091	0.00112	3.81325	29.62206	-16.83200	0.66592	0.07458
56100.564078	-21.03718	0.00124	3.82127	29.62559	-13.46300	0.62243	0.07483
56119.483508	-21.03475	0.00108	3.81842	29.63613	-14.56400	0.73965	0.07357
56150.591559	-21.03931	0.00109	3.82036	29.74521	-10.92000	0.81898	0.07572
56385.751865	-21.04222	0.00098	3.81371	29.63337	-10.76300	0.71539	0.07460
56386.770824	-21.04052	0.00103	3.81844	29.67964	-12.55800	0.65820	0.07439
56387.792386	-21.03726	0.00092	3.81029	29.74049	-11.78100	0.72738	0.07495
56388.769037	-21.03685	0.00100	3.81611	29.76710	-9.86400	0.61576	0.07414
56389.736044	-21.03830	0.00106	3.81143	29.65325	-13.85000	0.76534	0.07394
56390.747244	-21.03404	0.00121	3.81503	29.70144	-10.35100	0.65952	0.07405
56391.813227	-21.03450	0.00120	3.82083	29.77464	-12.10100	0.71923	0.07477
56394.785746	-21.03399	0.00114	3.81867	29.68909	-13.89200	0.64076	0.07473
56395.746716	-21.03776	0.00099	3.81310	29.64581	-10.45200	0.75007	0.07507
56396.794416	-21.03715	0.00105	3.82072	29.69707	-12.99200	0.69621	0.07394
56397.811337	-21.03324	0.00115	3.81613	29.66877	-10.88300	0.67807	0.07385
56398.690562	-21.03546	0.00131	3.81382	29.56450	-10.17900	0.68947	0.07345
56398.927360	-21.03481	0.00094	3.81807	29.66744	-15.50900	0.71962	0.07354
56399.706265	-21.03828	0.00098	3.81362	29.60735	-12.23900	0.70633	0.07295
56400.750962	-21.03859	0.00099	3.81964	29.71125	-14.72100	0.70244	0.07334
56401.719680	-21.03705	0.00102	3.80931	29.71102	-10.88800	0.64868	0.07348
56402.738528	-21.03331	0.00109	3.81755	29.70776	-13.19300	0.66750	0.07318
56403.732778	-21.03440	0.00106	3.81539	29.72983	-14.25900	0.66329	0.07406
56404.759609	-21.03662	0.00111	3.81661	29.65499	-10.11000	0.77237	0.07439
56405.894605	-21.03552	0.00115	3.81774	29.85775	-9.94600	0.72143	0.07360
56406.740208	-21.03456	0.00120	3.81993	29.82352	-14.33600	0.72669	0.07419
56407.695168	-21.03256	0.00110	3.81359	29.60134	-15.63300	0.70920	0.07465
56415.668008	-21.03662	0.00139	3.82129	29.55949	-14.10500	0.64940	0.07371
56415.779390	-21.03467	0.00148	3.83390	29.72448	-14.05600	0.71455	0.07412

Table 4. continued.

BJD - 2400000	RV [km s^{-1}]	σ_{RV} [km s^{-1}]	FWHM [km s^{-1}]	Contrast	BIS [km s^{-1}]	S-index	$H\alpha$
56416.707531	-21.03643	0.00101	3.81810	29.64671	-14.15500	0.80232	0.07423
56433.822483	-21.03652	0.00138	3.81790	29.58418	-16.32300	0.65912	0.07374
56452.637514	-21.03486	0.00095	3.81107	29.75017	-13.75000	0.65263	0.07411
56453.750191	-21.03072	0.00218	3.81240	29.44713	-13.66400	0.52168	0.07422
56454.576818	-21.03889	0.00122	3.81156	29.61765	-13.65100	0.75057	0.07466
56456.621577	-21.03266	0.00128	3.81601	29.77250	-9.32300	0.65904	0.07414
56459.602670	-21.03486	0.00098	3.81499	29.70580	-13.54200	0.67428	0.07328
56460.581195	-21.03286	0.00117	3.81579	29.74453	-12.91600	0.73618	0.07367
56467.721548	-21.03159	0.00127	3.82564	29.65161	-12.06000	0.68420	0.07433
56468.670282	-21.03719	0.00096	3.80961	29.56663	-14.63900	0.75087	0.07568
56469.573520	-21.03770	0.00098	3.81591	29.64044	-10.77500	0.79118	0.07630
56471.599078	-21.03543	0.00104	3.82143	29.69003	-17.16200	0.84916	0.07643
56472.612503	-21.03565	0.00097	3.82076	29.73460	-10.85000	0.69736	0.07397
56473.565061	-21.03717	0.00123	3.81395	29.88008	-13.54500	0.67735	0.07407
56474.582546	-21.03606	0.00120	3.82071	29.68392	-15.21200	0.68724	0.07355
56475.625201	-21.03356	0.00146	3.80712	29.83704	-9.08500	0.69556	0.07357
56476.551669	-21.03418	0.00106	3.80969	29.88073	-11.69200	0.65615	0.07375
56477.573477	-21.03471	0.00097	3.81894	29.75496	-13.81500	0.70699	0.07436
56481.550172	-21.02939	0.00113	3.81448	29.62782	-14.59500	1.96019	0.09191
56508.491034	-21.03812	0.00107	3.82046	29.71902	-13.22600	0.64301	0.07399
56728.910492	-21.03504	0.00097	3.82500	29.75477	-14.98800	0.58831	0.07371
56729.849217	-21.03309	0.00092	3.81440	29.69132	-11.25100	0.61797	0.07346
56732.847430	-21.03554	0.00115	3.81877	29.60389	-13.24700	0.63364	0.07364
56741.879057	-21.03733	0.00104	3.82538	29.71906	-14.84400	0.66620	0.07363
56742.830194	-21.03962	0.00099	3.81651	29.71470	-13.47300	0.57377	0.07331
56743.820860	-21.03773	0.00098	3.81371	29.64036	-10.62100	0.58088	0.07321
56744.838819	-21.03491	0.00095	3.81968	29.65426	-12.00700	0.58850	0.07264
56745.777198	-21.03319	0.00108	3.81495	29.62472	-11.09300	0.59745	0.07304
56746.846571	-21.03131	0.00153	3.82928	29.63570	-12.70400	0.55182	0.07340
56752.845395	-21.03829	0.00094	3.81700	29.75184	-14.06000	0.61436	0.07192
56754.870611	-21.03445	0.00165	3.82584	29.66639	-9.96800	0.46604	0.07254
56756.767444	-21.04072	0.00099	3.81570	29.67287	-11.93200	0.60350	0.07287
56756.889351	-21.04078	0.00087	3.82295	29.78539	-10.59100	0.58132	0.07292
56757.818795	-21.03977	0.00101	3.81853	29.69277	-12.62200	0.57528	0.07292
56758.837121	-21.03718	0.00257	3.80721	29.34789	-17.05100	0.05815	0.07438
56759.838142	-21.03684	0.00102	3.82147	29.65673	-10.46600	0.57260	0.07231
56760.824612	-21.03937	0.00102	3.81645	29.61767	-12.62800	0.54223	0.07273
56763.734927	-21.03761	0.00086	3.81459	29.61778	-10.42600	0.66000	0.07443
56764.787021	-21.03525	0.00097	3.81802	29.64064	-13.52100	0.76207	0.07542
56765.745347	-21.03668	0.00093	3.81730	29.46847	-13.55700	0.59231	0.07282
56766.775505	-21.03762	0.00090	3.81650	29.66796	-11.83900	0.64747	0.07306
56767.793091	-21.03850	0.00097	3.82151	29.64617	-12.82100	0.59777	0.07340
56768.780477	-21.03609	0.00089	3.81706	29.66137	-12.25100	0.59818	0.07329
56778.690297	-21.03769	0.00095	3.81349	29.64192	-13.21700	0.60622	0.07370
56779.783112	-21.03794	0.00107	3.82015	29.72665	-13.94800	0.62610	0.07330
56781.690717	-21.03766	0.00111	3.82007	29.60893	-13.11700	0.59434	0.07299
56783.736806	-21.03518	0.00096	3.81692	29.72172	-10.48900	0.63904	0.07303
56784.704805	-21.03187	0.00118	3.82099	29.61878	-14.25400	0.59723	0.07383
56785.625047	-21.03508	0.00111	3.81051	29.52198	-13.95500	0.64716	0.07335
56786.680164	-21.03692	0.00095	3.81366	29.63381	-15.14000	0.63646	0.07340
56817.691837	-21.03218	0.00131	3.82783	29.64171	-12.44600	0.60504	0.07321
56822.661214	-21.03234	0.00106	3.82016	29.68441	-14.71800	0.62893	0.07291
56823.724567	-21.03366	0.00110	3.81981	29.71198	-13.67800	0.62656	0.07268
56824.702469	-21.03578	0.00102	3.82337	29.81902	-13.50200	0.71863	0.07338
56825.666701	-21.03476	0.00105	3.81998	29.69412	-10.94900	0.71217	0.07365
56828.647510	-21.03619	0.00101	3.82720	29.78387	-9.57800	0.77022	0.07434
56837.742106	-21.03177	0.00106	3.81785	29.59583	-15.09500	0.67948	0.07337
56838.602389	-21.03142	0.00100	3.82349	29.71560	-15.70100	0.70379	0.07467
56839.599261	-21.03392	0.00107	3.82001	29.65510	-13.02800	0.67020	0.07362
56840.607775	-21.03573	0.00103	3.82299	29.74110	-13.89200	0.77562	0.07448
56842.505245	-21.03034	0.00118	2.97679	25.86681	-6.92100	0.71518	0.07301
56857.575771	-21.02994	0.00131	3.82407	29.76491	-12.45300	0.64550	0.07289
56858.591160	-21.03141	0.00094	3.82000	29.74665	-12.55700	0.82937	0.07390
56862.639442	-21.03168	0.00163	3.82337	29.50546	-15.39800	0.76169	0.07753
56863.567436	-21.03505	0.00105	3.82255	29.67961	-9.30500	0.69453	0.07359
56864.560703	-21.04031	0.00102	3.82542	29.79073	-14.82000	0.70451	0.07417

Table 4. continued.

BJD - 2400000	RV [kms^{-1}]	σ_{RV} [kms^{-1}]	FWHM [kms^{-1}]	Contrast	BIS [kms^{-1}]	S-index	$H\alpha$
56867.615838	-21.03540	0.00120	3.82053	29.68153	-12.59300	0.69146	0.07288
56871.640488	-21.03200	0.00122	3.81727	29.59402	-12.21000	0.70134	0.07379
56872.556590	-21.03169	0.00115	3.82406	29.72386	-12.39100	0.64048	0.07336
56920.501178	-21.03525	0.00143	3.81489	29.60122	-14.13600	0.76320	0.07368
56921.493865	-21.03652	0.00106	3.82537	29.74597	-15.09600	0.74328	0.07364
56922.518736	-21.03804	0.00092	3.81262	29.70174	-12.12700	0.71936	0.07326
56923.505383	-21.03576	0.00149	3.81921	29.62682	-14.90600	0.81708	0.07349
56924.492563	-21.03712	0.00118	3.82003	29.66977	-9.27500	0.86089	0.07358
56925.492960	-21.03277	0.00103	3.81241	29.66171	-13.52200	0.81023	0.07422
56926.483300	-21.03293	0.00102	3.81686	29.66027	-14.26000	0.73686	0.07439
56928.490972	-21.03366	0.00105	3.81418	29.61904	-13.03500	0.73980	0.07347
56931.482568	-21.03535	0.00096	2.97588	25.90034	-7.57500	0.67410	0.07372
56932.500110	-21.03466	0.00125	2.97926	25.84618	-12.84900	0.70888	0.07372
57061.879249	-21.03620	0.00099	2.97366	25.85982	-7.42400	0.82534	0.07245
57062.874065	-21.03525	0.00092	2.97238	25.83705	-9.37300	0.75282	0.07208
57075.891323	-21.03621	0.00102	2.98041	25.98974	-8.98900	0.68325	0.07294
57076.866870	-21.03365	0.00096	2.97932	26.00417	-10.35000	0.73074	0.07372
57077.894507	-21.03318	0.00118	2.98698	26.08231	-8.87800	0.83344	0.07506
57079.861021	-21.03859	0.00112	2.99151	26.17960	-4.04700	0.73765	0.07256
57082.873588	-21.03445	0.00095	2.97970	26.03923	-8.98400	0.75450	0.07276
57100.871196	-21.03746	0.00117	2.98565	25.99007	-8.44500	0.69009	0.07320
57101.845557	-21.03655	0.00097	2.98091	25.97553	-7.86800	0.75156	0.07355
57102.902853	-21.03570	0.00117	2.99316	26.05182	-8.56000	0.72155	0.07314
57114.877970	-21.04279	0.00107	2.98729	26.09924	-9.75100	0.66577	0.07291
57115.901283	-21.03915	0.00130	2.98883	26.02706	-7.30800	0.63521	0.07287
57116.796448	-21.03725	0.00103	2.97877	25.95115	-11.20600	0.66530	0.07266
57136.803148	-21.03668	0.00099	2.98684	26.06216	-8.88800	0.77239	0.07272
57140.817332	-21.03256	0.00091	2.98354	26.04445	-8.38200	0.75002	0.07234
57142.797626	-21.03594	0.00086	2.98762	26.07266	-7.62500	0.73667	0.07205
57143.797870	-21.03869	0.00093	2.98567	26.07215	-7.98500	0.76638	0.07203
57144.713698	-21.03527	0.00133	2.98486	25.89386	-13.74500	0.74788	0.07189
57145.833574	-21.03310	0.00139	2.98249	25.83493	-7.85900	0.65659	0.07151
57199.659083	-21.03755	0.00088	3.01184	25.64209	0.26000	0.69328	0.07303
57200.574275	-21.03662	0.00115	3.02311	25.91223	0.10600	0.67404	0.07389
57200.704512	-21.03870	0.00100	3.01190	25.62919	3.57100	0.65914	0.07347
57211.587042	-21.04082	0.00082	3.00979	25.58543	4.74100	0.72773	0.07244
57214.668498	-21.02925	0.00095	3.01268	25.63986	0.96700	0.74824	0.07275
57249.511994	-21.03617	0.00127	3.01641	25.63277	1.20100	0.68625	0.07309
57250.526632	-21.03796	0.00147	3.01227	25.59754	1.45500	0.67599	0.07408
57252.505034	-21.03505	0.00085	3.00972	25.53107	4.64200	0.73242	0.07285
57253.513954	-21.03481	0.00090	3.00912	25.60966	1.36900	0.74934	0.07238
57260.501166	-21.03894	0.00126	3.02070	25.67463	2.65100	0.70740	0.07262
57263.486849	-21.03380	0.00096	3.01464	25.74967	1.58000	0.68379	0.07137
57264.487619	-21.03518	0.00102	3.01084	25.71615	2.56700	0.73334	0.07226
57266.509576	-21.03358	0.00102	3.01052	25.66584	3.87600	0.77630	0.07231
57267.580490	-21.03122	0.00086	2.99880	25.34691	2.38700	0.77280	0.07233
57268.495205	-21.02950	0.00098	3.01538	25.78414	2.22300	0.75767	0.07314
57269.523288	-21.03331	0.00084	3.00779	25.53976	1.58800	0.80151	0.07290
57270.470476	-21.03506	0.00083	3.00771	25.52130	1.18800	0.81696	0.07435
57271.502355	-21.03192	0.00147	3.01524	25.60782	2.39100	0.66607	0.07272
57276.492036	-21.03114	0.00120	3.00929	25.55612	-2.28600	0.72487	0.07352
57277.486397	-21.02944	0.00094	3.00835	25.55858	1.86100	0.74105	0.07355
57292.489321	-21.03437	0.00098	3.00658	25.43699	0.99800	0.77391	0.07354
57293.479385	-21.03361	0.00115	3.00976	25.39352	2.05100	0.79542	0.07459
57294.486358	-21.03386	0.00095	3.00502	24.67654	0.91500	0.73370	0.07348

Table 5. Radial velocities time series for GJ 3293.

BJD - 2400000	RV [km s^{-1}]	σ_{RV} [km s^{-1}]	FWHM [km s^{-1}]	Contrast	BIS [km s^{-1}]	S-index	$H\alpha$
54805.684241	13.28713	0.00505	3.60254	25.79888	-17.14600	1.43841	0.06417
54825.640268	13.30974	0.00168	3.60782	25.14589	-5.88700	1.32105	0.06840
54826.634453	13.31091	0.00189	3.60512	25.07722	-3.29900	1.18284	0.06751
54827.648451	13.30608	0.00191	3.60538	25.03949	-10.48400	1.11380	0.06634
54828.660596	13.30306	0.00231	3.60655	24.93891	-3.71900	1.35938	0.06757
54829.769900	13.30342	0.00246	3.60755	24.76578	-10.29600	1.15427	0.06737
54830.663218	13.29975	0.00219	3.61464	25.10732	-14.16000	1.11939	0.06653
54831.658705	13.29811	0.00212	3.60920	25.18232	-14.41300	1.10805	0.06643
54832.672872	13.29703	0.00352	3.62180	24.78081	-11.90700	1.23669	0.06658
54833.660164	13.29660	0.00264	3.61949	25.03035	-8.65700	1.11968	0.06599
54834.716259	13.29360	0.00195	3.60456	25.03209	-9.87600	1.15549	0.06791
54848.620976	13.30462	0.00183	3.59771	25.10879	-15.04600	1.01176	0.06410
54850.614526	13.30238	0.00211	3.58700	25.11331	-17.36800	0.98858	0.06416
54852.633918	13.30558	0.00182	3.59572	25.10511	-6.39400	0.97414	0.06422
54854.626595	13.30206	0.00221	3.60632	24.87230	-15.97900	1.04855	0.06659
54879.591657	13.30399	0.00219	3.61009	24.97407	-7.65000	1.21610	0.06547
54881.624409	13.30019	0.00254	3.60531	24.80336	-19.38300	1.18238	0.06436
54883.524937	13.30109	0.00208	3.60588	24.97738	-19.55900	1.05619	0.06436
54885.564077	13.29958	0.00219	3.60068	24.90323	-11.28600	1.24502	0.06833
55045.922309	13.29203	0.00352	3.59152	24.95034	-5.09700	0.53175	0.06648
55047.913490	13.28496	0.00332	3.60761	24.95206	-7.97200	1.30462	0.06733
55049.922892	13.28501	0.00208	3.60038	24.98431	-14.02200	1.08683	0.06600
55052.903667	13.28672	0.00199	3.59689	25.03757	-8.62600	1.11384	0.06992
55121.838049	13.29815	0.00251	3.61245	24.90132	-21.51300	1.13064	0.06697
55126.731747	13.29901	0.00214	3.60909	24.87652	-10.83100	1.27585	0.06651
55129.712319	13.29939	0.00193	3.60236	24.96040	-9.03100	1.19116	0.06605
55132.803209	13.29488	0.00216	3.60264	24.91751	-7.52100	1.08551	0.06502
55135.700519	13.29045	0.00208	3.60418	24.92648	-6.98800	1.11731	0.06634
55137.706955	13.28465	0.00176	3.60414	24.99914	-2.58200	1.10078	0.06546
55139.738734	13.28315	0.00322	3.59590	24.69413	-19.69600	1.07615	0.06491
55141.715172	13.28170	0.00236	3.60172	24.98044	-17.63100	1.00666	0.06515
55143.683353	13.28291	0.00256	3.60443	25.03226	-13.76000	1.17939	0.06705
55168.598263	13.28956	0.00204	3.61057	24.94123	-15.05700	1.15850	0.06741
55169.623930	13.29192	0.00200	3.59617	24.94721	-1.72900	1.23873	0.06809
55230.607997	13.29238	0.00249	3.60718	24.79661	-6.60000	1.21420	0.06494
55403.920619	13.29736	0.00375	3.61997	24.81611	-7.91500	1.28338	0.06744
55411.880365	13.29398	0.00714	3.59996	25.14133	10.91200	0.89537	0.06577
55428.885351	13.30841	0.00295	3.59933	24.83009	-13.58100	1.21101	0.06618
55437.865289	13.30280	0.00194	3.60161	24.82933	-16.40300	1.21056	0.06798
55444.823799	13.29798	0.00217	3.60669	24.69761	-16.26800	1.10945	0.06544
55450.888963	13.29884	0.00222	3.60503	24.85917	-8.20600	1.23106	0.06706
55453.893332	13.30052	0.00228	3.61657	24.83225	-7.42100	1.14594	0.06651
55454.821713	13.30234	0.00229	3.60843	24.82226	-5.72200	1.11792	0.06483
55455.846302	13.30404	0.00322	3.61037	24.95592	3.99400	1.16694	0.06664
55456.833134	13.30144	0.00208	3.60504	24.86587	-7.48600	1.06433	0.06588
55457.863509	13.30340	0.00226	3.60461	24.85114	-13.88300	1.00624	0.06608
55493.821070	13.30954	0.00242	3.60987	24.95725	-7.36400	1.04942	0.06446
55494.769769	13.30636	0.00267	3.60567	24.84793	-10.00200	0.80874	0.06538
55495.880510	13.30440	0.00191	3.60457	24.68629	-14.22500	1.09695	0.06706
55497.750761	13.29962	0.00227	3.60157	24.88640	-11.72700	1.21370	0.06542
55500.806953	13.29395	0.00233	3.61028	25.10494	-8.35100	0.96037	0.06542
55501.751108	13.29091	0.00216	3.60475	24.90774	-2.33900	1.08924	0.06554
55505.644606	13.28513	0.00254	3.59661	24.78567	-0.57400	1.00832	0.06509
55514.687314	13.28332	0.00209	3.59658	24.93413	-9.79700	1.34571	0.06724
55521.726095	13.29687	0.00231	3.60660	24.80012	-14.61300	0.91468	0.06508
55523.713917	13.29907	0.00198	3.60248	25.04081	-12.85700	1.06428	0.06370
55547.633280	13.29914	0.00209	3.60517	24.93887	-5.94400	1.18103	0.06574
55548.599153	13.30039	0.00276	3.60506	24.76291	-7.40400	1.01141	0.06510
55549.699476	13.30187	0.00189	3.60281	25.05025	-3.73800	1.15391	0.06542
55576.599728	13.29620	0.00263	3.60982	25.12058	-14.86400	1.30366	0.06739
55579.692905	13.30124	0.00227	3.60891	24.79481	-1.77500	1.17443	0.06610
55586.579011	13.31356	0.00224	3.60733	24.96234	-7.36100	1.04879	0.06553
55612.549444	13.30545	0.00212	3.59664	24.89766	-8.20100	0.83286	0.06580
55615.505709	13.30639	0.00175	3.60687	24.94252	-13.07600	1.30558	0.07103
55621.499694	13.29374	0.00200	3.60026	24.85476	-5.67900	0.96816	0.06603
55817.894520	13.29746	0.00266	3.60730	25.03872	-9.59800	1.11978	0.06714

Table 5. continued.

BJD - 2400000	RV [$km s^{-1}$]	σ_{RV} [$km s^{-1}$]	FWHM [$km s^{-1}$]	Contrast	BIS [$km s^{-1}$]	S-index	$H\alpha$
55822.878882	13.30678	0.00194	3.61290	24.88298	-13.45800	1.00872	0.06714
55825.899099	13.30965	0.00207	3.61099	24.98686	-10.14400	1.23962	0.06781
55828.892018	13.30912	0.00193	3.60762	25.07880	-12.00000	1.15878	0.06632
55829.854215	13.30920	0.00207	3.60775	24.97491	-16.34000	1.07993	0.06585
55830.872340	13.30873	0.00230	3.59417	25.00099	-4.94500	1.02090	0.06623
55831.833656	13.30666	0.00190	3.59757	25.00945	-14.98000	1.19270	0.06634
55834.836217	13.30400	0.00235	3.59159	25.00795	-14.86600	0.94203	0.06550
55835.760676	13.30329	0.00237	3.60847	24.79972	-6.84700	0.93297	0.06503
55837.831271	13.30281	0.00173	3.59482	24.93214	-8.12700	1.02606	0.06454
55839.821106	13.29854	0.00254	3.60898	24.83951	-6.65200	1.24377	0.06410
55840.872050	13.29332	0.00201	3.61108	25.01686	-12.34300	0.97161	0.06538
55841.750218	13.29128	0.00279	3.59457	24.81362	-0.16500	1.05086	0.06592
55843.858883	13.28980	0.00200	3.61117	24.97364	-8.97300	1.01994	0.06570
55870.768892	13.28564	0.00233	3.60836	25.01811	-9.16100	1.03156	0.06598
55887.685025	13.29534	0.00352	3.59405	24.66931	-11.95900	1.28739	0.06655
55890.672969	13.30400	0.00202	3.60649	24.82451	-8.00100	1.18061	0.06655
55893.659583	13.30066	0.00238	3.61236	24.72070	-7.96700	1.12803	0.06615
55924.645449	13.30524	0.00227	3.61222	25.09914	-6.57800	1.14995	0.06596
55925.650070	13.30729	0.00221	3.59754	24.88584	-13.38200	0.96554	0.06551
55926.630663	13.30429	0.00209	3.61535	24.96683	-7.81600	1.17105	0.06725
55927.638592	13.30534	0.00262	3.60334	24.87551	-23.76800	1.04069	0.06554
55928.682457	13.30447	0.00240	3.59773	24.87190	-14.68300	0.98636	0.06414
55929.614705	13.30370	0.00238	3.60304	24.86785	-6.95300	0.92004	0.06481
55930.633059	13.30486	0.00236	3.60578	24.92209	-15.13200	1.23944	0.06516
55931.615824	13.30357	0.00255	3.60603	24.90897	-11.45500	0.94165	0.06441
55932.616260	13.30063	0.00213	3.59831	24.91965	-12.63100	1.24667	0.06490
55933.630897	13.30111	0.00213	3.61401	24.96484	-10.77800	1.16176	0.06497
55940.550353	13.29138	0.00326	3.61658	24.95451	-11.83200	1.54094	0.06589
55941.642143	13.29720	0.00197	3.61108	25.00144	-11.56500	1.21553	0.06546
55942.698321	13.29410	0.00262	3.60089	24.79415	-8.25300	0.93298	0.06504
55943.639459	13.29720	0.00276	3.60998	24.79693	-11.80900	1.28354	0.06656
55944.630164	13.30033	0.00254	3.60971	24.95140	-6.49700	1.12484	0.06530
55945.641378	13.30071	0.00229	3.61062	24.92532	-4.84600	1.17007	0.06588
55946.637012	13.30059	0.00225	3.60626	24.86616	-5.12000	1.10456	0.06607
55947.621339	13.29862	0.00210	3.60959	24.95253	-12.26500	1.05574	0.06560
55949.616275	13.30126	0.00208	3.60094	24.84526	-9.15500	1.15547	0.06456
55950.628075	13.30332	0.00221	3.61087	24.90341	2.25300	1.41267	0.06742
55997.531261	13.27845	0.00277	3.59258	24.73141	-10.15600	1.07665	0.06519
56001.488947	13.27650	0.00236	3.60593	24.70919	-11.71300	0.88176	0.06454
56008.507639	13.29077	0.00216	3.58326	24.82394	-12.39600	0.99871	0.06562
56010.513424	13.29979	0.00221	3.60673	24.81264	-13.23500	1.05353	0.06519
56022.505933	13.29589	0.00309	3.61053	24.63378	-12.26500	1.19487	0.06767
56025.484808	13.28653	0.00348	3.58540	24.36799	-6.58300	99.00000	0.07099
56030.485817	13.28159	0.00419	3.60485	24.67276	-0.97100	1.09692	0.06724
56032.474498	13.28279	0.00440	3.60567	24.96957	-6.90800	0.92325	0.06652
56158.864994	13.29341	0.00277	3.59488	24.71040	-8.84100	1.11252	0.06832
56160.886335	13.29645	0.00244	3.59963	24.74944	-10.13800	1.39606	0.07008
56171.846000	13.30447	0.00229	3.60866	24.69961	-11.02000	0.94568	0.06540
56208.855664	13.29245	0.00425	3.62924	24.56804	-21.13700	1.47928	0.06558
56209.863998	13.28855	0.00534	3.63220	24.65556	5.80800	1.03037	0.06537
56210.849414	13.29532	0.00249	3.60271	24.69381	-9.65000	1.15068	0.06601
56221.869314	13.30484	0.00297	3.60559	24.70250	-21.47600	1.22809	0.06715
56229.757114	13.30344	0.00231	3.60705	24.66251	-0.16900	1.04788	0.06887
56230.709142	13.30224	0.00286	3.60004	24.50700	-19.20800	1.14848	0.06644
56231.780904	13.29930	0.00225	3.61505	24.73681	-11.02500	1.11629	0.06950
56235.664393	13.29563	0.00328	3.60122	24.81693	-13.63900	1.34573	0.06669
56236.653139	13.29218	0.00300	3.61510	24.76089	-8.31900	1.22445	0.06724
56237.643597	13.28945	0.00256	3.60731	24.76752	-6.97100	0.90788	0.06623
56238.612526	13.28999	0.00253	3.61303	24.62477	-5.61600	0.81225	0.06595
56239.666512	13.28469	0.00306	3.61977	24.86813	-11.83600	1.32971	0.06737
56245.613388	13.28258	0.00305	3.60453	24.78696	-17.89300	0.93200	0.06829
56248.648511	13.28748	0.00333	3.59427	24.86074	-16.62300	0.94043	0.06525
56249.672532	13.28736	0.00269	3.60082	24.92011	-9.27900	1.00592	0.06562
56251.690105	13.29188	0.00215	3.60230	24.91233	-13.75500	0.86878	0.06497
56252.654029	13.29385	0.00211	3.59468	24.91635	-12.23900	0.98274	0.06597
56253.655857	13.29686	0.00274	3.59634	24.89247	-10.19900	1.03980	0.06534

Table 5. continued.

BJD - 2400000	RV [km s^{-1}]	σ_{RV} [km s^{-1}]	FWHM [km s^{-1}]	Contrast	BIS [km s^{-1}]	S-index	$H\alpha$
56256.689979	13.30274	0.00264	3.60931	24.72152	-16.32200	0.91314	0.06558
56257.729949	13.30044	0.00220	3.61488	24.95335	-9.61900	1.14283	0.06628
56259.643442	13.30647	0.00256	3.59588	24.67017	-19.92200	1.19137	0.06682
56263.636881	13.30173	0.00335	3.59387	24.89050	-17.24000	1.14028	0.06921
56264.781506	13.29858	0.00187	3.60065	24.90384	-18.88900	1.24327	0.06903
56283.565328	13.29808	0.00267	3.60422	24.84882	-22.31400	1.00336	0.06607
56304.652698	13.29348	0.00244	3.62495	25.00670	-8.39000	1.21849	0.06514
56307.607913	13.29730	0.00200	3.61245	24.91672	-10.32100	1.08507	0.06777
56312.606333	13.30707	0.00251	3.61586	24.87951	-11.24100	1.27828	0.06766
56314.608745	13.31175	0.00259	3.62399	24.80913	-11.77500	1.10909	0.06581
56316.642218	13.31726	0.00277	3.61573	24.41020	-12.50800	0.93183	0.06745
56318.644521	13.31766	0.00301	3.07817	22.24179	2.93000	1.25208	0.06638
56319.655672	13.31536	0.00330	3.09120	22.36275	-21.02100	1.13858	0.06621
56944.875495	13.29033	0.00334	3.09839	22.43077	-17.77300	1.20461	0.06588
56948.738510	13.28941	0.00225	3.08363	22.37577	-6.67600	1.15791	0.06478
56951.727579	13.29638	0.00256	3.08230	22.36371	-6.75900	1.19064	0.06591
56989.641550	13.29746	0.00223	3.07412	22.46412	-16.79800	1.22933	0.06614
56990.806123	13.30483	0.00325	3.07530	22.60035	-2.53900	0.94264	0.06651
56991.792259	13.30351	0.00314	3.08404	22.56076	-4.83400	0.84707	0.06788
56992.755154	13.30158	0.00213	3.08541	22.56358	-3.60500	1.01456	0.06490
56993.661520	13.30290	0.00253	3.08115	22.47170	-7.59100	1.17941	0.06620
56994.603856	13.30591	0.00280	3.07076	22.51368	-3.93400	1.18841	0.06605
56994.733368	13.30453	0.00353	3.10087	22.69729	9.62300	0.81696	0.06602
56995.802531	13.30280	0.00276	3.09021	22.54694	-14.52200	1.37627	0.06977
56996.785571	13.30061	0.00228	3.08671	22.35066	-6.97500	1.23102	0.06711
56997.655833	13.30052	0.00213	3.09408	22.37350	-7.08100	0.96771	0.06890
56998.663049	13.29502	0.00216	3.08858	22.44118	-9.97700	1.14880	0.06850
56999.668863	13.29641	0.00234	3.07803	22.48233	-4.72600	0.98808	0.06725
57000.654791	13.29701	0.00249	3.08333	22.43008	-7.55900	1.24177	0.06730
57001.820993	13.28997	0.00916	3.09250	21.81063	15.97700	99.00000	0.06765
57002.702894	13.29034	0.00350	3.09330	22.60877	-18.70400	1.53037	0.07309
57003.664549	13.28861	0.00226	3.09093	22.59631	-5.35200	1.09968	0.06981
57007.607232	13.29348	0.00234	3.08857	22.45094	-16.48600	1.54543	0.07707
57008.607445	13.28819	0.00332	3.08599	22.61984	-5.81900	1.46831	0.06992
57009.603861	13.28778	0.00259	3.08449	22.49648	-6.88100	1.40460	0.06853
57018.659726	13.29973	0.00249	3.09762	22.57869	-2.89000	1.12903	0.06581
57019.661710	13.30072	0.00307	3.08669	22.55093	-20.61600	0.95944	0.06610
57020.665730	13.30849	0.00265	3.09153	22.57849	-10.09500	0.97703	0.06621
57021.694899	13.29982	0.00232	3.07972	22.33433	-5.34500	1.37350	0.06822
57022.720536	13.29969	0.00195	3.07315	22.55126	-12.01300	1.06516	0.06615
57044.576456	13.29658	0.00220	3.09617	22.63819	-6.14800	1.23231	0.06933
57045.564149	13.29915	0.00244	3.10133	22.63253	-0.44100	1.31634	0.07132
57046.570464	13.29667	0.00217	3.08592	22.53196	-2.09000	1.38826	0.06776
57047.586268	13.30125	0.00239	3.09270	22.64925	-19.75800	1.28299	0.06645
57048.572374	13.30313	0.00219	3.09965	22.64557	1.82800	1.29567	0.06794
57049.588212	13.30270	0.00228	3.09083	22.76922	0.69800	1.25257	0.06699
57050.570857	13.30449	0.00207	3.09725	22.63409	-7.61500	1.13235	0.06665
57051.581509	13.30642	0.00178	3.08953	22.54361	-9.40600	1.37997	0.07088
57052.566353	13.30961	0.00290	3.09553	22.66150	-4.85400	1.36001	0.06812
57053.576344	13.30692	0.00280	3.09744	22.54724	-12.26100	1.43179	0.07159
57054.565561	13.30910	0.00263	3.10199	22.61545	-5.33200	1.17163	0.06638
57055.610735	13.30715	0.00249	3.08782	22.55037	-3.77700	0.91883	0.06719
57056.613122	13.30935	0.00233	3.08533	22.45494	-1.72500	1.08409	0.06610
57057.593021	13.30733	0.00221	3.09599	22.46527	-14.02700	1.33309	0.06724
57058.609562	13.30266	0.00201	3.08755	22.41164	-5.48000	1.20551	0.06693
57061.618211	13.30000	0.00237	3.08143	22.40497	-9.32900	1.37400	0.06514
57062.605528	13.29081	0.00233	3.07852	22.24424	-6.32300	1.06682	0.06459
57064.575184	13.29007	0.00251	3.07719	22.50249	-7.08800	1.13560	0.06403
57065.578206	13.28547	0.00186	3.08184	22.54842	-8.69100	0.98001	0.06432
57066.555800	13.28820	0.00311	3.07988	22.56901	-13.15700	1.07860	0.06542
57075.597614	13.28668	0.00295	3.06016	22.59752	-10.42700	0.95436	0.06529
57076.538475	13.29446	0.00229	3.08083	22.54411	-6.43100	1.08071	0.06578
57077.535801	13.29671	0.00224	3.08182	22.54988	-7.13200	0.88135	0.06737
57078.554770	13.29391	0.00311	3.09509	22.56209	-3.96200	1.20457	0.06621
57079.526694	13.29802	0.00234	3.07593	22.50782	-10.93200	1.30121	0.06797
57080.536497	13.30167	0.00359	3.08055	22.44380	-28.14000	0.84920	0.06879

Table 5. continued.

BJD - 2400000	RV [$km s^{-1}$]	σ_{RV} [$km s^{-1}$]	FWHM [$km s^{-1}$]	Contrast	BIS [$km s^{-1}$]	S-index	$H\alpha$
57082.521187	13.30657	0.00279	3.09246	22.44558	-11.85500	1.49421	0.07312
57100.516771	13.28156	0.00233	3.07021	22.32990	-6.87800	1.21035	0.06554
57101.501954	13.27843	0.00263	3.07428	22.36061	-8.09800	1.05274	0.06449
57102.522320	13.27361	0.00368	3.07704	22.23797	-8.78300	1.43611	0.06581
57103.495341	13.28431	0.00301	3.06985	22.35386	-9.84600	1.03031	0.06495
57104.531402	13.28163	0.00220	3.08003	22.30730	-1.47500	1.14905	0.06526
57114.510271	13.29542	0.00205	3.07382	22.42178	-7.59900	1.16808	0.06485
57115.481448	13.29545	0.00189	3.06996	22.44888	-9.00700	1.11991	0.06512
57116.504730	13.30226	0.00360	3.07454	22.26678	-16.72300	0.87480	0.06631